AD-A117 737 CITY COLL NEW YORK F/G 17/2
ACQUISITION, IMAGE AND DATA COMPRESSION.(U)
APR 82 D L SCHILLING, G EICHMANN AFOSR-81-0169
UNCLASSIFIED AFOSR-TR-82-0567 NL

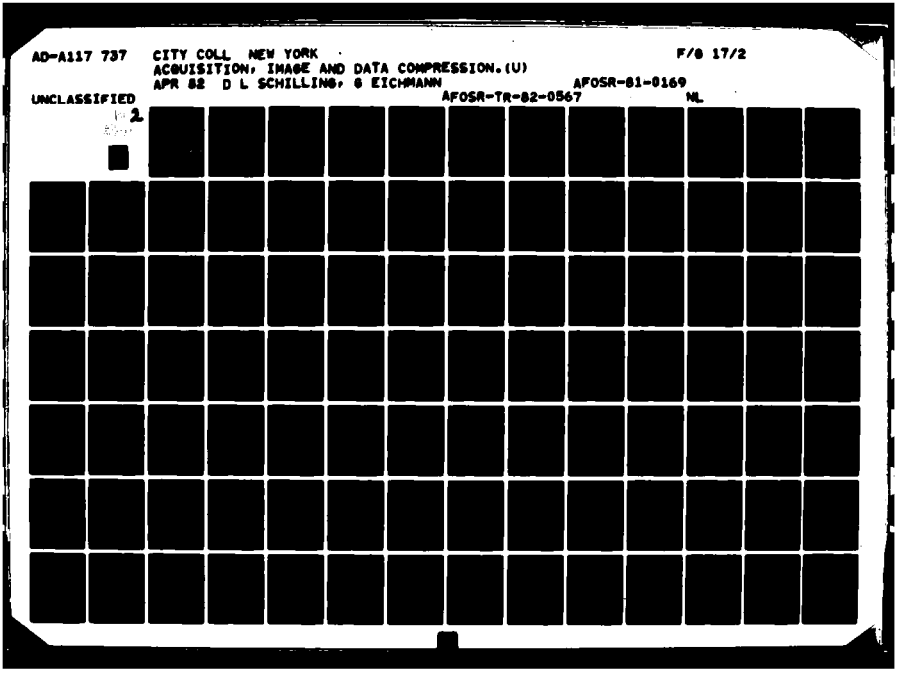

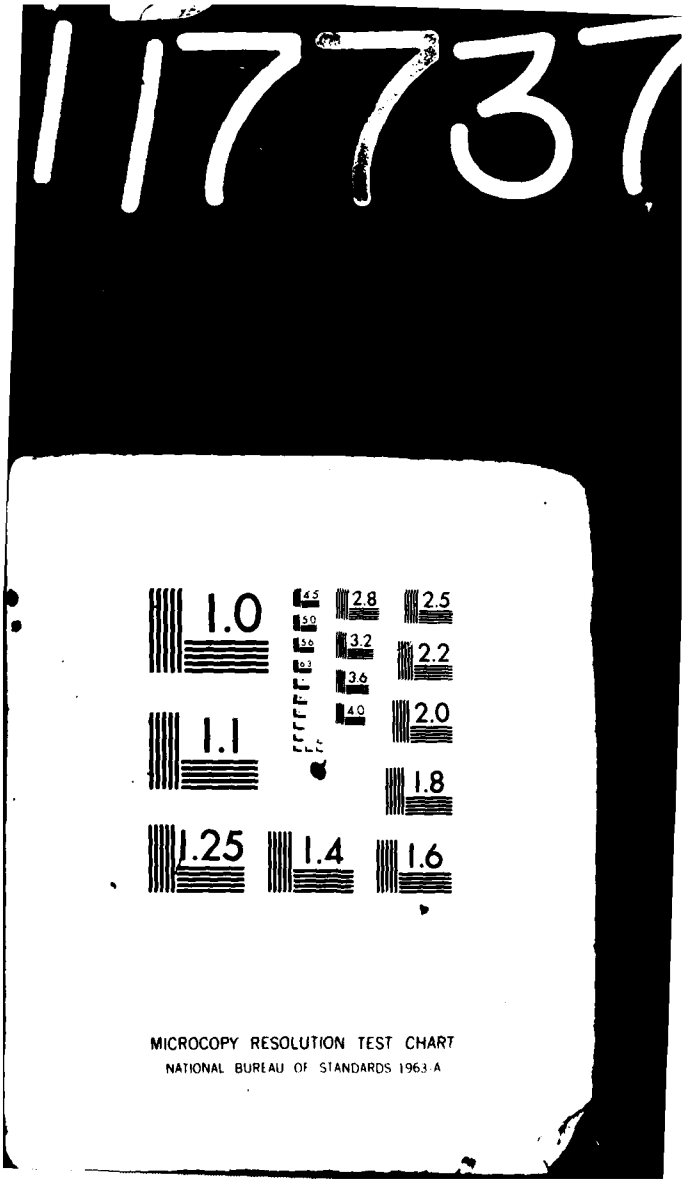
1.0
1.1
1.25
1.4
1.6
1.8
2.0
2.2
2.5
2.8
3.2
3.6
4.0
4.5
5.0
5.6
6.3
MICROCOPY RESOLUTION TEST CHART
NATIONAL BUREAU OF STANDARDS 1963-A

AFOSR-TR- 82-0567

(3)

ACQUISITION, IMAGE AND DATA COMPRESSION

Annual Technical Report - 5444-1

February 28, 1981 - March 1, 1981

Grant AFOSR-81-0169

AIR FORCE OFFICE OF SCIENTIFIC RESEARCH

Bolling Air Force Base

Washington, D. C. 20332

Donald L. Schilling
Professor
Co-Principal Investigator

George Eichmann
Professor
Co-Principal Investigator

DEPARTMENT OF ELECTRICAL ENGINEERING

THE CITY COLLEGE OF
THE CITY UNIVERSITY of NEW YORK

ACQUISITION, IMAGE AND DATA COMPRESSION

Annual Technical Report - 5444-1
February 28, 1981 - March 1, 1982

Grant AFOSR-81-0169
AIR FORCE OFFICE OF SCIENTIFIC RESEARCH
Bolling Air Force Base
Washington, D. C. 20332

Donald L. Schilling
Professor
Co-Principal Investigator

George Eichmann
Professor
Co-Principal Investigator

DEPARTMENT OF ELECTRICAL ENGINEERING

UNCLASSIFIED

SECURITY CLASSIFICATION OF THIS PAGE (When Data Entered)

REPORT DOCUMENTATION PAGE	READ INSTRUCTIONS BEFORE COMPLETING FORM
1. REPORT NUMBER AFOSR-TR- 82-0567	2. GOVT ACCESSION NO. AD-A117 737
	3. RECIPIENT'S CATALOG NUMBER
4. TITLE (and Subtitle) ACQUISITION, IMAGE AND DATA COMPRESSION	5. TYPE OF REPORT & PERIOD COVERED ANNUAL March 1,1981-Feb.28,1982
	6. PERFORMING ORG. REPORT NUMBER
7. AUTHOR(s) Donald L. Schilling Geore Eichmann	8. CONTRACT OR GRANT NUMBER(s) AFOSR-81-0169
9. PERFORMING ORGANIZATION NAME AND ADDRESS City College of New York New York, N. Y. 10031	10. PROGRAM ELEMENT, PROJECT, TASK AREA & WORK UNIT NUMBERS 2305/B1 61102F
11. CONTROLLING OFFICE NAME AND ADDRESS Air Force Office of Scientific Research Bolling, A.F.B, Washington, D.C. 20332	12. REPORT DATE April 30, 1982 13. NUMBER OF PAGES 91
14. MONITORING AGENCY NAME & ADDRESS(if different from Controlling Office)	15. SECURITY CLASS. (of this report) UNCLASSIFIED 15a. DECLASSIFICATION/DOWNGRADING SCHEDULE

16. DISTRIBUTION STATEMENT (of this Report)

Approved for public release;
distribution unlimited.

17. DISTRIBUTION STATEMENT (of the abstract entered in Block 20, if different from Report)

18. SUPPLEMENTARY NOTES

International Communications Conference - 6/82, INFOCOM 4/82
SPIA, San Diego, August 1981

19. KEY WORDS (Continue on reverse side if necessary and identify by block number)

Spread Spectrum, Optical Transforms, Acquisition, Delta Modulation, Simulation

20. ABSTRACT (Continue on reverse side if necessary and identify by block number)

This report discusses the following subjects:
A new reservation-based multiple access packet switching technique applicable to packet communications using a satellite channel is proposed. The objective of this research is to optimize the system performance in terms of throughput and delay and to develop analytical models to analyze the scheme.

DD FORM 1 JAN 73 1473 EDITION OF 1 NOV 65 IS OBSOLETE
S/N 0102-014-6601

UNCLASSIFIED
SECURITY CLASSIFICATION OF THIS PAGE (When Data Entered)

Simulation results show markedly improved delay-throughput characteristics over other existing and proposed multiple access techniques with especially significant performance gains at high traffic and also as the traffic imbalance among the users increases. A good agreement between the simulation results and the analytical results is obtained.

This report analyzes the slotted-ALOHA multiple access scheme for broadcast channels with a finite number of users, each having a buffer of infinite capacity. The analysis is based on the idea presented in (1), of having a two Markov chain model to describe the whole system. The model analyzed in this paper is simpler, gives further insight into the problem of interacting buffered users, and leads to one-dimentional Markov chains.

An upper bound on the worst case autocorrelation of PN sequences of a given length is obtained. The value of the worst case autocorrelation curve at some specific points is found and using interpolation methods a smooth curve fitting to the worst case autocorrelation curve is formulated.

(Continued on next page)

An infinite cyclic sequence of period p, where $p \leq 2^k$ for some positive integer k, is a shift register sequence if any block of k consecutive bits over one period of this sequence is not repeated. The sequence of period $p=2^k-1$ is known as the maximal length sequence and the sequence of length $p=2^k$ is called a deBruijn sequence [1]. For a given k the number of deBruijn sequences is $2^{2^{k-1}-k}$.

A linear maximal length sequence (also known as a PN sequence) can be generated by a k-stage linear feedback shift register (LFSR) with a primitive characteristic polynomial [2]. For a given k the number of linear maximal length sequences is $\phi(2^k-1)/k$,where ϕ is the Euler's ϕ-function. An efficient method to construct the nonlinear sequences is the cycle joining method [2],[3] which is based on joining the sequences of short period together to obtain a deBruijn sequence.

In the following a new property of the PN sequences is presented. For generation of nonlinear sequences of period $p=2^k$ this property and several other well known properties, [2], of the PN sequences are used to join the cycles of an LFSR with characteristic polynomial $G(x)=g(x)(1+x)^n$, where g(x) is a primitive polynomial of degree m and G(x) is of degree k=m+n.

Superresolving image restoration (SIR) in the presence of noise is considered. Few SIR algorithsm have demonstrated the ability to resolve two point sources spaced on-half of the Rayleigh distance apart. In this report, it is shown that the SIR of a two-point noncoherent source spaced one-tenth of a Rayleigh distance apart is possible. The method presented uses optimal data fitting techniques based on the method of linear programming. For noisy images, a combination of linear eigenvalue prefiltering and optimal data fitting is used. It is also shown that for a diffraction-limited (DL) image of two point sources spaced one-half of the Rayleigh distance apart, where the input is contaminated with sigificant noise, SIR is achievable. These results have important implications in atmospheric physics, geophysics, radio astronomy, medical diagnostics, and digital bandwidth-compression applications where the deconvolution of noisy bandwidth-compressed images is one of the fundamental limitations.

A method of restoring the discrete Fourier transform (DFT) spectrum of a DL image from a narrow observation segment of a DL image is also presented. The DL spectral restoration process is the dual of the more common DL image restoration process with the role of frequency and space reversed. Applications of a spectrum restoration include increasing the

field of view of existing imaging systems and extracting precise frequency components of a large DL image using only small segment of the entire image. This method could also be employed for image data compression which is of interest in digital video applications. Several differences between the implementation of the image and the spectrum restoration processes are described. The estimate is constrained to have an upper bound on the number of frequency components contained in the Fourier spectrum. The bound is the number of samples acquired at the Nyquist rate for the length of the image. The magnitude of the DFT spectrum is also bounded. These constraints define a large number of possible solutions. The desired solution is then selected such that the distance, defined in a function-theoretic sense, between the measured and the estimated image is an optimum. A number such measeures are investigated. Numerical experiments show that this approach yields results that are highly immune to measurement noise.

Signal-dependent noise encountered when sampling video signals at low sampling rate, while using an adaptive video delta modulator both as a source encoder and a video digitizer, is combated by using a white-light reflective transform optical preprocessor. While the white-light preprocessor works on black and white images, its main advantage is that it can simultaneously process using a single source many color channels. Further, the relative lack of both spatial and

temporal coherence aids in reducing speckle and interference noise effects. Experimental results on color video images, that have been preprocessed using a white light optical transform preprocessor and digitally encoded by sampling close to the Nyquist rate with an adaptive delta modulator, are presented.

I. Research Objectives

1. Dynamic Reservation Multiple Access Technique for Data Transmission via Satellites

A new reservation-based mulitiple access packet switching techniques applicable to packet communications using a satellite channel is proposed. The objective of this research is to optimize the system performance in terms of throughput and delay and to develop analytical models to analyze the scheme.

2. Analysis of Interacting Buffered Users in Slotted ALOHA

The objective of this research is to analyze the slotted ALOHA multiple access scheme for broadcase channels with a finite number of buffered users. Previous investigators of this problem have assumed that a user has a maximum of one packet in his buffer. In such a case, if a second packet arrived it would be automatically rejected and destroyed.

3. Worst Case Acquisition of PN Sequences

The objective of this study is to bound the autocorrelation of PN sequences. Using this bound more accurate estimates of the acquisition time in a spread spectrum system can be obtained.

4. Generation of Nonlinear Shift Register Sequences

Nonlinear sequences are more numerous and therefore more difficult to ascertain by an enemy, then linear sequences. The objective of this study is to present a new property of PN sequences and show how this property results in the generation of these sequences.

5. Superresolving Image Restoration

Superresolving image restoration in the presence of noise is considered.

6. Restoration of the DFT Spectra

Restoration of the DFT spectra of a narrow segment diffraction-limited image is described.

7. White-light Prefiltering

The use of a white-light preprocessor for color image bandwidth compression is described.

II. Status of the Research Effort

DYNAMIC RESERVATION MULTIPLE ACCESS TECHNIQUE FOR DATA TRANSMISSION VIA SATELLITES

D. K. Guha, D. L. Schilling, and T. N. Saadawi

Department of Electrical Engineering, City College of New York
New York, New York

Abstract

A new reservation-based multiple access packet switching technique applicable to packet communications using a satellite channel is proposed. The objective of this research is to optimize the system performance in terms of throughput and delay and to develop analytical models to analyze the scheme.

Simulation results show markedly improved delay-throughput characteristics over other existing and proposed multiple access techniques with especially significant performance gains at high traffic and also as the traffic imbalance among the users increases. A good agreement between the simulation results and the analytical results is obtained.

1.0 INTRODUCTION

The field of large data networks has seen a tremendous growth in the last decade. The simplest solution to providing communication between two points is to assign a dedicated channel for their use. This method is expensive in computer communications especially over long distances. Measurement studies conducted on time-sharing systems indicate that both computer and terminal data streams are *bursty*. That is, the peak data rate is much larger than the average data rate. Thus, if a channel is dynamically shared in some fashion among many users, the required channel capacity may be much less than the unshared case of dedicated channels. This concept is known as statistical load averaging and has been applied in many computer- communication schemes to various degrees of success. The application of packet switching techniques to radio communication (both satellite and ground radio channels), which is a multi-access broadcast medium, provides a solution.

In the subarea of multiple access schemes for networks that include broadcast (and particularly satellite) links a great deal of work has been done in inventing and analyzing strategies and protocols for the shared use of a common channel by geographically separated users. The problems of choosing the optimum access protocol (in the sense of minimizing both average and maximum delays per message for a given throughput) have not been formulated yet.

The basic goal of this paper is to develop control schemes that can be employed when using a geostationary satellite channel for intercommunications between a set of geographically distributed nodes and, more importantly, modeling and analysis of such schemes. Although many time-division multiplexed schemes have been proposed, very few of the schemes have been modeled analytically. In this paper, we develop and analyze a dynamic reservation-based multiple access packet switching technique, which minimizes both average and maximum delays and maximizes traffic throughput. The analysis is based on a combination of two Markov chain model; one Markov chain describes the status of the buffer contents of a typical user, we refer to it as the User Markov Chain and one that describes the status of all the users of the channel, we refer to it as the System Markov Chain.

Simulation results have been obtained for the system under various traffic distributions among nodes, and are presented later in the paper. These results show markedly improved delay-throughput characteristics over other existing and proposed multiple access techniques with especially significant performance gains as the traffic imbalance among the users increases. A good agreement between the simulation results and the analytic results is obtained.

For equal traffic distribution among nodes, each node needs approximately two (2) slots at most to transmit packets in a time frame to achieve the best performance. It is found that the average number of frame size is approximately 1 slot per node at low throughput and less than 2 slots per node at high throughput. In other words, the knowledge of the second preceeding reservation vector for a node is not necessary to have two slots at most in a time frame.

For unequal traffic distribution among nodes, on the other hand, the delay-throughput characteristic is improved by assigning variable slots to the nodes in a time frame. The knowledge of preceding reservation vectors is, therefore, necessary to assign variable slots to a node in a time frame. Optimum values of variable slots to be assigned to the nodes are obtained for unequal traffic among nodes in which the arrival rate of packets for one node is eight times higher than that of other nodes. However, these values will depend on the traffic distribution among nodes. Further analysis of these should be made.

In Section 2.0, we examine several existing and proposed satellite communication packet switching schemes. A new reservation multiple access scheme is then presented.

In Section 3.0, this proposed scheme is modeled and analyzed in a queuing theoretic framework. A numerical solution to the mathematical model is obtained. Steady-State System performance parameters, such as average queue sizes and waiting times which are useful in system design, are obtained.

In Section 4.0, a FORTRAN simulation model is developed, and a comparison is made between the analytical solution and the simulated performance. A good agreement between these two is obtained. The simulation results are compared with other existing and proposed satellite schemes and show markedly improved delay-throughput characteristics over the others. Simulation results are also obtained for the system using different arrival rates of two classes of traffic under various loads and node distributions. These results are presented later in this section.

In Section 5.0, conclusions and suggestions for further work are presented.

2.0 PACKET SWITCHING TECHNIQUES FOR SATELLITES

2.1 Background

Several techniques have been previously proposed for using a satellite channel in a packet-switching data network in a way which allows all stations to dynamically share the channel capacity. There is a variety of ways[1] allocating time slots to the nodes, such as fixed-assignments, random access, reservation-techniques, etc. The well-known ALOHA[2] and slotted-ALOHA[3] schemes are examples of random access techniques.

Reservation-ALOHA[4] used random-accessing in conjunction with a frame concept and dynamic ownership principle to allow full utilization of the channel capacity. A different reservation approach, described by Roberts,[5] uses a first-come first-served distributed queuing system in conjunction with a random-accessing technique for making reservations.

Binder's technique[6] consists of a dynamic time-assignment system superimposed on a fixed STDM structure. The approach retains the stability and allocation fairness of a fixed STDM while allowing nodes to make use of channel capacity otherwise wasted because of light traffic loads and a non-uniform distribution of traffic among the nodes.

Balgangadhar and Pickholtz[7] discuss a scheme where time is divided into frames, each frame consisting of reservation time slots, preassigned time slots and reservation access time slots. The idea behind this scheme is to make efficient channel utilization while circumventing the delay problem by introducing the pre-assigned slots, which force the frame size to be no smaller than one round-trip delay.

2.2 A Proposed New Reservation Technique

The proposed scheme consists of a dynamic reservation-based time-assignment packet switching technique. In this proposed scheme, time is divided into frames, each frame consisting of reservation time slots, preassigned fixed time slots and reservation-based variable time slots. At the beginning of each frame, there are M small slots (M is the number of users in the system), each large enough to transmit a reservation from one of the M nodes in the network. Following these small reservation slots, there are M preassigned fixed slots, with each node being permanently allocated one fixed slot per frame. The slot size and the number of nodes, as in Binder's Scheme, is such that the duration of these M fixed slots is at least as long as one round-trip delay to the satellite. At the end of these fixed slots come the reservation based variable slots (V). The number of these variable slots in each frame depends on the reservation vectors sent by the nodes at the beginning of the frames and the algorithm described in the following discussion. The idea behind this scheme is to make efficient channel utilization (hence, the asynchronous variable slots) but circumvent the delay problem by introducing the fixed slots, forcing the frame size to be no smaller than one round-trip delay. One major advantage of this scheme is that the reservation time is small enough to accommodate two bits of reservation vector for each node and thus a very small percentage of the total frame time, which is not true for other existing schemes. Figure 2.1 illustrates the frame structure and time-slot allocation.

The reservation vector is sent by each node as follows: The nodes examine the buffer contents (number of packets opened) just prior to sending the reservation information, subtract one from it (since they know that they will get one fixed slot in the frame) and sends two bits (0,0) (or only 0 in this case) or (0,1) or (1,0) or (1,1) into the two reservation slots assigned to it. The (0,0) vector represents the situation where the station does not have any packet for transmission, the (0,1) vector represents the station having only one packet to transmit, the (1,0) vector represents the station having only two packets to transmit, and the (1,1) vector represents the station having more than two packets to transmit. The number of variable slots assigned to each station in a time frame will be determined by the following algorithm:

A. There will be no time slot allotted for the station which has sent a (0,0) vector (or only '0' in this case).

B. There will be one time slot allotted for transmission for the station which has sent a (0,1) vector.

C. There will be two time slots allotted for transmission for the station which has sent a (1,0) vector.

D. The station which has sent a (1,1) vector will be allotted time slots (equal to or more than two) which will depend on its prior reservation vectors as follows:

   1. P (which is equal to or more than two) time slots will be reserved for transmission if the first preceding reservation vector is (0,0), or (0,1) or (1,0).
   2. Q (which is equal to or more than P) time slots will be reserved for transmission if the first preceding vector is also (1,1) but the second preceding vector is (0,0) or (0,1) or (1,0).
   3. R (which is equal to or more than Q) time slots will be reserved for transmission if the preceding two vectors are both (1,1).

The above algorithm is explained in Table 2.1.

Immediately, after all the nodes have transmitted their reservation, each node transmits (if it has any packets in its buffer), sequentially, one packet on the one fixed slot assigned to it. Since

Table 2.1

Algorithm for Slot Assignment

RESERVATION VECTORS SENT BY EACH NODE AT THE BEGINNING OF A FRAME			NO OF RESERVATION BASED VARIABLE SLOTS (V) ASSIGNED TO EACH NODE IN A TIME FRAME
PRESENT VECTOR	FIRST PRECEDING VECTOR	SECOND PRECEDING VECTOR	
(0,0)	—	—	0
(0,1)	—	—	1
(1,0)	—	—	2
(1,1)	(0,0) OR (0,1) OR (1,0)	—	P
(1,1)	(1,1)	(0,0) OR (0,1) OR (1,0)	Q≥P
(1,1)	(1,1)	(1,1)	R≥Q

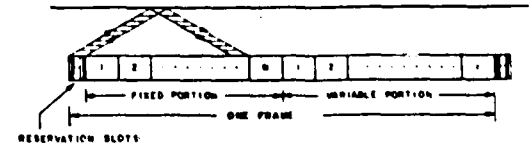

Figure 2.1a. Frame structure of proposed scheme.

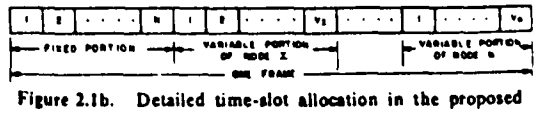

Figure 2.1b. Detailed time-slot allocation in the proposed scheme.

(NOTE: IN THE MATHEMATICAL MODEL, THE SMALL SEGMENTS AT THE BEGINNING OF A FRAME, WHERE THE RESERVATION VECTORS ARE SENT BY THE NODES, ARE ASSUMED TO BE OF ZERO DURATION.)

the duration of the M fixed slots is longer than a round-trip delay, by the end of the fixed slots all the nodes will have received the information for the variable slots assigned to them. Accordingly, each node will transmit its assigned packets, sequentially, in the variable portion of the time frame.

It is to be noted that the slot allocation is highly asymmetrical with regard to the terminals. It is intuitively obvious that the packets in station n have to wait longer than the packets of station (n-1) to get transmitted. To overcome this problem, the assignment of the slots can be done in a cyclic order: in frame (j), the sequence of slot allocations is (j,2,...,M); in frame (j+1), the sequence is changed to (2,3,...,M,1), and so forth; in frame (j+M+1), the sequence is again (1,2,...,M). In such a TDMA based reservation slot the *reservation minipackets* are quite short, because they would not have to carry identity and synchronization information.

The length of the frame is a random variable and depends on the number of users requesting transmission at the beginning of the frame. The mathematical model in section 4 is centered primarily around *the imbedded Markov chain*, imbedded at the special epochs which are the beginnings of the frames. The service order within the frame has no effect on the state of the system at these epochs. But the service order does affect the waiting time distribution for the packets queued at the terminals.

3.0 A MATHEMATICAL MODEL OF THE PROPOSED SCHEME

3.1 Introduction

The proposed system is a non-standard multi-queuing single-server queuing system. Multiqueues attended by a single-server have received a good deal of attention in the queuing theory literature.[8-11] What distinguishes the proposed system is primarily the service discipline.

Chu and Konheim[12] have developed a unified mathematical model for the analysis of synchronous TDM, the asynchronous TDM, and the "Hub polling" techniques. Specifically, they assume that the arrival pattern of packets at the stations is Poisson and, using a generating function approach, have developed equations leading to the queue size distributions of the buffers at the model and the waiting times experienced by the packet.

It is to be noted that the service time of a packet is dependent on the status of the remaining queues. If we let n_k represent the contents of the input buffer of the kth user, then a complete description of all M users requires the specification of the joint probability distribution $P(n_1,n_2,...,n_M)$. The determination of these probabilities is very complex, if not impossible and demands the solution of a large number of sets of equations. Fayolle and Iasnogorodski[13] showed the limitation of this direct approach. They considered the simple example of two parallel M/M/1 queuing systems with infinite capacities and with service rate for each system depending on the status of the other system's queue. They showed that the generating function F(x, y), corresponding to the joint probability of the two queue sizes can be continued as a meromorphic function to the whole complex plane. Using the theory of analytic continuation they reduced the problem to a Rieman-Hilbert problem and were able to obtain a closed form for F(x, y) which includes several elliptical integrals of the third kind. Extension of their analysis to the case of more than two users and to our problem seems unfeasible.

Leibowitz[14] presents an approximate method of treating multiqueue systems. He studied the case of N queues with a single server, in which the queues are served in cyclic order. He used the following argument to derived the probability distribution of the queues; if the server meets the same probability distribution of the number of customers, say P_a, at each of the queues on one cycle of the system, then the same distribution must meet him when he returns to the same queue.

Hashida[15] used Leibowitz's approximate approach in the analysis of multiqueue systems where the server serves, at most, K customers that were waiting when he arrived at a queue. Also in Reference 7, the authors used Leibowitz's approximation along with an independence assumption to obtain the queue size distribution for each user.

Besides introducing a new reservation scheme, we consider that the main contribution of this dissertation, is the mathematical model presented here to analyze interacting buffered terminals. The model, as mentioned earlier, is basically a combination of two Markov chains imbedded at the beginning of each frame; one Markov chain that describes the state of the user, referred to as the User Markov Chain and another Markov chain that describes the state of all the users in the systems, referred to as the System Markov Chain. T. T. Saadawi and A. Ephremides[16] used a similar approach to analyze the reservation scheme where they considered that each station transmits maximum one packet in a time frame.

In Section 3.2.1 we describe the System Markov Chain while in Section 3.2.2 the User Markov Chain is obtained. For the purpose of comparison with simulation results, the mathematical model is studied here for the reservation scheme where each station is allowed to transmit maximum two packets in a time frame, i.e., $P = Q = R = 1$. For other values of P, Q and R we will have similar analyses for the system.

3.2 The User Model

The system consists of M terminals, each of which has an infinite buffer. The arrival process at each of the M terminals is assumed to be a Bernoulli process with rate σ, i.e., the probability of arrival of a (single packet) message at any terminal in each slot is σ. The total arrival rate is, therefore, $M\sigma$ packets per slot, which is equal to the throughput rate. Most other studies of multiple access protocols have assumed a Poisson arrival process. The Bernoulli process is a discrete-time analog of the Poisson process, which is well-suited to the discrete time slot structure. The user may be in one of two states: an idle user, where his buffer is empty; or an active user, where his buffer is not empty.

As shown in Fig. 3.1 whenever the user has the packet(s) in his buffer, it sends a reservation request at the beginning of the frame*, the preassigned packet is transmitted to the fixed time slot and the reservation-based packet(s) are transmitted to the assigned slot(s) of the variable portion of the frame after it receives messages from the satellite at the end of a round-trip delay.

We need the following definitions;

π_i = steady state probability of having i packets in the buffer at the beginning of a frame.

Hence

π_0 = probability of an empty buffer

= probability of an idle user

$1 - \pi_0$ = probability of an active user

* In the mathematical model, the small segments at the beginning of a frame, where the reservation vectors are sent by the nodes, are assumed to be of zero duration.

3.2.1 The System Markov Chain The state of the system is described by the number of users requesting transmission at the beginning of the frame. Let us first define the following:

j_1 = number of users having only one packet requesting transmission at the beginning of a frame

j_2 = number of users having more than one packet requesting transmission at the beginning of a frame

L_{j_1,j_2} = length of a frame resulting from requests for transmission of j_1 and j_2 users at its beginning

= $(M+j_2)$ slots, where M is equal to or greater than one round-trip delay in time slots

P_{j_1,j_2} = steady state probability of having j_1 and j_2 users requesting transmission at the beginning of a frame

σ_{j_0} = probability of an idle user generating no packet during the frame of length L_{j_1,j_2}

$$= \binom{M+j_2}{0}(1-\sigma)^{M+j_2} \tag{3.1a}$$

σ_{j_1} = probability of an idle user generating one packet during the frame of length L_{j_1,j_2}

$$= \binom{M+j_2}{1}\sigma\,(1-\sigma)^{M+j_2-1} \tag{3.1b}$$

σ_{j_2} = probability of an idle user generating more than one packet during the frame of length L_{j_1,j_2}

$$= 1-\sigma_{j_0}-\sigma_{j_1} \tag{3.2}$$

F_0 = probability of having two packets only in the buffer at the beginning of a frame given user is active and having more than one packet

$$= \frac{\pi_2}{1-\pi_0-\pi_1} \tag{3.3}$$

F_1 = probability of having three packets in the buffer at the beginning of a frame given user is active and having more than two packets

$$= \frac{\pi_3}{1-\pi_0-\pi_1-\pi_2} \tag{3.4}$$

K_1 = number of users having one packet remain active out of j_2 users requesting transmission at the beginning of a frame

K_2 = number of users having more than one packet remain active out of j_2 users requesting transmission at the beginning of a frame

$M - K$ = number of idle users at the beginning of a frame where $K = K_1 + K_2$

$C(K_1,K_2,j_2)$ = probability [K_1 users having one packet and K_2 users having more than one packet remain active out of j_2 users requesting transmission at the beginning of a frame]

$$= \binom{j_2}{K_1+K_2}(1-F_0)^{K_1+K_2}(F_0)^{j_2-K_1-K_2}\cdot\binom{K_1+K_2}{K_2}(1-F_1)^{K_2}F_1^{K_1} \tag{3.5}$$

In the above binomial distribution, it is assumed that the probability a user remains active is independent from the state of the other users. A similar assumption has been stated and justified in Reference 15, where the case of a single server serving N lines in cyclic order is studied. In that analysis, the number of lines is assumed constant during a cycle and is determined by a binomial distribution.

$q(i_1,i_2,K_1,K_2,j_2)$ = probability [i_1 idle users receive one packet and i_2 idle users receive more than one packet out of (M-K) idle users during a frame given $K(=K_1+K_2)$ users remain active out of j_2 users requesting transmission at the beginning of a frame]

$$= \binom{M-K}{i_1+i_2-K}\cdot\left(1-\sigma_{j_0}\right)^{i_1+i_2-k}\cdot\left(\sigma_{j_0}\right)^{M-i_1-i_2}$$
$$\times\binom{i_1+i_2-K}{i_2-K_2}\cdot\left(\frac{1-\sigma_{j_0}-\sigma_{j_1}}{1-\sigma_{j_0}}\right)^{i_2-K_2}\cdot\left(\frac{\sigma_{j_1}}{1-\sigma_{j_0}}\right)^{i_1-K_1} \tag{3.6}$$

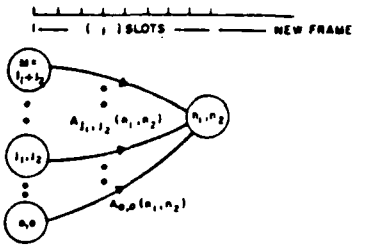

Figure 3.1a. System Markov Chain.

The System Markov Chain is illustrated in Fig. 3.1a. Therefore, P_{n_1,n_2}, the steady state probability of n_1 users having one packet and n_2 users having more than one packet, requesting transmission at the beginning of the frame is given by

$$P_{n_1,n_2} = \sum_{j_1=0}^{M}\sum_{j_2=0}^{M-j_1} A_{j_1,j_2}(n_1,n_2)P_{j_1,j_2} \tag{3.7}$$

where $A_{j_1,j_2}(n_1,n_2)$ is the transition probability from state (j_1,j_2) to state (n_1,n_2) and is given by

$$A_{j_1,j_2}(n_1,n_2) = \sum_{k_2=0}^{\min(j_2,n_2)}\sum_{K_1=0}^{\min(j_1-K_2,n_2)} Pr[K=(K_1+K_2) \text{ users remain active, } (n_1-K_1) \text{ idle users receive one packet only, and } (n_2-K_2) \text{ idle users receive more than one packet during a frame, given } j(=j_1+j_2) \text{ users request transmission at the beginning of a frame.}]$$

$$= \begin{cases} \sum_{k_2=0}^{\min(j_2,n_2)}\sum_{K_1=0}^{\min(j_1-K_2,n_2)} q(n_1-K_1,n_2-K_2,K_1,K_2,j_2)C(K_1,K_2,j_2) & \text{for } 1 \le j = j_1+j_2 \le M, \text{ and } 0 \le n = n_1+n_2 \le M \\ \binom{M}{n_1}\sigma^{n_1}(1-\sigma)^{M-n_1}, & \text{for } j=0, n_2=0, \text{ and } 0 \le n = n_1+n_2 \le M \end{cases} \tag{3.8}$$

3.2.2 The User Markov Chain The state of the user is described by the number of packets in the buffer at the beginning of the frame.
Let

n = number of packets in the buffer at the beginning of a frame

π_n = steady state probability of having n packets in the buffer at the beginning of a frame

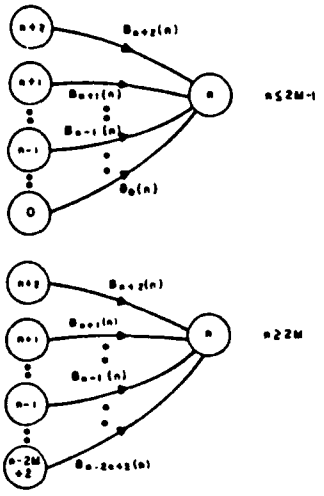

Figure 3.1b. User Markov Chain.

In Fig. 3.1.b, we show the User Markov Chain. Note that $B_{n-i}(n)$ is the transition probability from state (n-i) to state (n). Let us now determine these transition probabilities. Let

$g(i,L_{j_1j_2})$ = Pr[i packets arrive during the frame of length $L_{j_1j_2}$]

$$= \binom{M+j_2}{i}\sigma^i(1-\sigma)^{M+j_2-i} \tag{3.9}$$

$B_{n+2}(n)$ = Pr[two packets leave and no packet arrives during the frame of length $L_{j_1j_2}$]

$$= \sum_{j_2=1}^{M}\sum_{j_1=0}^{M-j_2} g(0,L_{j_1j_2})P_{j_1j_2}\Big/\left[1-\sum_{j_1=0}^{M}P_{j_1,0}\right], \quad n = 0,1,2\ldots \tag{3.10}$$

Similarly,

$B_{n+1}(n)$ = Pr[two packets leave and one packet arrives during the frame of length $L_{j_1j_2}$]

$$= \sum_{j_2=1}^{M}\sum_{j_1=0}^{M-j_2} g(1,L_{j_1j_2})P_{j_1j_2}\Big/\left[1-\sum_{j_1=0}^{M}P_{j_1,0}\right], \quad n = 1,2,\ldots \tag{3.11}$$

and

$B_1(0)$ = Pr[one packet leaves and no packet arrives during the frame of length $L_{j_1j_2}$]

$$= \sum_{j_1=1}^{M}\sum_{j_2=0}^{M-j_1} g(0,L_{j_1j_2})P_{j_1j_2}\Big/\left[1-\sum_{j_2=0}^{M}P_{0j_2}\right] \tag{3.12}$$

Similarly,

$B_n(n)$ = Pr[two packets leave and two packets arrive during the frame of length $L_{j_1j_2}$]

$$= \sum_{j_2=1}^{M}\sum_{j_1=0}^{M-j_2} g(2,L_{j_1j_2})P_{j_1j_2}\Big/\left[1-\sum_{j_1=0}^{M}P_{j_1,0}\right], \quad n = 2,3,\ldots \tag{3.13}$$

$B_1(1)$ = Pr[one packet leaves and one packet arrives during the frame of length $L_{j_1j_2}$]

$$= \sum_{j_1=1}^{M}\sum_{j_2=0}^{M-j_1} g\left(1,L_{j_1j_2}\right)P_{j_1j_2}\Big/\left[1-\sum_{j_2=0}^{M}P_{0j_2}\right] \tag{3.14}$$

and

$B_0(0)$ = Pr[no packet arrives during the frame of length of $L_{j_1j_2}$]

$$= \sum_{j_2=0}^{M-1}\sum_{j_1=0}^{M-1-j_2} g(0,L_{j_1j_2})P_{j_1j_2}\Big/\left[1-\sum_{j_2=0}^{M}P_{M-j_2j_2}\right] \tag{3.15}$$

Similarly,

$B_{n-i}(n)$ = Pr[two packets leave and (i+2) packets arrive during the frame of length $L_{j_1j_2}$]

$$= \sum_{j_2=1}^{M}\sum_{j_1=0}^{M-j_2} g\left(i+2,L_{j_1j_2}\right)P_{j_1j_2}\Big/\left[1-\sum_{j_1=0}^{M}P_{j_1,0}\right], \tag{3.16}$$

$$n = 3,4,\ldots$$

$$i = 1,\min(n-2,2M-2)$$

$B_i(n)$ = Pr[n packets arrive during the frame of length $L_{j_1j_2}$]

$$= \sum_{j_1=1}^{M}\sum_{j_2=0}^{M-j_1} g(n,L_{j_1j_2})P_{j_1j_2}\Big/\left[1-\sum_{j_2=0}^{M}P_{0j_2}\right], \tag{3.17}$$

$$n = 2,\ldots, 2M-1$$

and

$B_0(n)$ = Pr [n packets arrive during the frame of length $L_{j_1j_2}$]

$$= \sum_{j_2=0}^{M-1}\sum_{j_1=0}^{M-1-j_2} g(n,L_{j_1j_2})P_{j_1j_2}\Big/\left[1-\sum_{j_2=0}^{M}P_{M-j_2j_1}\right], \tag{3.18}$$

$$n = 1,\ldots,2M-1$$

We now can have a numerical solution for $\pi_n, n = 0,1,2,3,\ldots$ as described below.

3.2.3 Numerical Solutions Equations (3.1) through (3.6) provide the values of the quantities that were needed in order to solve the equations (3.7). However, some of these quantities are not expressed in terms of only the system parameter $M\sigma$, but, in terms of F_0 and F_1 which are function of π_0, π_1, π_2 and π_3, which in turn are expressed in terms of $[P_{n_1,n_2}]$. Thus, in total, we have a set of simultaneous, coupled non-linear equations in π_n and $[P_{n_1,n_2}]$. In

Fig. 3.2, we show the flow chart to solve for these values. We start with an initial value for F_0 and F_1, then solve equation (3.7) in $[P_{a_1,a_2}]$. Using the values of P_{a_1,a_2} we then determine the steady state probabilities π_a which satisfy the following matrix equation:

$$\pi_a = \pi_a B \tag{3.19}$$

where B is the transition probability matrix with elements $b_{ij} = B(i,j)$.

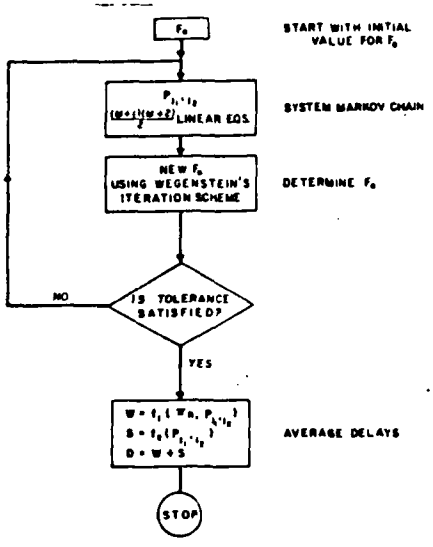

Figure 3.2. Flow chart to determine average delays for the proposed scheme.

The solution of n equations in n unknowns in equation (3.19) is straightforward using matrix inversion* and equations (3.9) through (3.18). Then, using Wegestein's iteration scheme[17], we obtain the new F_0 and F_1 and repeat it until it converges to a solution for π_a. A FORTRAN program was written to solve π_a. The analytical results are compared with the simulation results in the next chapter.

3.2.4 Delay Analysis The average total delay per packet, D, is the sum of the average waiting time in the buffer, W, plus the average time from the beginning of the frame till the packet is transmitted in its assigned slot. We refer to the latter as the service time, S. Hence,

$$D = W + S \tag{3.20}$$

Using Little's Result,[18] we can write W as;

$$W = \frac{Q}{\sigma} \tag{3.21}$$

where,

Q = Average Queue Size

$$= \sum_{n=0}^{\infty} n \cdot \pi_n$$

Assuming cyclic assignment discussed earlier in Section 2.2, the average service time is given by

$$S = \pi_1 \cdot \frac{M}{2} \frac{(1-\pi_0-\pi_1)}{2} \left[\frac{M}{2} + \frac{1}{2}(S_f+M)\right] \tag{3.22}$$

* When n is very large, it might be difficult to invert the matrix B. In that case, other standard methods should be used to solve equation (3.19).

The average frame size, another parameter of our interest, is given by

$$S_f = \sum_{j_1=0}^{M} \sum_{j_2=0}^{M-j_1} (M+j_2) P_{j_1,j_2} \tag{3.23}$$

Finally, we define stability as, "The system is said to be stable if the steady state probability of having a finite number of packets in the buffer exists and is non-zero."

4.0 SIMULATION RESULTS

A FORTRAN *simulation program* was written to find the throughput-delay performance of the proposed model described in the last chapter, under the following traffic conditions:

- Equal traffic distribution among nodes *in which traffic* was equally distributed among the nodes
- *Unequal traffic distribution among* nodes in which the arrival rate of packets for one "big" node is higher than that of other "small" nodes.

It will be assumed that the satellite channel *is a highly reliable data* link, in which noise may be neglected (a typical value for the capacity of the channel is 50,000 bits/sec). Packets of fixed length are used and time is slotted so that one packet is transmitted per slot. The slot size and the number of nodes is such that the duration of these M fixed slots is one round-trip delay to the satellite i.e., .27 sec.

4.1 Equal Traffic Among Nodes

In this case, the arrival process at each of the M terminals is assumed to be a Bernoulli process with rate σ, i.e., the probability of arrival of a (single packet) message at any terminal in each slot is σ. The total arrival rate is, therefore, M σ packets per slot, *which is same as the system throughput* or the system utilization factor. The Burnoulli process is well suited to the discrete time slot structure and is a discrete-time analog of the Poisson process. For varying M, the number of nodes and $M\sigma$, the system *utilization* factor, the following statistics have been collected from the simulation model. In a finite run-length simulation, the statistics are an arithmetic average over the M queues. Also, a comparison between these system performance parameters obtained by the mathematical model and those obtained by the simulation model has been made for M = 4 for the situation where each node is allowed to transmit maximum two packets in a time frame (i.e., P = Q = R = 1) for

(1) Mean and standard deviation of the queue sizes at the nodes at the beginning of a frame (Table 4.1).

(2) Mean and standard deviation of the frame length expressed in number of time slots (Table 4.2).

(3) Average and maximum delay for a packet at various loads (Figures 4.2 and 4.3). The analytical result for the average delay for M=4 and P=Q=R=1 is also compared with the simulation result in Figure 4.2.

Figure 4.1 compares the average delay for the proposed scheme with that for other protocols discussed in Section 2.0. It shows that the proposed scheme gives a significant improvement for delay over the other reservation schemes. It is also seen from Figures (4.2 and 4.3) that, for the traffic situation discussed above, each node needs approximately two (2) slots at most to transmit packets in a time frame to achieve the best performance. This result also agrees with the results of Balgangadhar and Pickholtz's scheme[7] where they have found out that the average number of frame size is approximately 1 slot per node at low throughput and less than 2 slots per node at high throughput (See Table 4.2). In other words,

the knowledge of the second preceding reservation vector for a node is not necessary to have two slots at most in a time frame.

The agreement between the analytical results and the simulation results is seen to be excellent over a wide range of $M\sigma$, the system utilization factor. For example, for M = 4 and the utilization factor of 0.4, the mean queue size at the epochs and the mean frame size, computed analytically, are 0.43 and 4.24 respectively (see Tables 4.1 and 4.2). For the same value of $M\sigma$, simulation results give the mean queue size at the epoch as 0.44 and the mean queue size at the epochs as 0.44 and the mean frame size as 4.29. The disagreement between these and the analytical values is about 2 percent and 1 percent, respectively.

The agreement between the analytical and the simulation results (Figure 4.2) is seen to be particularly good for low values of system utilization factor. It is difficult to argue why the independence assumption made in the mathematical analysis should hold for low values of the utilization factor. On the other hand, for large values of M, one might argue that because of the large number of queues, the different queues become decoupled and hence make the independence assumption valid. But further analysis of this should be made.

Table 4.1

Comparison Of Computed (Analytical) and Simulated Values for the Mean and Standard Deviation (In Parenthesis, Below the Mean) of Queue Sizes at the Beginning of a Frame, for Various Values of N and $N\sigma$ (the Number of Nodes and the System Utilization Factor, Respectively)

	$N\sigma$ = System Utilization							
	0.1	0.2	0.3	0.4	0.5	0.6	0.7	0.8
Analytical	.1	.2	.31	.43	.57	.72	.91	1.15
(M = 4)	(.3)	(.45)	(.54)	(.63)	(.7)	(.77)	(.86)	(0.88)
Simulated								
M = 4	.1	.2	.32	.44	.57	.72	.93	1.2
	(.3)	(.45)	(.54)	(.64)	(.72)	(.79)	(.9)	(1.1)
M = 12	.1	.2	.31	.43	.56	.72	.91	1.17
	(.3)	(.45)	(.55)	(.65)	(.75)	(.85)	(.96)	(1.09)
M = 20	.1	.2	.31	.42	.55	.74	.92	1.21
	(.31)	(.44)	(.56)	(.65)	(.74)	(.85)	(.97)	(1.12)

Table 4.2

Comparison Of Computed (Analytical) and Simulated Values for the Mean and Standard Deviation (In Parenthesis, Below the Mean) of Frame Size in Number of Slots, for Various Values of N and $N\sigma$ (the Number of Nodes and the System Utilization Factor, Respectively)

	$N\sigma$ = System Utilization							
	0.1	0.2	0.3	0.4	0.5	0.6	0.7	0.8
Analytical	4.02	4.08	4.13	4.24	4.4	4.6	5.0	5.5
(M = 4)	(.15)	(.3)	(.44)	(.55)	(.73)	(.9)	(.98)	(1.3)
Simulated								
M = 4	4.02	4.08	4.17	4.29	4.47	4.72	5.17	5.91
	(.15)	(.3)	(.45)	(.57)	(.76)	(.93)	(1.22)	(1.69)
M = 12	12.05	12.24	12.5	12.97	13.57	14.45	15.76	17.7
	(.24)	(.49)	(.74)	(1.02)	(1.41)	(1.82)	(2.37)	(3.24)
M = 20	20.08	20.34	20.88	21.59	22.53	24.08	26.09	29.37
	(.28)	(.62)	(.96)	(1.37)	(1.74)	(2.35)	(2.95)	(3.89)

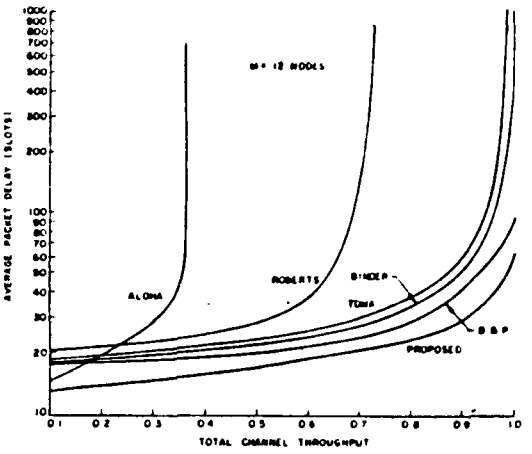

Figure 4.1. Comparison of various schemes (12 nodes): average packet delay vs. throughput.

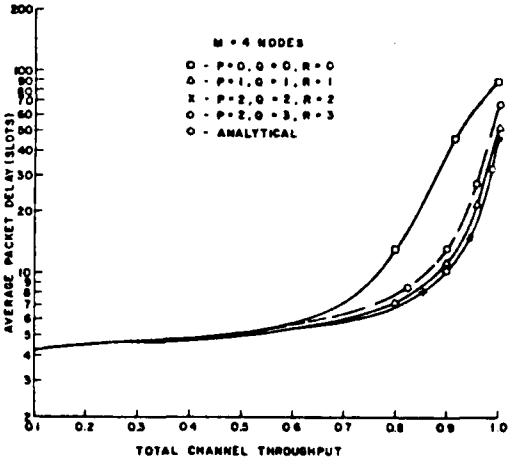

Figure 4.2. Average Packet Delay vs. Throughout (4 Nodes)

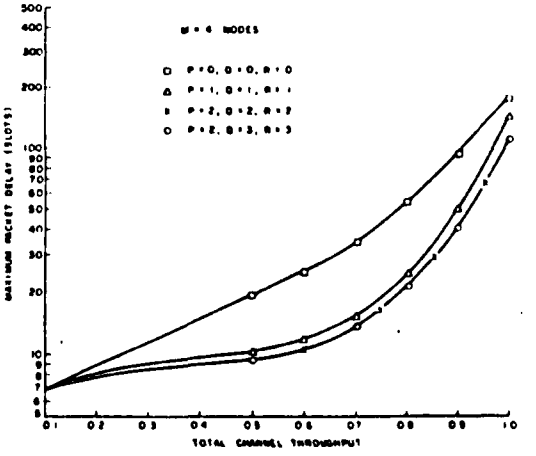

Figure 4.3. Maximum packet delay vs. throughput (4 nodes).

4.2 Unequal Traffic Among Nodes

In this case, it is considered that a "big" node consists of (single packet) messages whose arrival rate (σ_b) is eight times the arrival rate (σ_s) of (single packet) messages at other "small" nodes. Total small node traffic was divided equally among themselves. The total arrival rate is, therefore, $(\sigma_b+(M-1)\sigma_s)$, which is equal to the system throughput.

For varying M, the number of nodes, and the system throughput, the average (Figure 4.4) and maximum (Figure 4.5) delay for a packet at "small" and "big" nodes at various loads have been obtained from the simulation model. It is seen from these figures that by assigning variable slots to the "big" node we improve the average and maximum delay characteristics of the system. The knowledge of preceding reservation vectors, is, therefore, necessary to assign variable slots to a node in a time frame.

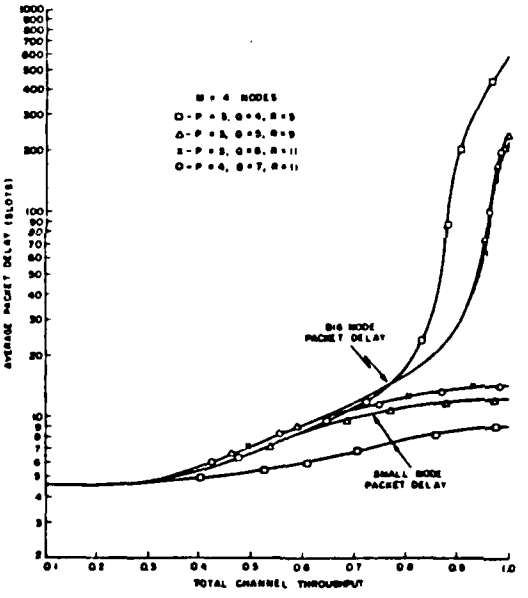

Figure 4.4. Average packet delay vs. throughput (4 nodes) packet arrival rate of 1 big node eight times higher than that of each of 3 small nodes.

The same algorithm for reservation of slots is applied to all nodes (Table 3.1). It is seen that the best performance is obtained for P=3, Q=6, and R=11 for the traffic situation discussed above. However, optimum values of P, Q and R and their relationships will depend on the ratio of the arrival rates at "big" and "small" nodes. Further analysis of these should be made. It is important to note here that an adaptive algorithm (similar to the algorithm discussed in this dissertation), where a node asking for more than two slots [by sending reservation vector (1.1)] is assigned some additional slots in addition to the slots assigned to it in the previous frame, is also studied and found not suitable in this case.

5.0 CONCLUSIONS AND SUGGESTIONS FOR FURTHER WORK

The field of large data networks has seen a tremendous growth in the last decade. In the subarea of multiple access schemes for neworks that include broadcast (and particularly satellite) links, many time-division multiplexed schemes have been proposed for the shared use of a common channel by geographically separated

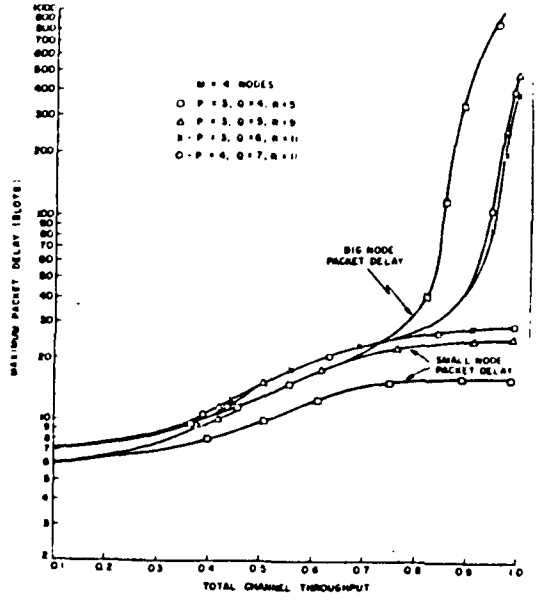

Figure 4.5. Maximum packet delay vs. throughput (4 nodes) packet arrival rate of 1 big node eight times higher than that of each of 3 small nodes.

users, but very few of the schemes have been modeled analytically. Also, the problems of choosing the optimum access protocol (in the sense of minimizing average delay per message for a given throughput) have not been formulated yet. In this paper we develop optimum control schemes that can be employed when using a geostationary satellite channel for intercommunications between a set of geographically distributed nodes and, more importantly, the modeling and analysis of such schemes.

Several existing and proposed satellite multiple access techniques are examined. In this dissertation, we develop and analyze a dynamic reservation-based multiple access packet switching technique, which minimizes both average and maximum delays and maximizes traffic throughput. The analysis is based on a combination of two Markov chain model; one Markov chain describes the status of the buffer contents of a typical user, we refer to it as the User Markov Chain and one that describes the status of all the users of the channel, we refer to it as the System Markov Chain.

Simulation results have been obtained under various traffic distributions among nodes. These results show markedly improved delay-throughput characteristics over other existing and proposed multiple access techniques with especially significant performance gains at high traffic and also as the traffic imbalance among the users increases. A good agreement between the simulation results and the analytical results is obtained.

For equal traffic distribution among nodes, each node needs approximately two (2) slots at most to transmit packets in a time frame to achieve the best performance. It is found that the average number of frame size is approximately 1 slot per node at low throughput and less than 2 slots per node at high throughput. In other words, the knowledge of the second preceding reservation vector for a node is not necessary to assign two slots at most in a time frame.

For unequal traffic distribution among nodes, on the other hand, the delay-throughput characteristic is improved by assigning variable slots to the nodes, in a time frame. The knowledge of preceding reservation vectors is, therefore, necessary to assign variable slots to a node in a time frame. The optimum values of variable slots to be assigned to the nodes are obtained for unequal traffic among nodes in which the arrival rate of packets for one node is eight times higher than that of other nodes. However, these values will depend on the traffic distribution among nodes. Further analysis of these should be made.

The proposed packet switching technique based upon dynamic reservation multiple access concept may also be applied to the use of ground radio channels for terminal-computer communications. In this case the analysis will be the same, except the time frame will consist of only reservation-based variable time slots but no preassigned fixed slots because there is no round-trip delay.

REFERENCES

1. Tobagi, F. A., "Multi-access Protocols in Packet Communication Systems," *IEEE Trans. Commun.*, Vol. 28, April 1980, pp. 468-488.
2. Abramson, N., "Packet Switching with Satellites," *AFIPS Conf. Proc.*, Vol. 42, June 1973.
3. Kleinrock, L. and Lam, S., "Packet-Switching in a Slotted Satellite Channel," *AFIPS Conf. Proc.*, Vol. 42, June 1973.
4. Crowther, W. R., Rettbert, R., Walden, D., Ornstein, S., and Heart, F., "A System for Broadcast Communication, Reservation-ALOHA," *Proc. 6th Hawaii Int. Syst. Sci. Conf.*, Jan. 1973.
5. Roberts, L., "Dynamic Allocation of Satellite Capacity Through Packet Reservation," *Proc. AFIPS Conf.*, Vol. 42, June 1973.
6. Binder, R., "A Dynamic Packet Switching System for Satellite Broadcast Channels," *Proc. ICC'75*, San Francisco, CA, June 1975.
7. Balgangadhar, M. M. and Pickholtz, L., "Analysis of Reservation Multiple Access Technique for Data Transmission Via Satellites", *IEEE Trans. Commun.*, Vol. COM-27, Oct. 1979.
8. Spragins, John D., "Loop Transmission Systems-Mean Value Analysis," *IEEE Trans. Commun.*, Vol. COM-20, No. 3, June 1972, pp. 592-602.
9. Konheim, A. G. & Meister, "Service in a Loop System," *JACM*, Vol. 19, No. 1, Jan. 1972, pp. 92-108.
10. Konheim, A. G., "Service Epochs in a Loop System," *Symposium on Computers and Communications Networks and Teletraffic*, Polytechnic Institute of Brooklyn, April 4-6, 1972, pp. 125-143.
11. Spragins, John D., "Loops Used for Data Collection," *Symposium on Computers and Communications Networks and Teletraffic*, Polytechnic Institute of Brooklyn, April 4-6, 1972, pp. 59-76.
12. Chu, W. W. and Konheim, A. G., "On the Analysis and Modeling of a Class of Computer Communication Systems," *IEEE Trans. Commun.* Vol. COM-20, No. 3, June 1972, pp. 645-660.
13. Fayolle, G. and Iasnogorodski, "Two Coupled Processors: The Reduction to a Riemann-Hilbert Problem" *Zeilschrififur Wahrscheinlichkeits Theory and Verwandte Gebiete*, by Springer-Verlag 1979.
14. Leibowitz, M. A., "An Approximate Method for Treating a Class of Multiqueue Problems," *IBM Journal of Research and Development*, Vol. 5, No. 3, July 1961, pp. 204-209.
15. Hashida, O., "Analysis of Multiqueue," *Review of the Electrical Comm. Lab.*, Nippon Telegraph and Telephone Public Corporation, Vol. 20, No. 3-4, March-April, 1972.
16. Saadawi, T. N. and Ephremides, A., "Stability and Optimization of Slotted ALOHA with a Finite Number of Buffered Users", *19th CDC Conference*, Albuquerque, New Mexico, Dec., 1980.
17. Lance, G. N., "Numerical Methods for High Speed Computers", *Iliffe*, London, 1960, pp. 134-138.
18. Little, D. C., "A Proof of the Queuing Formula: $L = \lambda W$", *Operations Research*, Vol. 9, 1961, pp. 383-387.

ANALYSIS OF INTERACTING BUFFERED USERS IN SLOTTED ALOHA

by

Tarek N. Saadawi and Donald L. Schilling

City College of New York

ABSTRACT:

This paper analyzes the slotted-ALOHA multiple access scheme for broadcast channels with a finite number of users, each having a buffer of infinite capacity. The analysis is based on the idea presented in (1), of having a two Markov chain model to describe the whole system. The model analyzed in this paper is simpler, gives further insight into the problem of interacting buffered users, and leads to one-dimensional Markov chains.

1. INTRODUCTION

The problem of analyzing random access schemes for a finite number of buffered users is still an open problem.

In most of the previous analysis for random access schemes, (2),(3), (4) and (5), it was assumed that a user can have a maximum of one packet in his buffer. Any packet that is generated, while there is a packet in the buffer, is assumed to be rejected.

Buffering is essential in most practical applications, such as satellite access networks. When buffering is not used, packet rejection is often employed. Packet rejection is costly and represents a drastic means of

flow control.

In this paper, and as a typical example of a random access scheme, we analyze the slotted ALOHA system with a finite number of buffered users. The approach here is similar to the one presented in (1), yet the model presented here is simpler and gives further insight into the problem. The approach is based on modelling the interaction between the competing terminals by a combination of two Markov chains. The key idea behind the interaction is the fact that successful transmission of a packet by a user depends on the status of the other users. Thus it is possible to consider the state of a user (represented by the size of his queue) modeled by an imbedded Markov chain, whose parameters (transition probabilities) depend on the state of the system (basically, the number of users who need service, and those who do not). The latter state is represented by an imbedded Markov chain whose parameters in turn functions of the state of the users. It is possible to obtain sets of coupled equations for the steady state equilibrium distribution of these states. They are solved numerically and curves for the average waiting, service and total delay, are obtained. The model in this paper leads to one-dimensional Markov chains, as opposed to two-dimensional Markov chains obtained in (1).

II THE MODEL

The user terminal is shown in Fig.1. The buffer

has unlimited capacity; time is slotted. Packets are assumed to be of fixed length L, with one time slot equivilant to a packet length. It is assumed also that the sensing of a collision is instantaneous.* The arrival process is modeled as a Bernoulli process with average rate of arrival (or, equivilantly probability of an arrival in a given slot) equal to σ.

The packet of the head-of-line (HOL) in the buffer enters the transmitter, with probability f, and is transmitted. At the same time a replica of the packet remains in the buffer (as HOL). In the case of success, (the terminal is in the unblocked state), the replica packet is discarded and the following packet becomes HOL. In the case of collision, (the terminal is in the blocked state), the replica packet enters the transmitter with probability f, (the same probability by which the HOL packet in the unblocked terminal is transmitted), for retransmission. A packet that arrives at an idle user goes directly to the transmitter without incrementing the buffer content.

Hence, the terminal (or user) can be in one of two states, an idle state or an active state. In the idle state, the terminal is unblocked and the buffer is empty, hence a packet is generated with probability σ and transmitted instantaneously. In the active state, the

---

* Instantaneous sensing of collisions is clearly not possible for satellite channels.

packet (whether it is the HOL packet in an unblocked state or it is the replica packet in the blocked state), is transmitted with probability f.

In the following we describe the user Markov chain and the system Markov chain:

a) The User Markov Chain.

The state of the user is denoted by (i), where i=0,1,2,... indicates the number of packets in the buffer. Let

$\pi_i \triangleq$ steady state probability of the state (i)

and

$$G(z) \triangleq \sum_{i=0}^{\infty} \pi_i z^i \qquad (1)$$

In order to characterize the transition probabilities of the user Markov chain, we need to define the following additional quantities;

r = Prob.[successful transmission/user is active]

q_1 = Prob. [success/user is idle]

$= \sigma q$

where q is the probability of success, assuming a packet has already arrived, given the user is idle. Now, the transition probability of the user Markov chain can be obtained as shown in Fig.2, where:

A = Prob. [no packets arrive to the active terminal and a packet succeeds]

$= (1-\sigma)r$

B = Prob. [no packets arrive and no transmission, or transmission and no success, OR 1 packet arrives and one

success]

$= (1-\sigma)(1-r)+\sigma r$

C = Prob. [one arrival and no transmission, or transmission with failure]

$= \sigma(1-r)$

D = Prob. [1 arrives and collides]

$= \sigma(1-q)$

E = Prob. [no arrivals or 1 arrives and succeeds]

$= (1-\sigma)+\sigma q$

Hence

$$\pi_j = A\pi_{j+1} + B\pi_j + C\pi_{j-1} \qquad j \geq 2 \qquad (2.a)$$

$$\pi_1 = A\pi_2 + B\pi_1 + D\pi_0 \qquad (2.b)$$

$$\pi_0 = A\pi_1 + E\pi_0 \qquad (2.c)$$

Applying Eqn.(1), we get:

$$G(z) = [Az^{-1}+B+Cz]G(z)+[-Az^{-1}+(D-C)z+(E-B)]\,\pi_0 \qquad (3)$$

Differentiating (3) with respect to z and evaluating at z=1, we get

$$\pi_0 = \frac{A-C}{A-C+D}$$

i.e.

$$\pi_0 = \frac{r-\sigma}{r-\sigma(1-q)} \qquad (4)$$

To determine the average buffer size, Q, we differentiate (3) twice and evaluate at z=1; we then obtain $Q = \acute{G}(1)$ as;

$$\frac{A[1-\pi_0]}{A-C}$$

$$= \frac{(1-\sigma)r[1-\pi_0]}{r-\sigma} \qquad (5)$$

b) The System Markov Chain.

The state of the system is described by the number of active users. Let

M $\triangleq$ total number of users in the system

and

n $\triangleq$ number of active users.

Then

M-n = number of idle users

P_n $\triangleq$ steady stat probability of having n active users in the system.

Fig. 3 shows the system Markov chain. To obtain the transition probabilities we need the following definition;

$g_i(n) \triangleq$ Prob.[i out of n blocked users attempt transmission]

$$= \binom{n}{i} f^i (1-f)^{n-i}$$

$q_j(n)$ = Prob.[j out of M-n idle users attempt transmission]

$$= \binom{M-n}{j} \sigma^j (1-\sigma)^{M-n-j}$$

E $\triangleq$ The conditional probability that the buffer size equals unity given that the user is active.

$$= \frac{\pi_1}{1-\pi_o}$$

Referring to Fig.3, we can write P_n as;

$$P_n = q_o(n+1)\,g_1(n+1)\,E\,P_{n+1} + \left\{q_o(n)\,|1-g_1(n)E| + q_1(n)\,g_o(n)\right\} P_n$$

$$+ q_1(n-1)\,|1-g_o(n-1)|\,P_{n-1} + \sum_{i=2}^{n} q_i(n-i)\,P_{n-i}$$

$$1 \le n \le (M-1) \qquad (6.a)$$

$$P_1 = q_o(1)\,g_1(2)\,E\,P_2 + \left\{q_o(1)\,|1-g_1(1)E| + q_1(1)\,g_o(1)\right\} P_1 \qquad (6.b)$$

$$P_o = q_o(1)\,g_1(1)\,E\,P_1 + |q_o(o) + q_1(M)|\,P_o \qquad (6.c)$$

The first term in Eqn. (6.a) is the probability that only the active user, with buffer contents equal to unity, transmits, times the probability the system is in state (n+1). The second term is the probability that either none or at least two active users or one active with buffer contents greater than one transmit, or no active but one idle transmit, times the probability that the system is in state (n). The third term is the probability that one idle user and at least one active user transmits, times the probability of being in state (n-1). The last term is the probability that the i idle users generate and transmit a packet times the probability of being in state (n-i). We then sum over i, $(2 \le i \le n)$.

III. SUCCESS AND COLLISION PROBABILITIES.

The success and collision probabilities are determined as follows;

r = Prob. [successful transmission/user is active]

$$= \frac{f \sum_{n=1}^{M} (1-\sigma)^{M-n} (1-f)^{n-1} P_n}{1 - P_o} \qquad (7)$$

Where the expression in the denominator represents the probability that there is at least one active user. The numerator represents the probability that the active user under consideration attempts transmission times the probability that (M-n) idle users don't receive a packet arrival and (n-1) remaining active users don't attempt transmission times the probability that there are n active users in the system. We sum over all possible values of n. Similarly,

$$q_1 = \frac{\sigma \sum_{n=0}^{M-1} (1-\sigma)^{M-n-1} (1-f)^{n} P_n}{1 - P_M}$$

$$= \sigma q \qquad (8)$$

IV. AVERAGE PACKET DELAY

The average total delay per packet is the sum of the average waiting time in the buffer, W, plus the average time spent from the first attempted transmission to the final successful one, (the service time S).

From Eqn.(5) and applying Little's result, we get

$$W = \frac{Q}{\sigma}$$

$$= \frac{r(1-q)}{r-\sigma q} \qquad (9)$$

To determine the service time S, we note that the average transmission time given that the terminal is either idle and collision occurs or the terminal is active, equals to

$$\sum_{n=1}^{\infty} n(1-r)^{n-1} = \frac{1}{r}$$

When success occurs on the first attempt of transmission, the service time is one packet long. Hence S is given by

$$S = \frac{1}{r}[(1-\pi_o) + \pi_o(1-q)] + 1 \times \pi_o q$$

$$= \frac{1}{r}[1-\pi_o q] + \pi_o q \qquad (10)$$

V. NUMERICAL RESULTS

The set of coupled non-linear equation (2) through (8) were solved numerically to obtain the probabilities $[P_j]$, π_o, π_1, and Q. This has been carried out iteratively as follows: Referring to Fig.4, we start with an initial value for E, the conditional probability that the buffer size equals unity given that the user is active, solve the set of linear simultaneous equations for the system Markov chain and obtain $[P_j]$. With these values of P_j's, we obtain the values of r and q as given by equations (7) and (8) and then using Eqns. (2.c), (4) and a proper iteration scheme, we obtain the new value for E. In Fig.5,

and for M=4, P=0.3, we plot the probabilities P_0, P_1 and P_2 versus throughput. Fig.6 is a plot for the probabilities π_0, π_1, and E versus throughput. Then Fig. 7 is the delay throughput curves. We notice that for M=4 and P=0.3, the maximum throughput is 0.466, while for the model presented in (1) and for the same value of M and P, it is 0.434.

VI. CONCLUSION

This paper considered the problem of interacting buffered terminals in multiple access schemes. The analysis of the slotted-ALOHA multiple access scheme with a finite number of buffered terminals has been presented. The analysis is based on the idea of using two Markov chains (system and user Markov chains) that partially accounts for the interaction between the users. The model here is simple and leads to one-dimensional Markov chains.

REFERENCES

(1) Tarek N. Saadawi and Anthony Ephremides, "Analysis, Stability, and Optimization of slotted ALOHA with a Finite Number of Buffered Users", IEEE Transactions on Automatic Control, June, 1981.

(2) Norman Abramson, "The ALOHA System - Another alternative for Computer Communications" AFIPS Conference Proceedings, 1970 Fall Joint Computer Conference, Vol.37, 281-285.

(3) S.S. Lam, "Packet Switching in a Multi-Access Broadcast

Channel with Applications to Satellite Communication in a Computer Network", Computer Science Department, March 1974 (Ph.D. Dissertation).

(4)L. Kleinrock and Y. Yemini, "An Optimal Adaptive Scheme for Multiple Access Broadcast Communication", International Conference on Communications, Toronto, Canada, June, 1978.

(5) J. Capetanakis, "Tree Algorithms for Packet Broadcast Channels", IEEE Transactions on IT, Vol.25, No.5, Sept. 1979, pp.505-515.

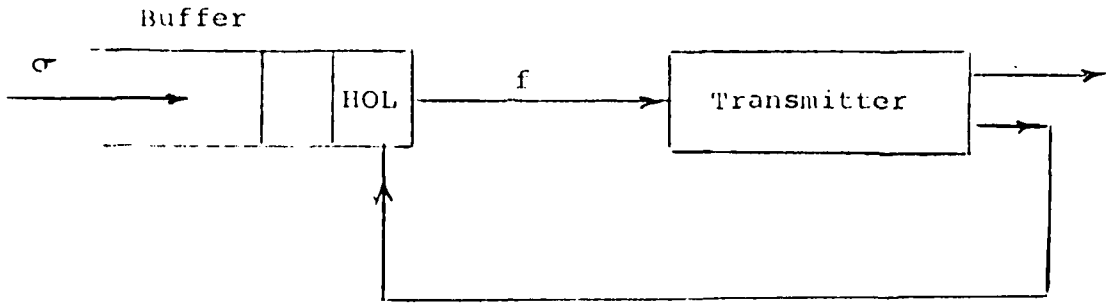

Fig. 1 The User Terminal

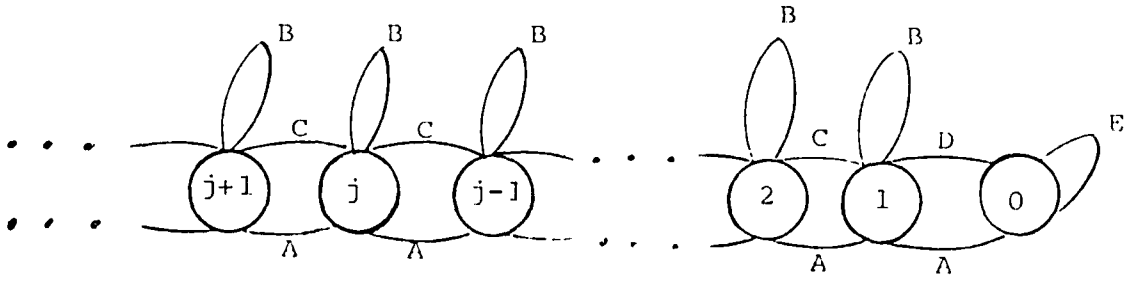

Fig. 2 The User Markov Chain

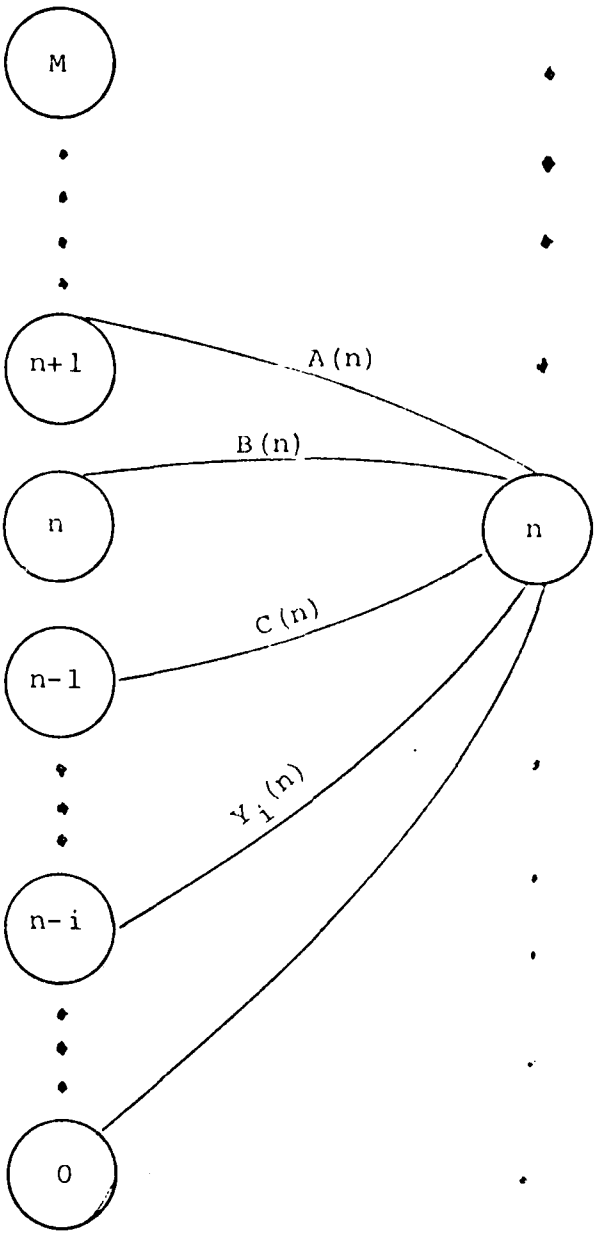

Fig.3 The System Markov Chain

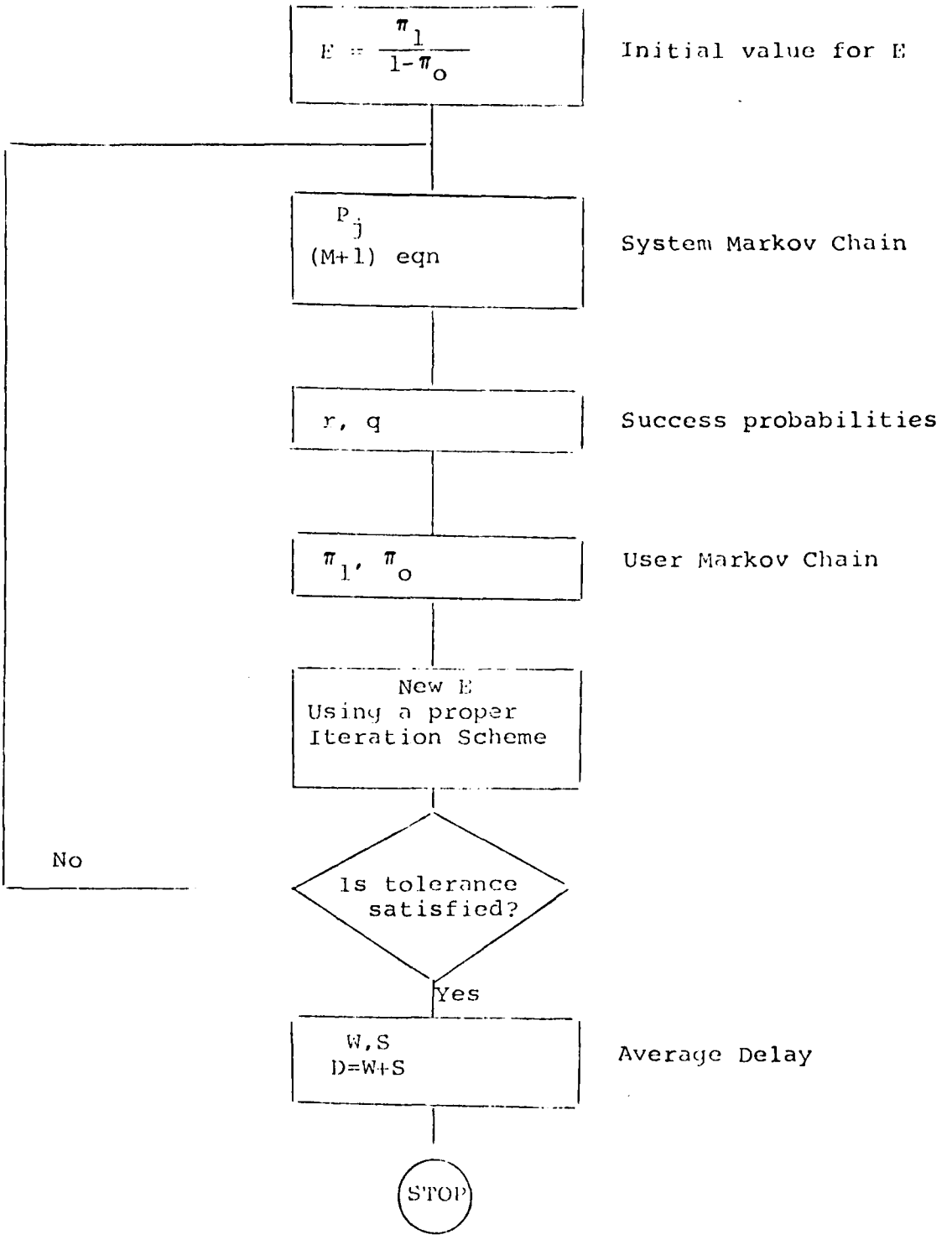

Fig.4 Flow Chart for the Calculation of the Average Delays

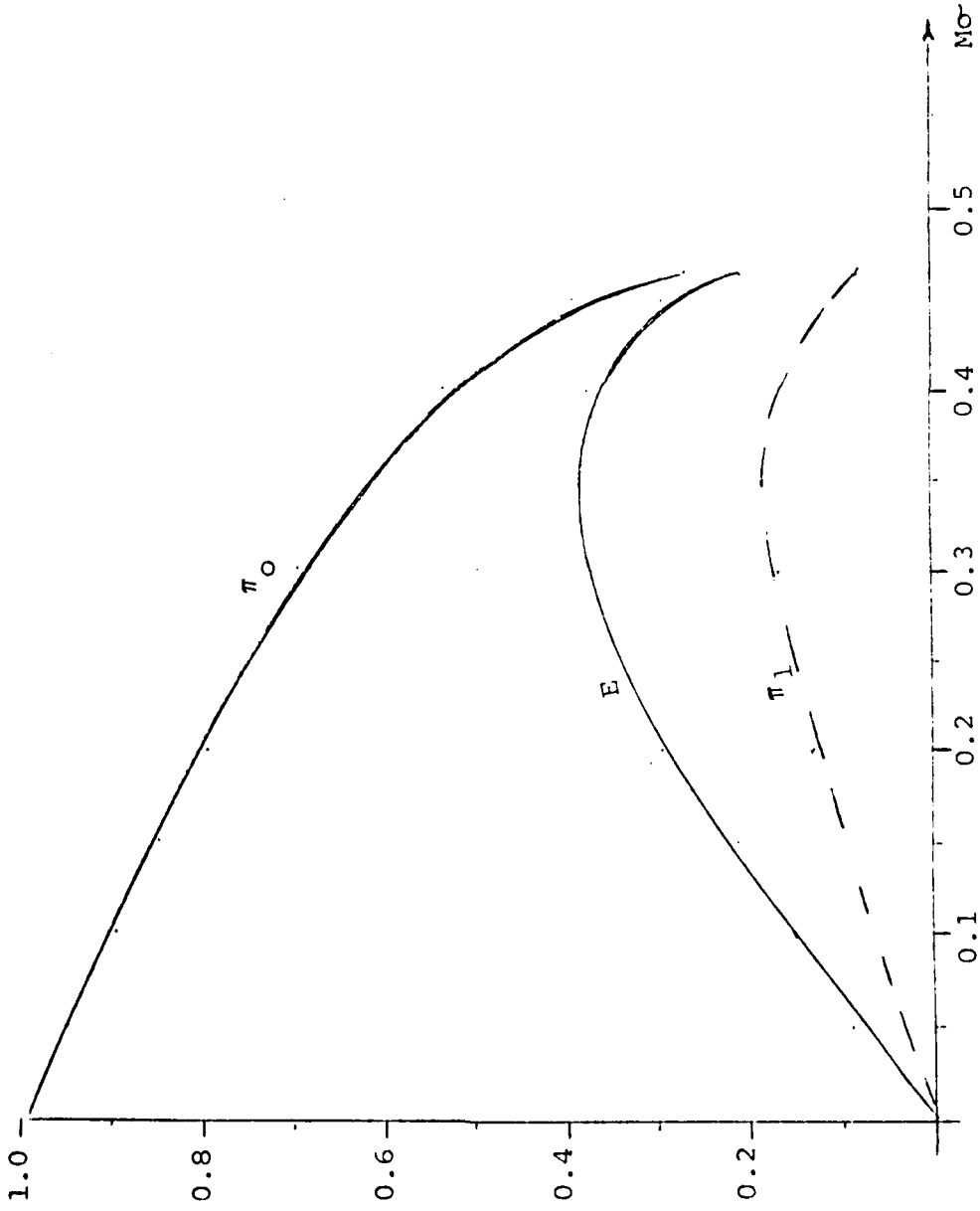

Fig.5 The Probabilities π_o, π_1, E versus channel Throughput

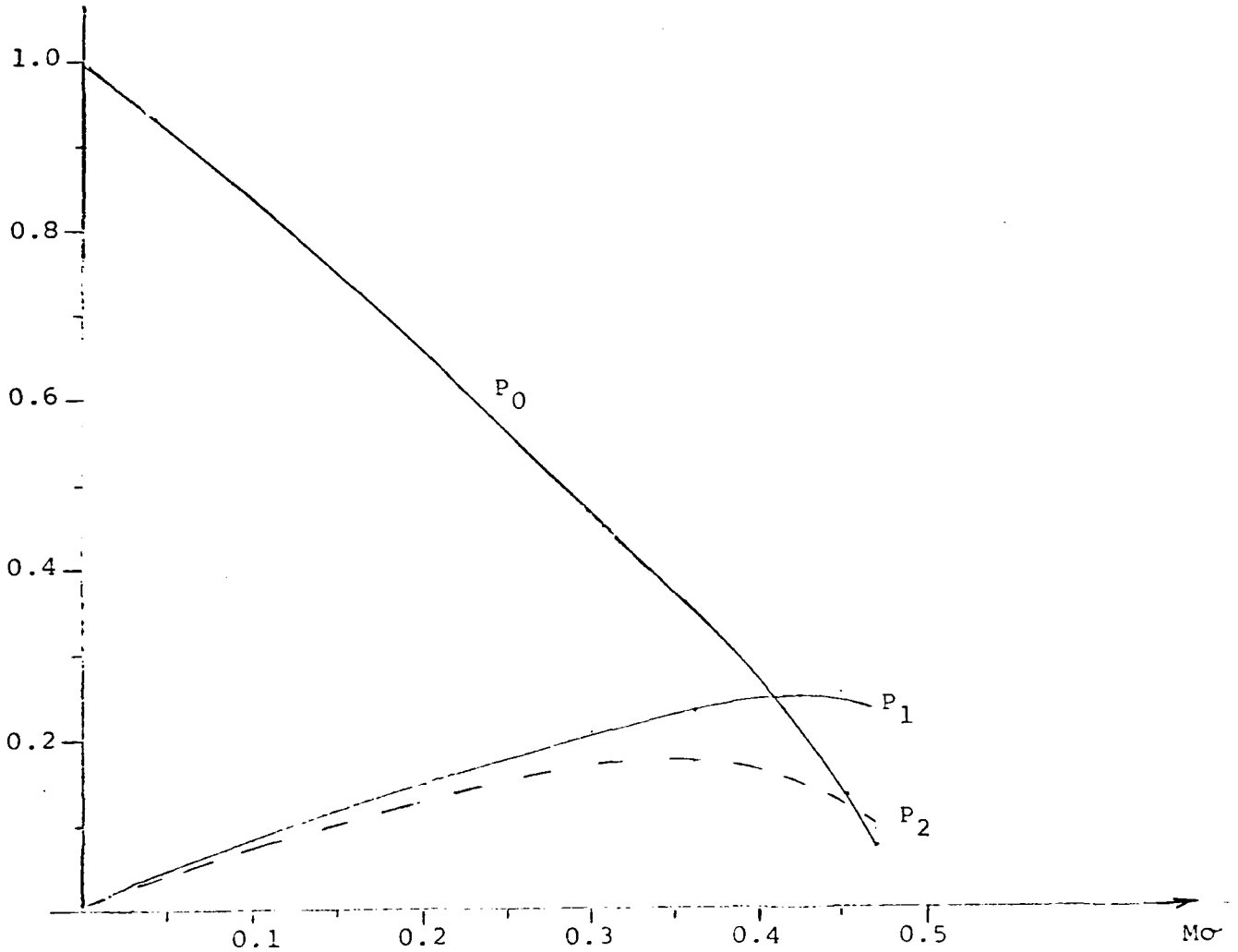

Fig. 6 The Probabilities P_0, P_1 and P_2 versus channel Throughput

(M=4, P=0.3)

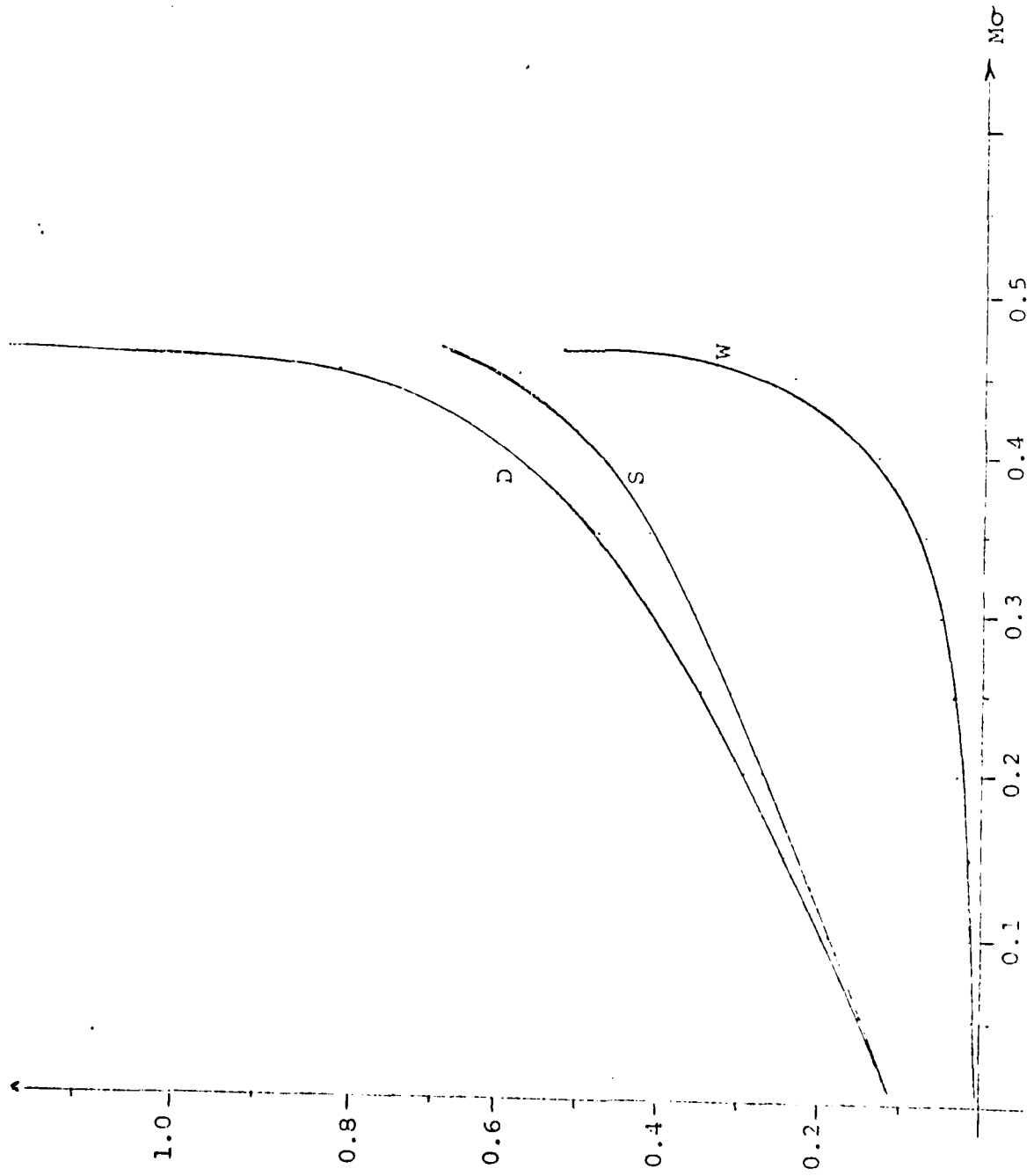

Fig. 7. The Average Packet Delays versus Channel Throughput (M=4, P=0.3)

Worst Case Aquisition of PN Sequences

Farhad Hemmati Donald L. Schilling
Department of Electrical Engineering
City College of New York
New York, N. Y. 10031

Abstract

An upper bound on the worst case autocorrelation of PN sequences of a given length is obtained. The value of the worst case autocorrelation curve at some specific points is found and using interpolation methods a smooth curve fitting to the worst case autocorrelation curve is formulated.

Introduction

Let $g(0), g(1), g(2), \cdots, g(L-1)$ be a PN sequence of length $L = 2^n - 1$. The autocorrelation of the PN sequence is defined as

$$R_\tau(\gamma) = \sum_{j=0}^{\gamma-1} (-1)^{g(j) + g(j+\tau)} \tag{1}$$

where γ is the partial correlation length. For $\tau = 0$, i.e., for correlated sequences $R_0(\gamma) = \gamma$. Furthermore, $R_\tau(L) = -1$ for $1 \leq \tau \leq L-1$. $R_\tau(\gamma)$ depends on the specific selected PN sequence and the phase τ.

For a given value of τ let us define

$$h(k) = g(j) + g(j+\tau) \tag{1a}$$

The shift and add property of PN sequences implies that $h(0), h(1), h(2), \cdots, h(L-1)$ is again a PN sequence. Therefore $R_\tau(\gamma)$ depends on the arrangement of the zeros and ones in the PN sequence $h(k)$. Figure 1 shows a typical

---

The research performed for this paper was partially supported under AFOSR grant 05431 and RADC Contract F19628-80-C-0095

example of the correlation of such a PN sequence.

The worst case of $R_\tau(\gamma)$, for all γ , is the one which over the set of all PN sequences of a given length and all possible phases $1 \leq \tau \leq L-1$, is as close to $R_0(\gamma)$ as possible. A sequence h(k) produces the worst case autocorrelation if it starts with the longest possible run of zeros, which is n-1, followed by the shortest possible run of ones followed by the longest possible run of zeros followed by the next shortest possible run of ones and so on. This sequence was invented by Davidovici and Schilling [1] and is known as a pseudo-pseudo-noise, (PPN), sequence. As an example the PPN sequence of length L=31 is 0000100010010010110110111011111. The PPN sequence is very close to the actual worst case of the PN sequences for short length codes. Unfortunately, it was observed that for long codes the obtained upper bound on the worst case autocorrelation of PN sequences based on the structure of PPN sequence is not very tight. In this paper we add to the above construction procedure the condition that each n-tuple along the sequence must appear only one time (window property). This condition results in the following well known construction technique:

1. The Worst Case Sequence Generation Algorithm

1. Generate n ones and set i = 0.
2. Append a zero and check if the generated n-tuple had not previously occurred. If not set i = i+1, go to 2, otherwise change the last generated bit to one, set i = i+1 and go to 3.
3. If $i=2^n$ go to 4. Otherwise go to 2.
4. Delete the first n+1 bits and stop.

Example: The generated sequence for n=5 is

111110000100011001010011101011011111.

The above construction technique was originally given by Ford [2] and is generalized by Golomb [3] and is extensively studied by Fredrickson[4]. Note that the generated sequence satisfies the run property and the window property of the PN sequences while the PPN sequence only satisfies the run property. Moreover, the sequence constructed by the above algorithm can be generated by an n-stage nonlinear feedback shift register.

A pure cycling shift register is an n-stage shift register with the last stage connected to the first stage of the register. The length of the cycles generated by the pure cycling shift register are divisors of n and the number of cycles is [5],

$$Z(n) = \frac{1}{n} \sum_{d|n} \phi(d) 2^{n/d}, \tag{2}$$

where ϕ (d) is the Euler's ϕ-function. In the following we summarize the properties of the nonlinear sequences generated by the above algorithm [6]:

Property 1:

The nonlinear sequence is constructed by joining the cycles of the pure cycling feedback shift register.

Property 2:

The breadth of a vector is defined as the longest number of contiguous zeros in the vector. Then: the algorithm exhausts, in order, the cycles of breadth n-1, n-2, n-3, etc.

2. Formulation of the Upper Bound

Properties 1 and 2 stated above can be used to find the value of the worst case autocorrelation at some specific points. The first exhausted cycle is the cycle of breadth n-1. Hence

$$R_{\tau}(n) = n-2 \tag{3}$$

There is one cycle of breadth n-2, two cycles of breadth n-3, and in general 2^{n-2-b} cycles of breadth b for $N_1 \leq b \leq n-2$, where $N_1 = \frac{n-1}{2}$ for n odd and $N_1 = \frac{n}{2}$ for n even. The weight of a cycle is the number of ones in that cycle. For $b < N_1$ there are less than 2^{n-2-b} cycles of breadth b since all of the low weight cycles of length n have already been exhausted. Since a cycle of length less than n cannot have a breadth greater than N_1, all the cycles exhausted up to the breadth N_1 are of length n.

The partial correlation of two sequences $\underline{x}$ and $\underline{y}$ can be also defined by

$$R_\tau(\gamma) = \gamma - 2 \cdot W_H^\gamma (\underline{x} + \underline{y}) \tag{4}$$

where $W_H^\gamma (\underline{z})$ is the Hamming weight of the sequence $\underline{z} = \underline{x} + \underline{y}$ truncated to length γ. Using property 2 and Eq. (4) we can find N_1 points of the worst case autocorrelation by the recursive relation

$$R_\tau(n \cdot 2^j) = R_\tau(n \cdot 2^{j-1}) + n \cdot 2^{j-1} - 2\left[\tfrac{1}{2}(i-1)2^{i-1}\right] - 2 \cdot 2\left[2^{i-1}\right] \quad \text{for } 1 \leq i \leq N_1 \tag{5}$$

The second term is the right hand side (rhs) of (5) is the number of bits in all cycles of breadth b=n-1-i. The third term in the rhs of (5) corresponds to the fact that in the set of all binary (i-1)-tuples the number of ones is equal to the number of zeros, and the last term of (5) considers the two ones at the beginning and at the end of each breadth.

Equations (3) and (5) can be rewritten as

$$\begin{cases} R_\tau(n) = n-2 \\ R_\tau(n \cdot 2^i) = R_\tau(n \cdot 2^{i-1}) + (n-i-3)2^{i-1} & \text{for } 1 \leq i \leq N_1 \end{cases}$$

or

$$R_\tau(n \cdot 2^i) = n-2 + \sum_{j=1}^{i} (n-j-3)\, 2^{j-1} \quad \text{for } 1 \leq i \leq N_1 \tag{6}$$

Using $\sum_{j=1}^{i} j \cdot 2^{j-1} = (i-1)2^{i} + 1$ in (6), the final result is

$$\begin{cases} R_\tau(n) = n-2 \\ R_\tau(n \cdot 2^i) = (n-i-2)2^i \quad , \quad 1 \le i \le N_1 \end{cases} \tag{7}$$

Observe that in the set of all cycles of a given breadth b, the last cycle exhausted is the cycle consisting of b zeros followed by n-b ones. Application of this observation in (7) gives another set of points of $R_\tau(\gamma)$, namely

$$\begin{cases} R_\tau(n-1) = n-1 \\ R_\tau(n \cdot 2^i - 1 - i) = (n-i-2)2^i + i + 1 \quad , \quad 1 \le i \le N_1 \end{cases} \tag{8}$$

The formulation of $R_\tau(\gamma)$ for $\gamma > n \cdot 2^{N_1}$ in general is rather complicated. However for the case that n is a prime number, we note from (1) that the cycles of the pure cycling register are of length one or n. In this case there are two cycles of length one and there are N_W^n cycles of length n and weight W where

$$N_W^n = \frac{1}{n}\binom{n}{W} \quad , \quad 0 \le W \le n-1 \tag{9}$$

In order to find an upper bound on the value of the worst case autocorrelation we assume that n is a prime and the worst case sequence begins with the cycle of length n and weight one, followed by the cycles of weight two, followed by the cycles of weight three, etc. With this assumption the worst case autocorrelation at partial length γ is upper bounded by

$$R_\tau(\gamma) \leq \sum_{W=1}^{k} n \cdot N_W^n - 2\sum_{W=1}^{k} W \cdot N_W^n \tag{10}$$

where k is the weight of the highest weight cycles in the partial length γ. Substituting (9) into (10) the result is

$$R_\tau(\gamma) \leq \sum_{W=1}^{k} \binom{n}{W} - 2\sum_{W=1}^{k} \frac{W}{n} \binom{n}{W}$$

Since $\frac{W}{n}\binom{n}{W} = \binom{n-1}{W-1}$ we have

$$R_\tau(\gamma) \leq \sum_{W=1}^{k} \binom{n}{W} - 2\sum_{W=1}^{k} \binom{n-1}{W-1} \tag{11}$$

where

$$\gamma = n \sum_{W=1}^{k} N_W^n = \sum_{W=1}^{k} \binom{n}{W} \tag{12}$$

In particular for $k = \frac{1}{2}(n-1)$ we have from (12)

$$\gamma = \sum_{W=1}^{\frac{n-1}{2}} \binom{n}{W} = 2^{n-1} - 1,$$

and from (11)

$$R_\tau(2^{n-1}-1) \leq \sum_{W=1}^{\frac{n-1}{2}} \binom{n}{W} - 2\sum_{W=1}^{\frac{n-1}{2}} \binom{n-1}{W-1} = \binom{n-1}{\frac{n-1}{2}} - 1 \tag{13}$$

Using Stirling's Formula for factorials, (13) reduces to

$$R_\tau(2^{n-1}-1) \leq \frac{2^n}{\sqrt{2\pi(n-1)}}$$

For n large, $L' = 2^n - 2 \approx 2^n$ and

$$R_\tau(L'/2) \leq \frac{L'}{\sqrt{2\pi(n-1)}} \tag{14}$$

To find a smooth curve for the upper bound on the worst case autocorrelation of the PN sequences we can use any interpolation technique, e.g. Lagrange's method among the specific values of $R_\tau(\gamma)$ given in (7), (8), (11), and (14). The simplest case is an interpolation among the three points $R_\tau(0) = 0$, $R_\tau(L') = 0$ and $R_\tau(L'/2)$ given by (14), which yields a second degree polynomial,

$$R_\tau(\gamma) \approx \frac{4\gamma}{\sqrt{2\pi(n-1)}}(1-\gamma/L') \qquad (15)$$

Obviously a higher degree polynomial will give a better approximation to the worst case autocorrelation curve.

In Fig. 2 the worst case curve for n=11 generated by the algorithm described in Sec. 1, is compared with the approximation curve of (15) and a five point interpolation curve. Figure 3 is the same as Fig. 2 but for n=13. It should be mentioned that in the formulation of $R_\tau(\gamma)$ we have assumed that the worst case curve is symmetrical with respect to the line $\gamma = L'/2$.

In the case that n is not a prime number the length of the cycles of the pure cycling shift register are divisors of n. An upper bound on the worst case autocorrelation curve for n a nonprime number can again be obtained similar to the upper bounds of (11) and (12). Since the average weight per length of the short length cycles is approximately equal to the average weight per length of the long length cycles, the upper bounds of (11), (12), and (15) obtained for n a prime number are valid for any n.

Figures 4 and 5 compare the worst case autocorrelation curve generated by the algorithm for n=8 and n=10 with the three point interpolation curve of Eq. (15).

3. Conclusions

This paper has presented an upper bound on the worst case partial autocorrelation of nonlinear PN sequence. The results take the form of a readily implementable algorithm and an approximate, easily used, equation which upper bounds the algorithm, namely (15).

It is interesting to compare (15) with the results obtained by Davidovici and Schilling [1] who found

$$R_\tau(\gamma) < \gamma\left(1 - \frac{\gamma}{L}\right) \quad , L = 2^n - 1 \tag{16}$$

Note that both results are of the same form, and partial autocorrelation of [1] exceeds the bound developed in this paper by the factor

$$F = \sqrt{\frac{\pi(n-1)}{8}} \tag{17}$$

Hence for n=13, F = 1.77.

When using (15) or (16) to determine the probability of false alarm or detection when acquiring a PN sequence, a value of F of the order of (17) is often extremely significant.

References

(1) S. Davidovici and D. L. Schilling "Minimum Aquisition time of a PN sequence", NTC 1979.

(2) L. R. Ford, "A Cyclic Arrangement of M-tuples, Report No. P-1071, RAND Corp, 1957.

(3) S. Golomb, Shift Register Sequences, Holden-Day, San Francisco, 1967.

(4) H. Fredrickson "The Lexicographically least deBruijn Cycles", J. Combinatorial Theory 9, 1970, pp. 1-5.

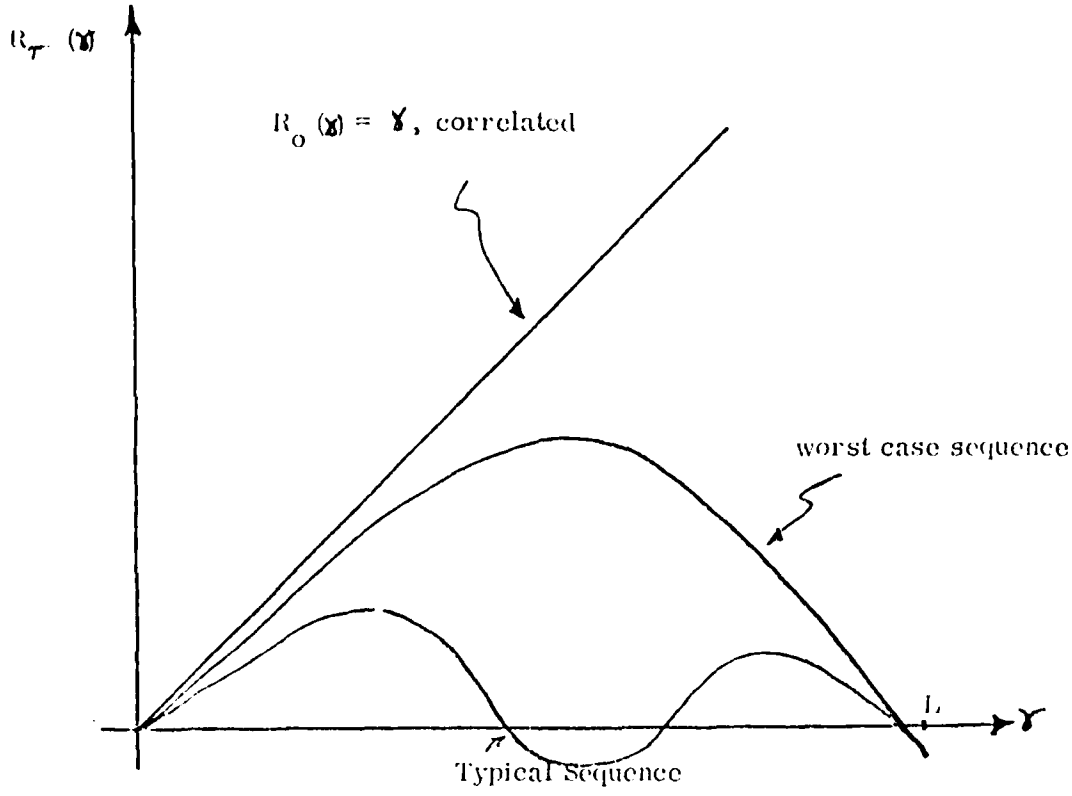

Fig. 1 A Typical Example of the Partial Autocorrelation of a PN Sequence

——— worst case curve generated by the Algorithm (Sec. 1)

—·— 3 point interpolation

——··—— five point interpolation

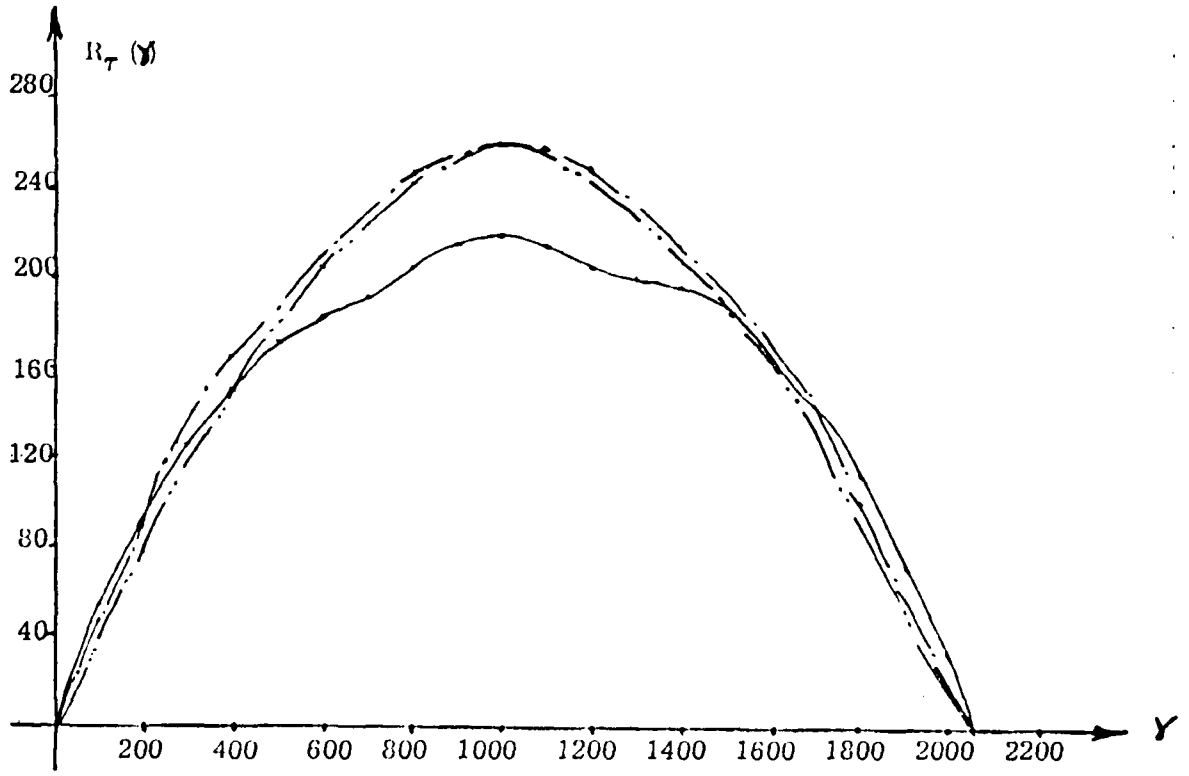

Fig. 2 Worst case sequence of length L=2047 generated by the algorithm, a three point and a five point interpolation curve.

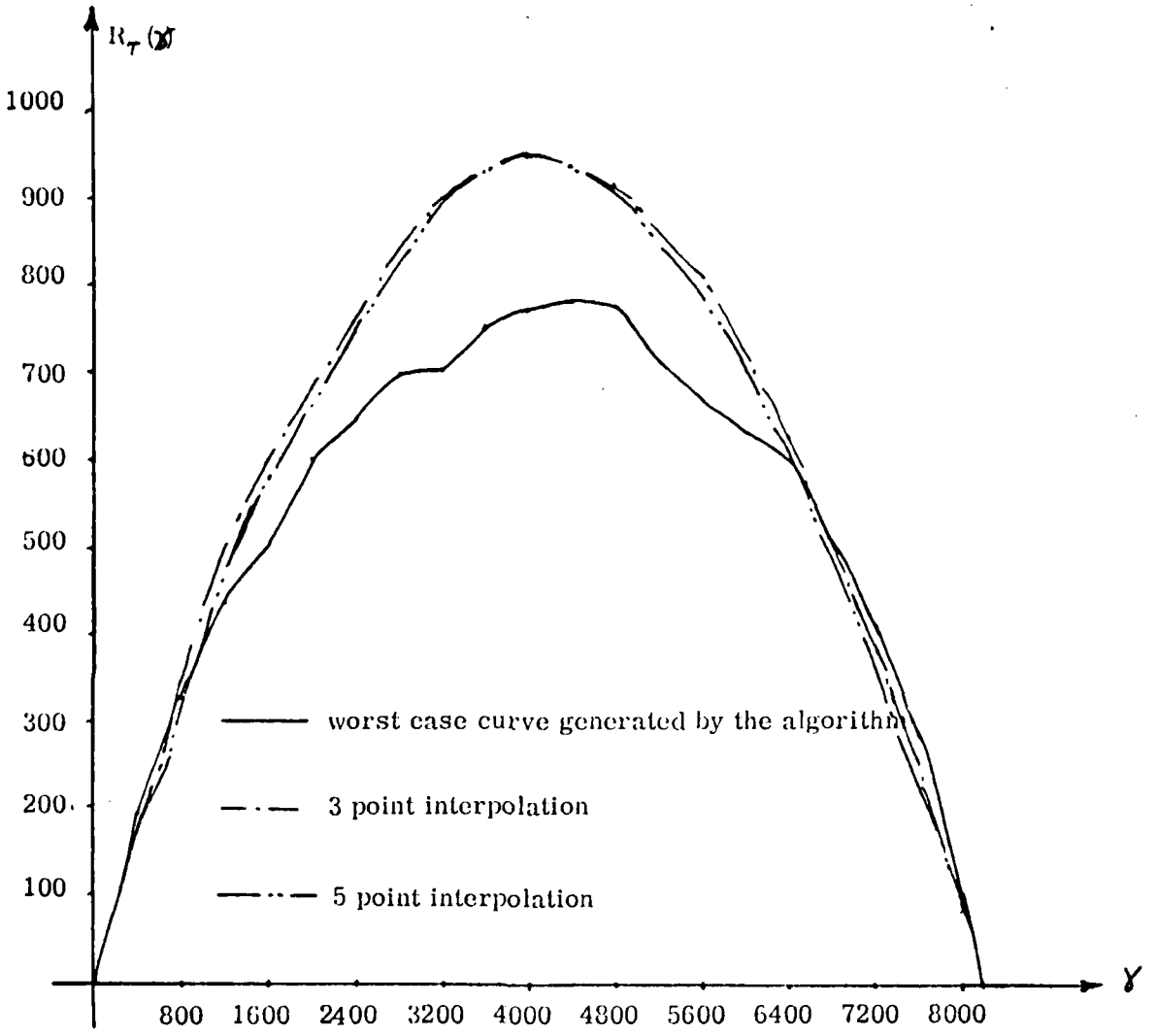

Fig. 3 Worst case sequence of length L = 8191 generated by the Algorithm, a three point and a five point interpolation curve.

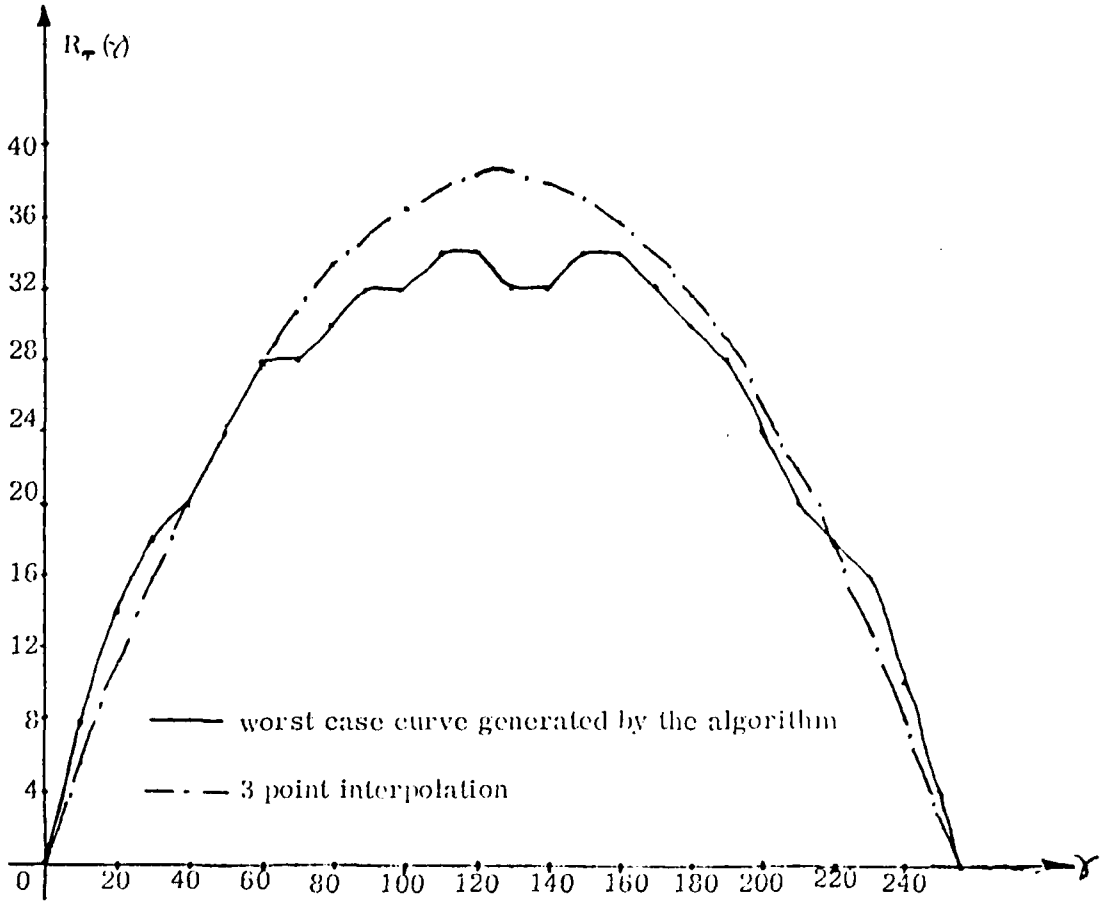

Fig. 4 Worst case sequence of length $L = 255$ generated by the algorithm and a three point interpolation curve.

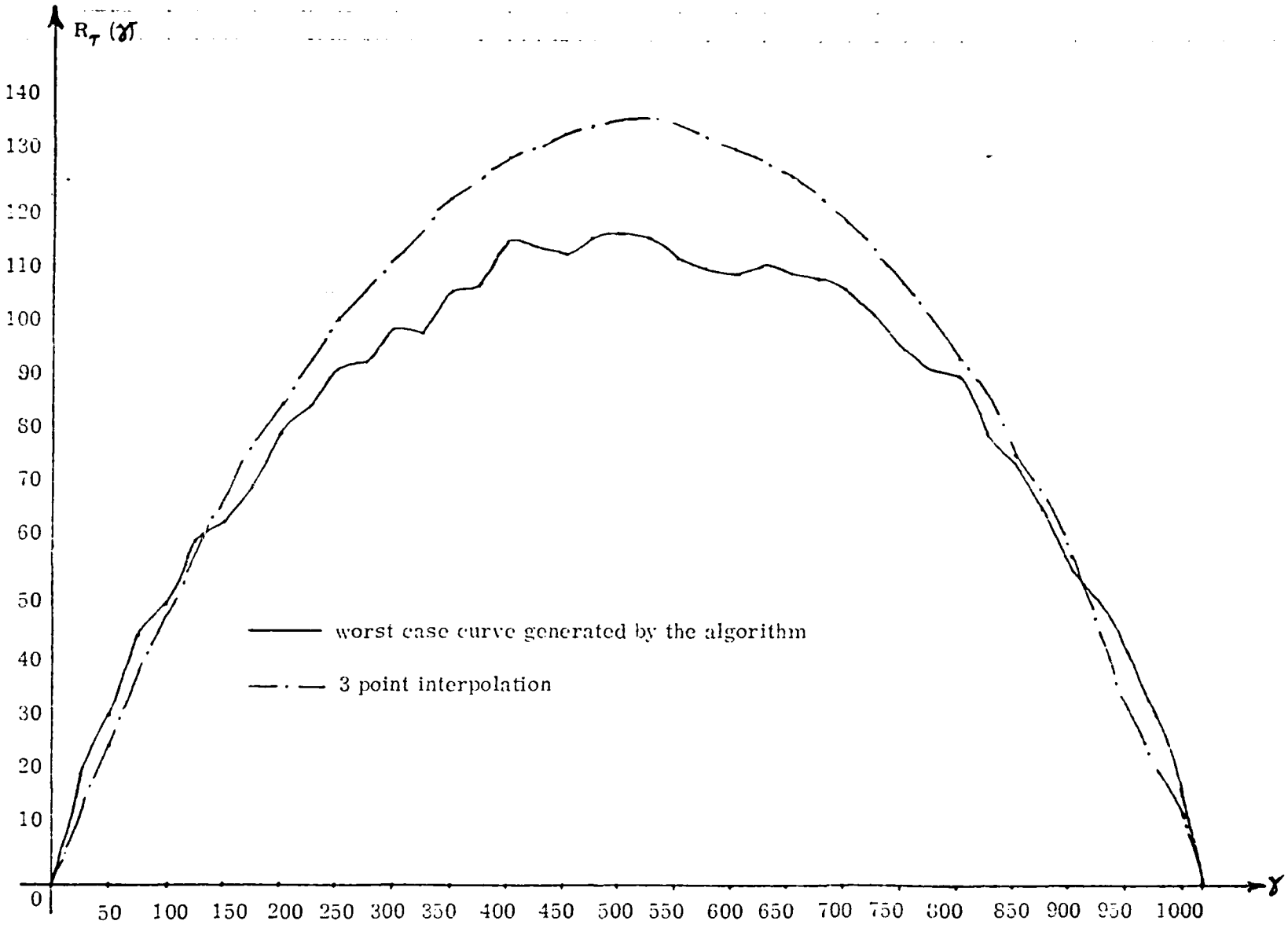

Fig. 5 Worst case sequence of length L = 1023 generated by the algorithm and a three point interpolation curve.

Generation of Nonlinear Shift Register Sequences

By

Farhad Hemmati

and

Donald L. Schilling

Department of Electrical Engineering

City College of New York

New York, N.Y. 10031

Submitted to the 19th Annual Allerton Conference on Communication, Control and Computing.

This work was partially supported by AFOSR under grant no. 5444.

Summary

An infinite cyclic sequence of period p, where $p \leq 2^k$ for some positive integer k, is a shift register sequence if any block of k consecutive bits over one period of this sequence is not repeated. The sequence of period $p=2^k-1$ is known as the maximal length sequence and the sequence of length $p=2^k$ is called a deBruijn sequence [1]. For a given k the number of deBruijn sequences is $2^{2^{k-1}-k}$.

A linear maximal length sequence (also known as a PN sequence) can be generated by a k-stage linear feedback shift register (LFSR) with a primitive characteristic polynomial [2]. For a given k the number of linear maximal length sequences is $\varphi(2^k-1)/k$,where φ is the Euler's φ-function. An efficient method to construct the nonlinear sequences is the cycle joining method [2],[3] which is based on joining the sequences of short period together to obtain a deBruijn sequence.

In the following a new property of the PN sequences is presented. For generation of nonlinear sequences of period $p=2^k$ this property and several other well known properties, [2], of the PN sequences are used to join the cycles of an LFSR with characteristic polynomial $G(x)=g(x)(1+x)^n$, where g(x) is a primitive polynomial of degree m and G(x) is of degree k=m+n.

A block of length m+j consecutive bits on a PN sequence generated by an m-stage LFSR is called an extended state of

degree j of the shift register and is represented by the (m+j)-tuple $\underline{S}=(s_{m+j},s_{m+j-1},\ldots,s_2,s_1)$. The conjugate of $\underline{S}$, [3], is defined by $\hat{\underline{S}}=(s_{m+j},s_{m+j-1},\ldots,s_2,\bar{s}_1)$, where $\bar{s}_1$ is the binary complement of s_1. A characteristic state over a PN sequence is defined as an extended state of degree j over the PN sequence such that its conjugate satisfies the recurrence relation of $(1+x)^j$.

Property: There exists a characteristic state on every PN sequence for any $j \geq 1$.

Proof: The proof is by induction. The property is obviously true for j=1. Since there exists a block of m consecutive ones followed by a zero ,(1,1,...,1,0), on every PN sequence and the conjugate of this extended state is a block of m+1 consecutive ones (1,1,...,1,1) which satisfies the recurrence relation of 1+x. Now, if we assume that the property is true for j=i, Lempel's homomorphism [3], can be used to prove that the property is also true for j=i+1. Moreover, the proof gives an itterative method to find the characteristic states of a PN sequence for any $j \geq 1$. Characteristic states of the PN sequence 1110010 for $1 \leq j \leq 8$ is shown in Table I.

Let C_k be the set of all cycles of a LFSR with the characteristic polynomial $g(x)(1+x)^n$,[4]. C_k can be divided into four subsets A,B,C and D. The subset A consists of cycles of length $(2^m-1)2^{e(j)}$ which satisfy the recurrence

relation of $g(x)(1+x)^j$, $0 \leq j \leq n-1$, where $e(j)$ is an integer such that $2^{e(j)-1} < j \leq 2^{e(j)}$. The subset B consists of cycles of length $(2^m-1)2^{e(n)}$ which satisfy the recurrence relation of $g(x)(1+x)^n$. Similarly the subset C consists of cycles of length $2^{e(j)}$ which satisfy the recurrence relation of $(1+x)^j$ $0 \leq j \leq n-1$. And finally the subset D consists of cycles of length $2^{e(n)}$ which satisfy the recurrence relation of $(1+x)^n$. The existence of a characteristic state on every PN sequence for any $j \geq 1$ can be used to prove the following theorem.

Theorem: Let α be a cycle of length $(2^m-1)2^{e(j)}$ in the set A. There exists $2^{e(j)}$ states on α such that their conjugates are in the set D. The conjugates of the $(2^m-2)2^{e(j)}$ remaining states on α are in the set B.

Corollary: Let β be a cycle of length $(2^m-1)2^{e(n)}$ in the set B. There exists $2^{e(n)}$ states on β such that their conjugates are in the set C. The conjugates of the $(2^m-2)2^{e(n)}$ remaining states on β are in the set A.

Since the number of cycles of an LFSR with the characteristic polynomial $g(x)(1+x)^n$ increases exponentially with respect to n ,[3],[4], the number of different deBruijn cycles which can be constructed by joining the cycles of $g(x)(1+x)^n$ increases double exponentially with respect to n.

References

[1] N.G. deBruijn, "A Combinatorial Problem", Nedel. Akad. Wetench. Proc. 49, pp. 758-764.

[2] S.W. Golomb, Shift Register Sequences, Holden-Day, San Francisco, 1967.

[3] A. Lempel, "On a Homomorphism of the deBruijn Graph and its Applications to the Design of Feedback Shift Registers", IEEE Trans. Computers C-19, 1970, pp. 1204-1209.

[4] B. Elspas, "Theory of Autonomous Linear Sequential Networks", IRE Trans. Circuit Theory T-6, 1959, pp. 45-60.

Table I. Characteristic States of the PN Sequence 1110010 for $1 \leq j \leq 8$.

j	$\underline{S}$	$\hat{\underline{S}}$	$(1+x)^j$
1	1110	1111	$1+x$
2	01011	01010	$1+x^2$
3	110010	110011	$1+x+x^2+x3$
4	1011100	1011101	$1+x^4$
5	10010111	10010110	$1+x+x^4+x^5$
6	011100101	011100100	$1+x^2+x^4+x^6$
7	0010111001	0010111000	$1+x+x^2+x^3+x^4+x^5+x^6+x^7$
8	11100101110	11100101111	$1+x^8$

Reprinted from APPLIED OPTICS, Vol. 21, page 496, February 1, 1982

Superresolving image restoration using linear programming

R. Mammone and G. Eichmann

Superresolving image restoration (SIR) in the presence of noise is considered. Few SIR algorithms have demonstrated the ability to resolve two point sources spaced one-half of the Rayleigh distance apart. In this paper, it is shown that the SIR of a two point noncoherent source spaced one-tenth of a Rayleigh distance apart is possible. The method presented uses optimal data fitting techniques based on the methods of linear programming. For noisy images, a combination of linear eigenvalue prefiltering and optimal data fitting is used. It is also shown that for a diffraction-limited image of two-point sources spaced one-half of the Rayleigh distance apart, where the input is contaminated with significant noise, SIR is achievable. These results have important implications in atmospheric physics, geophysics, radio astronomy, medical diagnostics, and digital bandwidth compression applications where the deconvolution of noisy bandwidth-compressed images is one of the fundamental limitations. The techniques described are specifically designed for impulsive-type images.

I. Introduction

The problem of restoring a linearly degraded image has been the subject of extensive investigations.[1] The mathematical formulation of the image restoration problem is common to many diverse fields such as atmospheric physics,[2] geophysics,[3] spectroscopy,[4] radio astronomy,[5,6] as well as the general subject of numerical analysis.[7] In general, the inversion of a linear degradation can be accomplished in a number of ways.[1] When the measurement error, which is the noise, is negligible and the degradation process is well-behaved, the direct inversion of the degradation process can easily be performed. For a well-conditioned degradation process, in the presence of noise, methods such as Wiener filtering are appropriate.[8] However, in many cases the degradation process is ill-conditioned. In this case the measurement errors are greatly amplified in the restoration process leading to an image estimate that is dominated by noise. In this paper we discuss the restoration of ill-conditioned linearly degraded images that have been corrupted by appreciable noise.

While many types of ill-conditioned image restoration can be considered, a particular ill-conditioned image restoration, the restoration of a diffraction-limited image of finite extent, has been used in this paper as a bench mark to provide a stringent test of the algorithm. Furthermore, this model has many other important applications such as the restoration of a severely bandwidth-compressed video images. Such images are of interest in digital TV applications.

It has been shown[9,10] that for images of finite extent, in the absence of noise, spectral components of the signal that have been removed can be reconstructed from the low passband information using analytic continuation. The extrapolation in the spatial frequency domain represents an increase in the spatial resolution in the spatial domain. An image restoration process which provides this increase in resolution is called a superresolving image restoration (SIR) process. A complete survey of recent restoration methods including SIR has been given by Frieden.[1] In general, statistical image restoration methods are not superresolving. Deterministic methods use various forms of regularization[11] to provide stability for the image restoration. Linear shift-invariant filters, while they provide stability, are also not superresolving. It has been postulated that only nonlinear filtering methods will provide SIR in the presence of noise.[1] The purpose of this paper is to show that the combination of linear shift-invariant filtering of the image and nonlinear restoration does provide SIR capability in a realistic noise environment.

The optimal data fitting step uses linear programming (LP) techniques. The LP method provides both cost and time effective ways to produce SIR. Although methods similar to LP have been suggested for image processing,[12-14] we have specifically addressed ill-con-

The authors are with City College of City University of New York, Department of Electrical Engineering, New York, New York 10031.

Received 4 June 1981.
0003-6935/82/030496-06$01.00/0.

ditioned problems and have incorporated a stabilizing presmoothing step, which also yields computational advantages.

II. Formulation

The SIR problem requires the inversion of a Fredholm integral equation of the first kind with a sinc function kernel. The integral equation corresponding to the coherent 1-D case is

$$g(x) = \int_{-b}^{b} \frac{\sin f_c \pi(x-y)}{\pi(x-y)} f(y)dy, \tag{1}$$

where $g(x)$ is the diffraction-limited (DL) image, $f(y)$ is the original image of length $2b$, and f_c is the cutoff frequency of the transfer function. It is well-known that the incoherent bandlimiting kernel has twice the spatial cutoff frequency as compared with the corresponding coherent kernel. Therefore, the coherent SIR is more stringent and thus provides a better bench mark than the corresponding incoherent kernel.

The discretized form of the image restoration problem can be formulated as a solution to the matrix linear equation

$$\mathbf{g} = H\mathbf{f} + \mathbf{n}, \tag{2}$$

where $\mathbf{f}$,$\mathbf{g}$ are the sampled values of the restored (desired) diffraction-limited and measured bandlimited images, respectively, $\mathbf{n}$ is the sampled noise vector, and H is a matrix representing the sinc integral operator obtained by using some appropriate quadrature rule. Without loss of generality we shall take $\mathbf{f}$, $\mathbf{g}$, and $\mathbf{n}$ to be N-dimensional vectors. Thus H is an $N \times N$ square matrix. The system of linear equations, represented by Eq. (2), is underdetermined since there are N equations and $2N$ unknowns. The unknowns are the components of the N-dimensional vectors $\mathbf{f}$ and $\mathbf{n}$. Neglecting the noise vector does not per se simplify the problem because for SIR the H, the degradation, matrix is nearly singular. Because of the rank deficiency of the H matrix, the inverse H is highly unstable.

To stabilize the inverse H matrix, the eigenvalues and the eigenvectors of the inverse matrix are filtered. The eigenvectors of the H matrix are similar to the discrete prolate spheroidal wave sequences,[15] the analog of the prolate spheroidal wave functions of the continuous case. The eigenvalues of the H matrix change abruptly from approximately unity to nearly zero as a function of the space–bandwidth product. The high order eigensequences, corresponding to rapidly oscillating functions, represent the eigenvalues close to zero. The instability of the inverse matrix is due to the near zero eigenvalues of the H matrix. By filtering (attenuation) of the image components corresponding to those eigenvalues, stable inversion can be obtained. There are a number of linear filtering schemes that have been suggested to do this filtering.[16,17] While these schemes stabilize the inversion process of the H matrix, since they do so at the expense of the high order eigenvalue components, which are precisely those components that contain the high spatial frequency information necessary for superresolution, these methods are not SIR methods. Furthermore, since this approach does not take into account the measurement errors, a critical factor in a highly unstable matrix inversion, other methods must be sought.

Additional information or constraints must be utilized to obtain SIR. Methods of image restoration that impose non-negativity constraints on the restored image to obtain stability[12,13] have been described. We use non-negativity, boundedness, and derivative constraints together with eigenvalue filtering to obtain SIR. The addition of these constraints stabilizes the restoration process. This method of restoration can be formulated as a data fitting problem where it is desired to obtain a restored image, which, when degraded, is as close as possible in some sense to the measured image. Two measures, or norms, of closeness were investigated, the l_1 and l_∞ norms. The l_1 norm of a vector is the sum of the absolute values of the elements of the vector, while the l_∞ norm of a vector is the maximum absolute value of the vector. The method which minimizes this norm is frequently called the minimax method.

Thus the method consists of two steps: (1) presmoothing the measured image to attenuate or eliminate image components which effectively could be due only to noise; (2) selection of the closest restored image estimate corresponding to the measured image. Two measures of closeness were examined yielding the minimal l_1 and minimax methods.

A. Presmoothing the Measured Image

A method of stabilizing the problem is to smooth the elements of the measured image vector $\mathbf{g}$. Ideally this smoothing can be accomplished by passing the measured image $\mathbf{g}$ through a filter which eliminates the frequency components for frequencies higher than f_c. This filters out the components due only to noise. This preprocessing step is straightforward if the DL image is provided in its entirety. However, the original image must be of finite duration for a solution to exist. Thus the DL image must be infinite in extent, although, for practical reasons, some finite interval of the DL image must be selected. Because the measured image is not bandlimited, some other linear filtering process must be used.

A method of smoothing the measured DL image can be obtained by examining the singular value decomposition (SVD)[17] of the degradation matrix H. From Eq. (2), neglecting the noise term, we have

$$\mathbf{g} = H\mathbf{f} = U\Lambda^{1/2}V^T\mathbf{f}, \tag{3}$$

where U and V^T are orthogonal matrices, Λ is a diagonal matrix comprised of the eigenvalues of the symmetric matrix HH^T, and superscripts T and $1/2$ denote matrix transpose and square root, respectively. The standard form of the SVD is used, where the eigenvalues are in decreasing order from left to right in Λ. These eigenvalues fall abruptly to practically zero, indicating the ill-conditioned nature of H. This SVD decomposition is commonly interpreted as a decomposition of the image into eigenimages. The higher order eigenvalues correspond to the higher order eigenimages. The amount of zero crossing is proportional to the order.

Thus the high order components correspond to the high frequency content of the image. We may rewrite Eq. (2) in a transformed coordinate system

$$\mathbf{G} = \Lambda^{1/2}\mathbf{F}, \tag{4}$$

where

$$\mathbf{G} = U^{-1}\mathbf{g}, \tag{5}$$

$$\mathbf{F} = V^T\mathbf{f}. \tag{6}$$

The interpretation of $\mathbf{G}$ and $\mathbf{F}$ is similar to that of a discrete Fourier transform (DFT).[18] Since the elements of the diagonal matrix decrease abruptly to zero, it is seen from Eq. (4) that the high order components (high frequency components) are greatly attenuated. This is to be expected since filtering in the DFT domain is consistent with low pass filtering in the diagonalized coordinate system.

The smoothing is accomplished by preprocessing the measured image via the singular value transform (SVF) Eq. (5) and forming

$$\hat{\mathbf{g}} = U\tilde{\mathbf{G}}, \tag{7}$$

where $\tilde{\mathbf{G}}$ is $\mathbf{G}$ modified by replacing all elements of index greater than r with zero. The index r corresponds to the largest order eigenvalue of the matrix HH^T whose value is greater than the standard deviation of the error. This elimination of the high order noisy components of the observed image also yields a reduction in the rank of the degradation matrix. This resulting rank deficiency has two effects on the problem: first, it yields an underdetermined system of equations with many possible solutions. We shall define an optimal solution and present a method of obtaining this solution later. The other effect is to make the system inconsistent; that is, the left-hand side of Eq. (2), neglecting the noise term, may have two identical adjacent rows of H due to the linear dependence, but as a result of the random noise, the left-hand side will be very different. Thus inconsistencies in the equations result from the noise. Therefore, we eliminate all but r linearly independent equations in H. The resulting reduced system of r equations is well-conditioned and consistent. This reduction of the number of equations gives the additional advantage of reducing the number of computations necessary in the next step.

At this point the pseudoinverse solution might suggest itself. The problem with this or any other linear solution is that it will not extrapolate the high order components. Thus we find a constrained optimal solution from this reduced system of equations using LP.

B. Constrained Estimate

The general LP problem can be formulated as follows[19]:

$$\text{minimize } \mathbf{c}^T\mathbf{x}, \tag{8}$$

$$\text{subject to } A\mathbf{x} \geq \mathbf{b}, \tag{9}$$

$$\text{where } \mathbf{x} \geq 0, \tag{10}$$

and $\mathbf{c}$ is called the cost vector, $\mathbf{x}$ is the M-dimensional vector denoting the variables, the $r \times M$ matrix A is called the constraint matrix, and $\mathbf{b}$ is an r-dimensional constraint vector. The most frequently used algorithm to solve linear programming problems is the simplex algorithm. This algorithm produces one of three mutually exclusive results: first, an indication that the problem is infeasible (the problem is feasible if all the constraints can be simultaneously satisfied for some choice of variables; the problem is infeasible otherwise); second, an indication that the problem is feasible but the optimal solution is unbounded; or, third, an optimal solution.

The minimal l_1 formulation of the image restoration will now be addressed. We define two N-dimensional vectors $\mathbf{n}^+$ and $\mathbf{n}^-$ so that they contain the negative and positive components of $\mathbf{n}$, respectively. For any given row, one of the two vectors $\mathbf{n}^+$ and $\mathbf{n}^-$ has one zero element, and the other has a positive element. Thus we may write

$$\mathbf{g} = H\mathbf{f} + \mathbf{n}^+ - \mathbf{n}^-, \tag{11}$$

so that $\mathbf{n}^+$, $\mathbf{n}^-$, and $\mathbf{f}$ are all positive N-dimensional vectors. If we consider the positive sum for row i,

$$n_i^+ + n_i^- = |g_i - h_i f|, \tag{12}$$

where h_i is the ith row of H. This is seen to be the absolute value of the residual of the difference between $\mathbf{g}$ and $h\mathbf{f}$. Taking the sum over all N rows yields the l_1 norm of the residual error. This will be the cost function that will be minimized subject to the constraints. The LP formulation of the minimal l_1 problem is:

$$\text{minimize } n_1^+ + n_1^- + n_2^+ + n_2^- + \ldots n_n^+ + n_n^-, \tag{13}$$

$$\text{subject to } \mathbf{g} = H\mathbf{f} + \mathbf{n}^+ - \mathbf{n}^-, \tag{13a}$$

$$\text{with } 0 \leq \mathbf{f} \leq f_{\max}. \tag{13b}$$

An alternate interpretation of minimizing the residual can be obtained by examining the process in terms of the solution vector. The l_1 norm is bounded by zero. If this bound is obtained, the residual error is zero and the solution vector is completely in $\mathbf{f}$. This case pertains to a direct inversion of the degradation matrix H. In general, this inversion is not possible, since the measured image $\mathbf{g}$ is usually not consistent with all the constraints. Thus $\mathbf{n}$ will contain nonzero elements, and $\mathbf{f}$ must contain corresponding zero elements as well.

Following a similar procedure, the minimax estimate can be obtained by LP. First, we let E represent a scalar variable denoting the largest positive deviation of the degraded estimate from the measured image. Then we write the LP formulation as:

$$\text{minimize } E, \tag{14a}$$

$$\text{subject to } \mathbf{g} = H\mathbf{f} + E\mathbf{e}_r, \tag{14b}$$

$$\mathbf{g} = H\mathbf{f} - E\mathbf{e}_r, \tag{14c}$$

where $\mathbf{e}_r$ is the r-dimensional unity vector. These equations can be solved by the method of LP. Thus the minimax formulation requires N more constraints than the minimal l_1 formulation of the same problem.

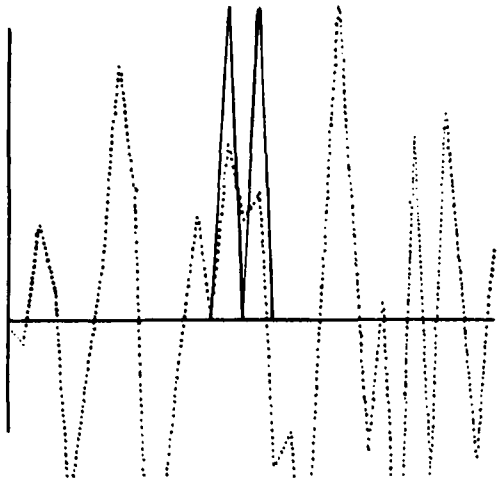

Fig. 1. Direct inverse solution for two impulses separated by one-eighth of the Rayleigh distance.

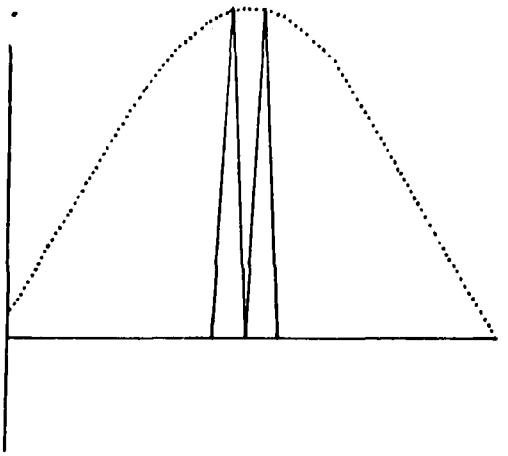

Fig. 2. Constrained minimal l_1 solution for two impulses separated by one eighth of the Rayleigh distance.

C. Numerical Results

A figure of merit of the SIR is the Rayleigh distance. The Rayleigh distance is inversely proportional to the bandwidth of the transfer function. Very few restoration methods achieve resolution of one-half of the Rayleigh distance.[1] This measure of resolution will be used for both noncoherent and coherent imaging systems. It should be remembered that the Rayleigh distance for a coherent imaging system is a more stringent criterion than for noncoherent imaging system.

The methods were simulated using the simplex linear programming subroutines contained in the International Mathematical and Statistical Library (IMSL) FORTRAN callable subroutine package. CUNY's Central Computing Facility was used. The bench mark example is the diffraction limitation of a coherent 1-D system. Figure 1 illustrates reconstruction of two impulses spaced one eighth of the Rayleigh distance with no added measurement noise. The image is composed of thirty-two samples. The direct inverse solution (dotted line) demonstrates very unstable behavior, even though the only error is that due to the finite precision of the computer used and arithmetic errors which are propagated numerically through the inversion process. The exact solution is shown by the two impulses (solid line). Figure 2 illustrates a perfect restoration of two impulses separated by one-eighth of the Rayleigh distance by the minimal l_1 norm method. The dotted curve is the DL image. It is approximately the main lobe of a sinc function centered at the center of the graph. The method completely restored the two impulses. The estimate is, the chain dot curve, completely coincident with the exact curve (solid line).

The minimax method did not provide the high resolution performance obtained with the minimal l_1 method for two-point restoration. Figure 3 gives an indication of this difference. The minimax estimate (chain-dot) curve is shifted. The second impulse is down by 80%, and the interimpulse trough is down to 50% of the actual peak amplitude. There is also a small artifact which appears just to the left of the first impulse. Although this estimate might actually be acceptable for many applications, it is clear that the minimal l_1 estimate is preferable. This was found to be the case in all situations investigated. The reason, we believe, for this discrepancy is the increase in computations needed for the minimax method and thus the greater the propagations of precision errors.

The method of restoration is robust to noise yielding estimates with an SNR of comparable magnitudes to the SNR of the measured signal. Here the SNR of the estimate is defined as

$$\mathrm{SNR}_f = 10 \log \left[\frac{\sum_{i=1}^{N} (f_i \text{ estimate} - f_i \text{ original})^2}{\sum_{i=1}^{N} (f_i \text{ original})^2} \right], \quad (15)$$

and the SNR of the measurement is defined as

$$\mathrm{SNR}_g = 10 \log \left[\frac{\frac{1}{N} \sum_{i=1}^{N} (g_i \text{ measured})^2}{\sigma^2_{\text{noise}}} \right]. \quad (16)$$

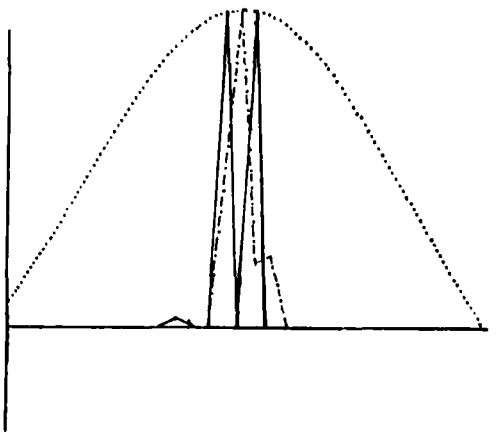

Fig. 3. Constrained minimax solution for two impulses separated by one eighth of the Rayleigh distance.

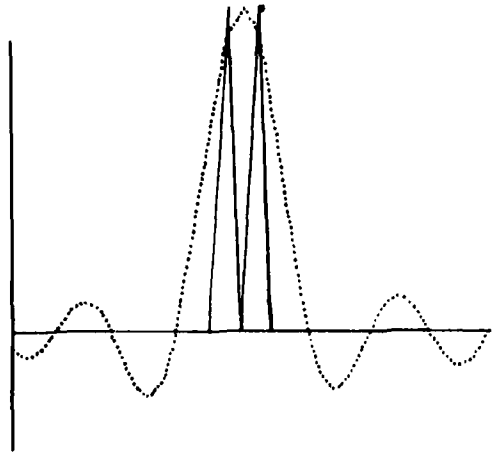

Fig. 4. l_1 estimate with no SVD prefiltering impulses separated by one-half of the Rayleigh distance with white noise added, $\sigma = 0.3$.

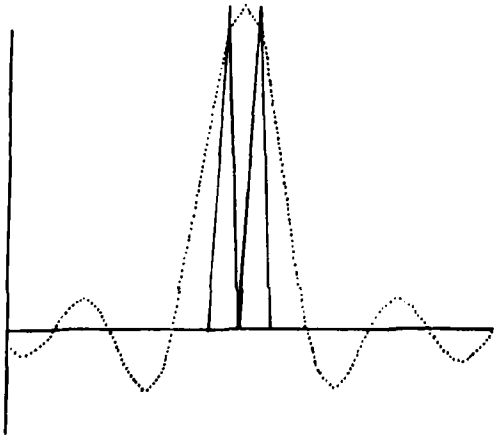

Fig. 5. l_1 estimate with SVD prefiltering, of two impulses separated by one-half of the Rayleigh distance with white noise added, $\sigma = 0.3$.

Figure 4 illustrates the minimal l_1 estimate (chain–dot curve) with no SVD prefiltering of two impulses separated by one-half of the Rayleigh distance. White Gaussian noise with zero mean and a $\sigma = 0.3$ has been added to the measured image. The corresponding SNR of the measured image is 21 dB. The restored image had an SNR of 14 dB. The diffraction-limited image (dotted line) has a jagged appearance due to the added noise. Figure 5 illustrates the effect of the SVD prefiltering. The example is identical to that in Fig. 4 except that prefiltering of the measured image has been performed. The diffraction-limited image (dotted line) appears much smoother than in Fig. 4. The improvement in the estimate is obvious. The estimate (chain–dot curve) lies almost completely coincident to the exact image (solid line) curve. The peak values of the estimate are 10% lower than the exact solution, and the interimpulse trough is 10% higher than the exact solution.

The method presented will find r nonzero elements for the $2N$ variables. Thus the formulation given by Eqs. (13) and (14) applies to impulsive-type images. A more general class of images can be restored if smoothness constraints of the form $f_{i+1} - f_i \leq \delta f_i$ are appended to the formulations, where δf_i is a bound on the first order difference (derivative) of the image to be restored. Higher order differences information can also be appended.

The methods presented have also been investigated for the case of a diffraction-limited noncoherent imaging system. The discrete formulation of the noncoherent case possesses an effectively higher rank than the coherent case as a result of the larger spatial bandwidth. Thus a better two-point resolution is obtained as shown in Fig. 6 where the restored image (chain–dot curve) is almost identical to the original image (solid line), and the dotted curve represents the measured DL image. The discrete spectrum, similar to the continuous transfer function, takes on intermediate values between zero and unity. Therefore, the elimination of noisy image components in the presmoothing step is not as effective. Since the image components retained will represent much of the measurement noise, this is demonstrated in Fig. 7 where the noncoherent DL image is shown by the dotted curve. The restored image

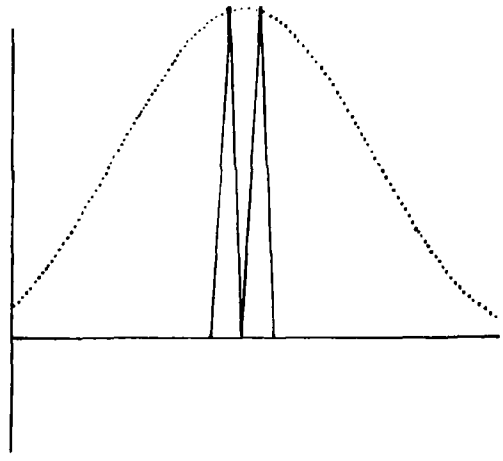

Fig. 6. Noncoherent restoration of two impulses separated by one-tenth of the Rayleigh distance.

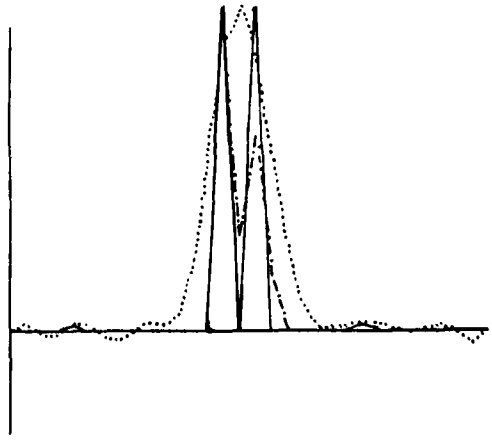

Fig. 7. Noncoherent restoration of two impulses separated by one-half of the Rayleigh distance with SNR of 24 dB.

(chain–dot) does not approximate the original image (solid line) as well as for the coherent case. Although the SNR is 4 dB larger than in that of the coherent case (Fig. 5), the restoration, although acceptable for many applications, is not as close as in the corresponding coherent example.

III. Summary and Conclusions

A new approach to image restoration has been introduced. The method is highly immune to measurement errors and noise. The ill-conditioned nature of the problem is accounted for in such a way as to reduce the amount of computations necessary. The capability of the method to yield superresolving restorations is demonstrated. This property of increasing the resolution of a measured image beyond that dictated by the diffraction limit is demonstrated even in the presence of very significant noise. The method is particularly well-suited for impulsive image applications.

This paper is based on a portion of a dissertation submitted by R. J. Mammone in partial fulfillment of the requirements for the Ph.D. in Electrical Engineering to the City University of New York, N.Y.

This work was supported in part by a grant under AFOSR 77-3217. Some of this material was presented at the 1980 OSA Annual Meeting, Chicago.

References

1. B. R. Frieden, "Image Enhancement and Restoration," in *Picture Processing and Digital Filtering*, T. S. Huang, Ed. (Springer, New York, 1975).
2. S. Twomey, J. Franklin Inst. **279,** 95 (1965).
3. J. P. Burg, "Maximum Entropy Spectral Analysis," presented at the 37th Annual Meeting of the Society of Exploration Geophysicists, Oklahoma, City, Okla. (1967).
4. P. A. Jansson, R. H. Hunt, and E. K. Plyler, J. Opt. Soc. Am. **60,** 596 (1970).
5. A. C. Schnell, Radio Electron. Eng. **29,** 21 (1965).
6. Y. Biraud, Astron. Astrophys. **1,** 124 (1969).
7. D. L. Phillips, J. Assoc. Comput. Mach. **9,** 84 (1962).
8. C. W. Helstrom, J. Opt. Soc. Am. **57,** 297 (1967).
9. J. L. Harris, Sr., J. Opt. Soc. Am. **56,** 569 (1966).
10. D. Slepian and H. O. Pollak, Bell Syst. Tech. J. **40,** 43 (1961).
11. A. N. Tikhonov, Sov. Math. **4,** 1035 (1963).
12. D. P. MacAdam, J. Opt. Soc. Am. **60,** 1617 (1970).
13. E. B. Barrett and R. N. Devich, Proc. Soc. Photo-Opt. Instrum. Eng. **74,** 152 (1976).
14. N. D. A. Mascarenhas and W. K. Pratt, IEEE Trans. Circuits Syst. **CAS-22,** 252 (1975).
15. D. Slepian, Bell Syst. Tech. J. **57,** 1371 (1978).
16. H. C. Andrews and C. L. Patterson, IEEE Trans. Acoust. Speech Signal Process. **ASSP-24,** 26 (1976).
17. H. C. Andrews and B. R. Hunt, Digital Image Restoration (Prentice-Hall, Englewood Cliffs, N.J., 1977).
18. B. R. Hunt, IEEE Trans. Audio Electroacoust. **A-19,** 283 (1971).
19. G. Hadley, *Linear Programming* (Addison-Wesley, Reading, Mass., 1962).

Restoration of discrete Fourier spectra using linear programming *

R. Mammone** and G. Eichmann

Department of Electrical Engineering
The City College of the City University of New York
New York, New York, 10031

ABSTRACT

A method of restoring the discrete Fourier transform (DFT) spectrum of a diffraction-limited (DL) image from a narrow observation segment of the DL image is presented. The DL spectral restoration process is the dual of the more common DL image restoration process with the roles of the frequency and space reversed. Applications of a spectrum restoration include increasing the field of view of existing imaging systems and extracting precise frequency components of a large DL image using only a small segment of the entire image. This method could also be employed for image data compression which is of interest in digital video applications. Several differences between the implementations of the image and the spectrum restoration processes are described. The estimate is constrained to have an upper bound on the number of frequency components contained in the Fourier spectrum. The bound is the number of samples acquired at the Nyquist rate for the length of the image. The magnitude of the discrete Fourier transform (DFT) spectrum is also bounded. These constraints define a large number of possible solutions. The desired solution is then

selected such that the distance, defined in a function-theoretic sense, between the measured and the estimated image is an optimum. A number of such measures are investigated. Numerical experiments show that this approach yields results that are highly immune to measurement noise.

* This paper is based on a portion of a dissertation submitted by R.J.Mammone in partial fulfillment of the requirements for the Ph.D. degree in Engineering to the City University of New York. This work was supported in part under a grant from the Air Force Office of Scientific Research AFOSR 81-0169 and a contract from the Rome Air Development Center F19628-80-C-0095

** presently with the Department of Electrical Engineering, Rutgers University, Piscataway, N.J. 08854

INTRODUCTION

The finite aperture of any physical imaging system eliminates the high spatial frequency components of the object from appearing in the image. The lack of high frequency detail results in a loss of resolution in the observed image. It has been shown [1], that for an object of finite extent, an exact restoration of the object from the diffraction-limited (DL) image is possible. The restoration of the DL object can be viewed as a continuation of the spatial Fourier spectrum beyond the spatial cutoff frequency imposed by the DL system. However, numerical implementation of DL image restoration process are highly unstable in the presence of measurement noise. The restoration process can be stabilized by imposing additional constraints [2]. Many restoration methods are available such as those of Frieden [2], Schell [3], Biraud [4], Jansson [5] and Burg [6]. Recently, Howard [7] has demonstrated a computationally inexpensive method using a least-squares approach. This approach was further elaborated on by Rushforth et al.[8]. A new method of obtaining an increase of image resolution using linear programmming techniques has recently been given by Mammone and Eichmann [9].

In this paper, the dual of the DL image restoration problem is considered. Here the extrapolation of a finite segment of the DL

(i.e. spatial bandlimited) image data in the presence of measurement noise is presented. The restoration of the discrete Fourier transform (DFT) spectrum may be interpreted as an extrapolation of the truncated spatial image. Application of a spectrum restoration include increasing the field of view of existing imaging systems and extracting exact frequency components of a large DL image when only a smaller image segment of the entire image is available. This reduction would be also of interest in image data compression applications such as the transmission of digital video images. While spectral restoration yields the same mathematical formulation as that obtained for DL image restoration, with the role of space and spatial frequency reversed, there are significant differences as well. Here the unknowns are Fourier coefficients which are complex numbers. This fact appears to double the numerical complexity of the problem. Also, the circulant convolutional operator which results from approximating the exact Fourier transform with a DFT leads to additional considerations. Finally, while the restored DL object is non-negative, the restored DFT spectrum need not be real nor non-negative. Thus, the powerful non-negativity constraint used in the DL image restoration can not be directly used.

The motivation of this research is to provide high resolution frequency estimates of data available only on an incomplete observation length using the computationally efficent FFT

algorithms. In order to simplify the discussion 1-D images are considered. For a DL (bandlimited) image truncated to lie within an interval S, the spatial frequency resolution is limited by the uncertainty principle [12]. The lack of spectral resolution is related to the infinite limits of integration in the definition of the Fourier transform. Since the image is available over a finite observation length, the calculated Fourier transform is distorted. It is convolved with a sinc function with mainlobe width D_f. For the case of two different sinusoidal images the uncertainty principle states that the difference in the frequency between the images can not be less than D_f otherwise there will be a significant overlap of the transforms. This overlap would not permit the two separate responses to be distinguishable. Thus, the frequency resolution is limited to

$$D_f \geq 1/S \qquad (1)$$

In many practical situations, the image is not available for an interval of sufficient length S for the desired frequency resolution D_f. It is then desirable to process the spectrum of the observed signal such that the spectral resolution is greater than that given by Eq.(1). If there is no source of measurement error, it is well known [1] that the spectrum can exactly be restored. However, there is always noise and/or error present due to, if nothing else, the finite numerical precision necessary to carry out the computation. Therefore, noise or measurement error must be considered as part of the formulation

of the problem. In this case, the restoration process becomes highly unstable.

It has been [2] found that the imposition of a priori constraints, such as nonnegativity of the estimate, will stabilize the restoration process. Since the maximum number of independent equations that can be generated is equal to the number of spatial samples r acquired at the Nyquist rate, we shall restrict the spectrum restoration method to situations where the number of frequency components is less then or equal to r. This limit on the dimension of the estimate has been obtained by several other studies [12,13,14]. The sinusoidal frequency components will be further assumed to be harmonics of the same fundamental frequency. This latter assumption is not necessary but is made to facilitate the use of the fast Fourier transform (FFT) approximation of the Fourier spectrum. The periodic frequency spectrum is obtained by zero-padding the truncated space sequence such that the total number of elements is L, an integer that is a power of two. This step allows a finer frequency scale to be generated.

The optimal data fitting employs linear programming (LP) techniques. The LP method provides both cost and time effective ways of selecting the optimal r-tuple estimate. LP methods have been used previously for the general image restoration problem [9,10,11]. The advantage of the LP techniques for the unstable

DL image restoration problem has also been addressed [9]. In this paper we demonstrate the advantage of this approach for the rank deficient spectrum restoration problem. Since the rank, the number of independent equations, is less then the number of unknowns, many solutions exist. The deficiency of the rank occurs due to the DFT low-pass filter effect that eliminates all but r discrete frequency components. This efffect is in contrast to the linear discrete convolution case [9] which yields a system of equations which has a full rank. However, because the adjacent equations are almost identical, when a finite arithmetic machine representation is used, the system of equations is ill-posed, i.e. nearly rank deficient.

FORMULATION

For the following discussion, it will be helpful to define negative spatial and frequency samples. The first (L/2+1) elements of the sequence f_n or F_k correspond to the positive spatial or frquency samples, respectively, in ascending order and the remaining (L/2-1) elements correspond to the negative spatial or frequency samples, respectively, in descending order. This is consistent with the idea of extending the sequences in a periodic manner. The spatial truncation operation, the model for a short observation segment, is characterized by multiplication of the spatial sequence by the unit rectangle sequence R_r where r is the number of adjacent unity elements centered about the

zero element and with all other elements are equal to zero. The DFT of the rectangle sequence is real and even, since R_r is real and even, and is similar to a sampled sinc function. Let the column vector h be defined as a vector whose elements are

$$h_n = \mathrm{DFT}\{ R_r \} \tag{2}$$

We shall use the circulant convolution theorem [15] to examine the relationship between the truncated and the exact sequence. The circulant convolution matrix for the discrete spatial truncation operator R is given by the circulant matrix

$$\underline{H} = \begin{vmatrix} h_0 & h_1 & h_2 & \cdots & h_{L-1} \\ h_{L-1} & h_0 & h_1 & \cdots & h_{L-2} \\ \cdot & \cdot & \cdot & & \\ \cdot & \cdot & \cdot & & \\ & & & & \\ & & & & \\ \cdot & \cdot & \cdot & & \\ h_1 & h_2 & h_3 & \cdots & h_0 \end{vmatrix} \tag{3}$$

and therefore

$$G = \underline{H}F + N \tag{4}$$

where G and F are the DFT of the measured and the actual sequence vectors, respectively, and N is the complex error (noise) vector. It is well known [15] that the eigen-values of a circulant matrix $\underline{H}$ are the coefficients of the DFT of the first row of the circulant matrix and the eigen-vectors are the DFT basis vectors. Therefore, the rank, which is equivalent to the number of nonzero eigenvalues, of $\underline{H}$ is equal to the number of

non-zero elements r in the rectangle sequence R . Since the vectors G, F and N are complex, Eq.(4) represents 2L real scalar equations. But all the spatial sequences are real and therefore, the DFT sequences must have symmetry. The symmetry in turn introduces redundancies in Eq.(4). The elimination of this redundancy reduces the 2L to L real equations. In order to obtain these L equations we must examine some properties of the DFT.

Similar to the properties of the Fourier transform, the DFT of a real sequence possesses an even real and an odd imaginary part. Since we wish to use the computationally efficient radix two FFT algorithm, the sequences must consist of an even number of points. The existing symmetry can be displayed in the following way. There is one element for the dc, the zeroth, component, (L/2-1) negative as well as positive elements and one remaining, the L/2 , element. This can be seen by noticing that the L/2th row of the DFT matrix is a sequence of alternating positive and negative unities. Thus, the center and the dc frequency components are always real. The remaining (L-2) elements consist of complex conjugate pairs, between the first and the last elements and the second and the second to the last elements and so on. There are (L/2+1) distinct real and (L/2-1) imaginary elements. We form the concatenated sequence of the distinct elements. Let the real and the imaginary parts of the ith element be denoted by the subscript Ri and Ii, respectively,

then

$$\hat{G} = \{ G_{R0}, G_{R1}, \cdots, G_{R(L/2+1)}, G_{I(L/2-1)}, \cdots, G_{I1} \}^T$$
$$\hat{F} = \{ F_{R0}, F_{R1}, \cdots, F_{R(L/2+1)}, F_{I(L/2-1)}, \cdots, F_{I1} \}^T \quad (5)$$
$$\hat{N} = \{ N_{R0}, N_{R1}, \cdots, N_{R(L/2+1)}, N_{I(L/2-1)}, \cdots, N_{I1} \}^T$$

where the superscript T stands for the transpose operation. The relation Eq.(4) can now be written in reduced form

$$\hat{G} = \hat{\underline{H}} \hat{F} + \hat{N} \quad (6)$$

where if we decompose the degradation matrix

$$\underline{H} = \left| \begin{array}{c|c} \underline{A} & \underline{B} \\ \hline e \; \underline{C} \; p & \underline{D} \end{array} \right| \quad (7)$$

where $\underline{A}$ is a $(L/2+1)\times(L/2+1)$, $\underline{B}$ is a $(L/2+1)\times(L/2-1)$, $\underline{C}$ and $\underline{D}$ are $(L/2-1)\times(L/2-1)$ submatrices of $\underline{H}$ and e and p are unused column vectors. If we denote the null vector and matrix 0 and $\underline{0}$, respectively, and define

$$\hat{\underline{B}} = \{ 0 \; \underline{B} \; 0 \} \quad (8)$$
$$\hat{\underline{C}} = \{ 0 \; 0 \; \underline{C} \} \quad (9)$$
$$\hat{\underline{D}} = \{ 0 \; 0 \; \underline{D} \} \quad (10)$$

then

$$\hat{\underline{H}} = \left| \begin{array}{c|c} \underline{A}+\underline{B} & \underline{0} \\ \hline \underline{0} & \underline{D}-\underline{C} \end{array} \right| \quad (11)$$

Thus Eq.(6) represents L real equations in the 2L variables $\hat{F}$ and $\hat{N}$. Here, $\hat{\underline{H}}$ denotes the space truncation operator in the DFT domain. This underdetermined system of equations has many solutions. For example, the pseudo-inverse solution might be used

[16], although this would produce an unconstrained estimate. In order that we may be able to impose constraints on and simultaneously choose an optimal solution, that is one close in some sense to the measured image, we use a method of optimization known as linear programming.

CONSTRAINED OPTIMAL SOLUTIONS

The basic linear programming (LP) problem is formulated in the following way [17] :

$$\text{Minimize the cost function} : c^T x$$

$$\text{Subject to} : \underline{A}x \leq b \qquad (12)$$

$$x \geq 0$$

where c and x are the known cost and unknown M-dimensional variable vectors, respectively, b is an r-dimensional constraint vector and $\underline{A}$ is a rxM constraint matrix. The most often used LP technique is the simplex method [17]. The output obtained from a simplex LP algorithm will correspond to one of the following three situations: either there is no feasible solution, that is, all of the constraints cannot simultaneously be satisfied, or the optimal solution is feasible but is unbounded. The third alternative is that the solution is feasible and bounded and then an optimal solution is provided.

The first step in the simplex method is to convert the inequality constraints into equalities. This step is accomplished by

introducing additional variables, called slack variables. The resulting system of equations will have more unknowns than equation leading to an underdetermined system of equations. From the many possible solutions the simplex method seeks a solution that minimizes the cost function. The basic premise of LP is that the solution vecor x will consist of at most r non-zero elements, where r equals to the number of independent equations, and the remaining M-r elements will be equal to zero. In a vector space interpretation of LP, the inequalities define intersecting hyper-planes which form a region of possible solutions. This region is an r dimensional polygon or simplex. The simplex will always lie in the positive octant of the vector space. The cost function also defines a hyper-plane for a fixed cost value. For this value to be minimum, the cost function hyper-plane must lie on an edge of the simplex. The coordinates of each edge contain at most r numbers. The simplex method is an iterative technique which begins with a feasible solution, at a particular edge of the simplex and, progresses to an adjacent edge in such a way as to yield a reduction in the cost value until no further reduction is possible. The coordinates of the resulting edge yields the optimal solution.

In a LP formulation of the spectral estimation problem, we now take Eq.(6) to to be part of the constraint matrix. In order to guarantee that all the variables are non-negative, a necessary requirement in LP, we next define the vectors in Eq.(6) in terms

of the nonnegative component vectors $\hat{F}^+$, $\hat{F}^-$, $\hat{N}^+$ and $\hat{N}^-$ such that

$$\hat{F} = \hat{F}^+ - \hat{F}^- \tag{13}$$

and

$$\hat{N} = \hat{N}^+ - \hat{N}^- \tag{14}$$

If we examine the sum

$$\hat{N}^+ + \hat{N}^- = \left|\hat{G} - \underline{\hat{H}}\hat{F}\right| \tag{15}$$

we observe that Eq.(15) is the l_1 norm of the error between the spectrum of the measured signal $\hat{G}$ and the spectrum of the spatially truncated image estimate $\hat{F}$. This is the error measure to be minimized. Thus the LP formulation of the l_1 spectral estimation problem is

$$\begin{aligned} &\text{Minimize} \quad : \quad \hat{N}^+ + \hat{N}^- \\ &\text{Subject to} \quad : \quad \hat{G} = \underline{\hat{H}}(\hat{F}^+ - \hat{F}^-) + \hat{N}^+ - \hat{N}^- \\ &\qquad\qquad\quad \hat{F}^+ \leq \hat{F}^+_{max} \\ &\qquad\qquad\quad \hat{F}^- \leq \hat{F}^-_{max} \\ &\qquad\qquad\quad \hat{F}^+, \hat{F}^-, \hat{N}^+, \hat{N}^- \geq 0 \end{aligned} \tag{16}$$

The l_1 norm is not the only measure of error that can be minimized. The l_{inf} norm or maximal deviation can also be employed. This can be seen by defining a scalar E to be the absolute value of the maximum element of the error vector given by Eq.(15). Thus the LP formulation of the l_{inf} spectral estimation problem is

$$\begin{aligned} &\text{Minimize} \quad : \quad E \\ &\text{Subject to} \quad : \quad \hat{G} \leq \underline{\hat{H}}(\hat{F}^+ - \hat{F}^-) + E e_n \end{aligned}$$

$$\begin{aligned} \hat{G} &\geq \underline{\hat{H}}(\hat{F}^{+}-\hat{F}^{-})-Ee_n \\ \hat{F}^{+} &\leq \hat{F}^{+}_{max} \\ \hat{F}^{-} &\leq \hat{F}^{-}_{max} \\ \hat{F}^{+}, \hat{F}^{-}, E &\geq 0 \end{aligned} \qquad (17)$$

where e_n is an L dimensional unit vector.

The l_2 norm or the sum of the squares of the error can also be minimized using a formulation similar to that of the l_1 norm. Here quadratic programming methods are used. Quadratic programming techniques provide an estimate with at most r positive elements with all other elements as zero. In general, quadratic programming techniques use computationally efficient LP methods but on larger augmented matrices. These methods are well known and many published computer routines are available [18,19]. There is usually more than one least-square estimate to an underdetermined system of equations like Eq.(4). For example, the pseudo-inverse solution [15] provides an unconstrained leastsquare estimate with lowest l_2 norm as well as the minimum square-error. Howard [7] has demonstrated a constrained least-squares approach for the dual problem incorporating a penalty function to force the solution to become nonnegative. Rushforth et al. [8] developed this approach for ill-posed DL image restoration problem.

The estimates obtained by optimizing the l_1, l_2 and l_{inf} norms are maximum likelihood estimates when the noise is modeled as a random variable with uniform, gaussian or exponential probability density

functions (pdf), respectively [20]. It was found, however, that for the low noise situation of interest, the pdf of the noise did not appreciably effect the estimates. In terms of increased frequency resolution, the l_1 norm consistently offered the best estimate irrespective of the noise pdf. This fact can be attributed to the relatively fewer numerical operations needed as well as the strongest bounds on the individual spectral components for the l_1 estimate. The constrained minimal l_2 norm using quadratic programming techniques requires much more numerical operations. Also, optimizing the l_2 norm is equivalent to minimizing the total noise spectral energy. While this is a desirable feature in general, for the purpose of increased frequency resolution, it tends to be counterproductive. The minimization of the global spectral error noise energy distribution tends to overly smooth the estimate leading to a decrease in frequency resolution.

NUMERICAL RESULTS

The observed spectrum is a smoothed version of the desired spectrum. Fig. 1 illustrates the inadequacy of simply taking the FFT of a truncated sequence. Here as well as in all subsequent Figures the magnitude of the Fourier spectrum is plotted. The dotted line represents a 32 point FFT of 23 samples of a cos $(w_L x)$ sequence, where w_L is the fundamental frequency 2pi/32. Here, only seven data samples have been replaced by zeros. The solid line

illustrates the exact spectrum of the full 32 sample sequence. The lack of resolution conceals the fact that only the fundamental frequency is present. The size of the FFT as well as the number of samples acquired are known a priori. This information, together with the bounds on the amplitude spectrum, is used to estimate the actual spectrum. Fig. 2 illustrates the performance of the l_1 norm when only seven out of the thirty-two samples of the fundamental cosinusoid is available. The dotted line curve represents the overly smooth estimate of the direct FFT spectrum. The minimal l_1 estimate, the dotted line, is very close to the original spectrum. The dotted line curve lies completely on the solid line curve. Thus, a complete restoration is possible even when only seven out of thirty two samples are available. Fig. 3 illustrates the extrapolated space domain sequence corresponding to Fig. 2. The acquired samples are illustrated by the solid line segment and the extrapolated curve by the dotted line curve.

The method is quite robust to measurement noise. Fig. 4 illustrates the restoration of the fundamental cosinusoidal waveform from fifteen samples of a thirty-two point FFT with white gaussian noise added. The variance of the noise is one tenth of the amplitude of the function. Thus, an increase on the order of a factor of two in resolution is obtained even in the presence of very significant measurement noise. The corresponding spatial extrapolation is depicted in Fig. 5. Here the incomplete observation is shown by the dotted line curve. The extrapolated

waveform (the chain dotted curve) follows the exact curve (solid line) very closely. In many applications it is desired to resolve two frequency components spaced very close together. Fig. 6 demonstrates the performance of the l_1 norm in this case. Here the first and the fifth harmonics are sampled with eleven out of the possible thirty-two samples. The direct application of the FFT provides the blurred spectrum indicated by the dotted curve. The estimated Fourier spectrum is represented by the solid line where again, the estimate follows the exact spectrum so closely that the curves are indistinguishable.

SUMMARY AND CONCLUSIONS

A new method of extrapolating a DL image from a measured spatially truncated image is presented. The method directly addresses the issue of the finite degree of freedom of the DL image. The feasible image estimates are constrained to have an upper bound on the number of frequency components comprising the image. A geometric approach has been taken, that is, various error measures were optimized subject to given constraints. Three error norms were discussed: the l_1, l_2 and l_{inf} norm. This method allows the addition of other linear constraints on the desired image. That is, any inequality possessing a linear combination of the unknown samples on one side of the inequality and a scalar value on the other side can also be ac . The inclusion of constraints of this type have been found to stabilize the otherwise unstable problem.

Numerical results demonstrate the increase in resolution as well as its robustness to measurement noise. In terms of resolution, the l_1 norm was found to give consistently the best spectral estimates.

REFERENCES

[1] D.Slepian and H.O. Pollak, " Prolate Spheroidal wave functions, Fourier Analysis and Uncertainty - I", Bell System Tech. J.,vol 40,43-63 (1961)

[2] B.R. Frieden, "Image Enhancement and Restoration", In Picture Processing and Digital Filtering, T.S.Huang,Ed., Springer-Verlag, New York (1975)

[3] A.C. Schell, "Enhancing the angular resolution of incoherent sources", Radio Electr. Eng.,vol 29, 21-26 (1965)

[4] Y. Biraud, " A new approach for increasing the resolving power by data processing", Astron. Astrophys., vol 1, 124-127 (1969)

[5] P.A. Jansson, R.H. Hunt and E.K. Plyer, " Resolution enhancement of spectra", J.Opt.Soc. America, vol. 60, 596-599 (1970)

[6] J.P.Burg," Maximum Entropy Spectral Analysis", presented at the 37th Annual meeting of Society of Exploration Geophysicist, Oklahoma City, Okl. 1967

[7] S.J. Howard, " Continuation of discrete Fourier spectra using a minimum-negativity constraint", J.Opt.Soc.America, vol.71, 819-824 (1981)

[8] C.K. Rushforth, A.E. Crawford, and Y. Zhou, "Least-squares reconstruction of objets with missing high-frequency components", J. Opt. Soc. Am., vol. 72, pp. 204-211 (1982)

[9] R. Mammone and G. Eichmann, "Superresolving image restoration

using linear programming", Appl. Opt., vol. 21, pp. 496-501 (1982)

[10] D.P. MacAdam, " Digital Image Restoration by Constrained Convolution", J. Opt.Soc.America, vol.60, 1617-1627 (1970)

[11] N.D.A. Mascarenhas and W.K.Pratt, "Digital Restoration under a regression model", IEEE Trans on Circuits and Systems, CAS-22, 252-266 (1975)

[12] A. Papoulis,Signal Analysis (McGraw-Hill,New York,1977)

[13] H.J. Landau and H.O. Pollak," Prolate Spheroidal wave functions, Fourier Analysis and Uncertainty- III: The dimension of the space of essentially time- and band-limited signals", Bell System Tech. J., vol. 41, 1295-1336 (1962)

[14] G. Toraldo de Francia, " Degrees of freedom of an image", J. Opt.Soc. Amer., vol. 59, 799-804 (1969)

[15] B.R. Hunt, "A matrix theory proof of the discrete convolution theorem", IEEE Trans. Audio Electroaccust., AU-19, 285-288 (1971)

[16] A. Albert, Regression and the Moore-Penrose Pseudoinverse (Academic Press, New York, 1972)

[17] G.Hadley, Linear Programming (Addison-Wesley, Reading, Ma., 1962)

[18] H.P. Kunzi, H.G. Tzschach and C.A.Zehnder, Numerical Methods of Mathematical Optimiztion (Academic Press, New York, 1971)

[19] C.L. Lawson and R.J. Hanson, Solving Least-squares Problems (Prentice Hall, Englewood Cliffs, 1974)

[20] S.M.Pizer, Numerical computing and mathematical analysis (Science Research Association, Chicago, Ill. 1975)

LIST OF CAPTIONS

Figure 1 The 32 point FFT of 23 sample points of $\cos(w_L x)$ (dotted line curve) and the exact DFT spectrum (solid line)

Figure 2 The restoration of the DFT of $\cos(w_L x)$ from the 32 point FFT of 7 spatial domain sample points (dotted line curve) and the estimated spectrum (solid line)

Figure 3 Extrapolation of $\cos(w_L x)$ in the spatial domain (dotted line curve) from 7 sample points (solid line)

Figure 4 Restoration of the $\cos(w_L x)$ from 15 spatial sample points (dotted line curve) with white gaussian noise. The noise variance is 0.1. The restored spectrum is depicted by a solid line.

Figure 5 Extrapolation of $\cos(w_L x)$ (chain-dot curve) in the spatial domain corresponding to frequency domain plot of Fig.4. The dotted curve indicates the incomplete observation with measurement error. The extrapolated curve (chain-dot) follows the actual waveform closely (solid line curve) very closely

Figure 6 Restoration of $\cos(w_L x) + \cos(5w_L x)$ using a 32 point FFT from 11 spatial domain sample points. The DFT is depicted with dotted and the restored waveform is shown with the solid curve.

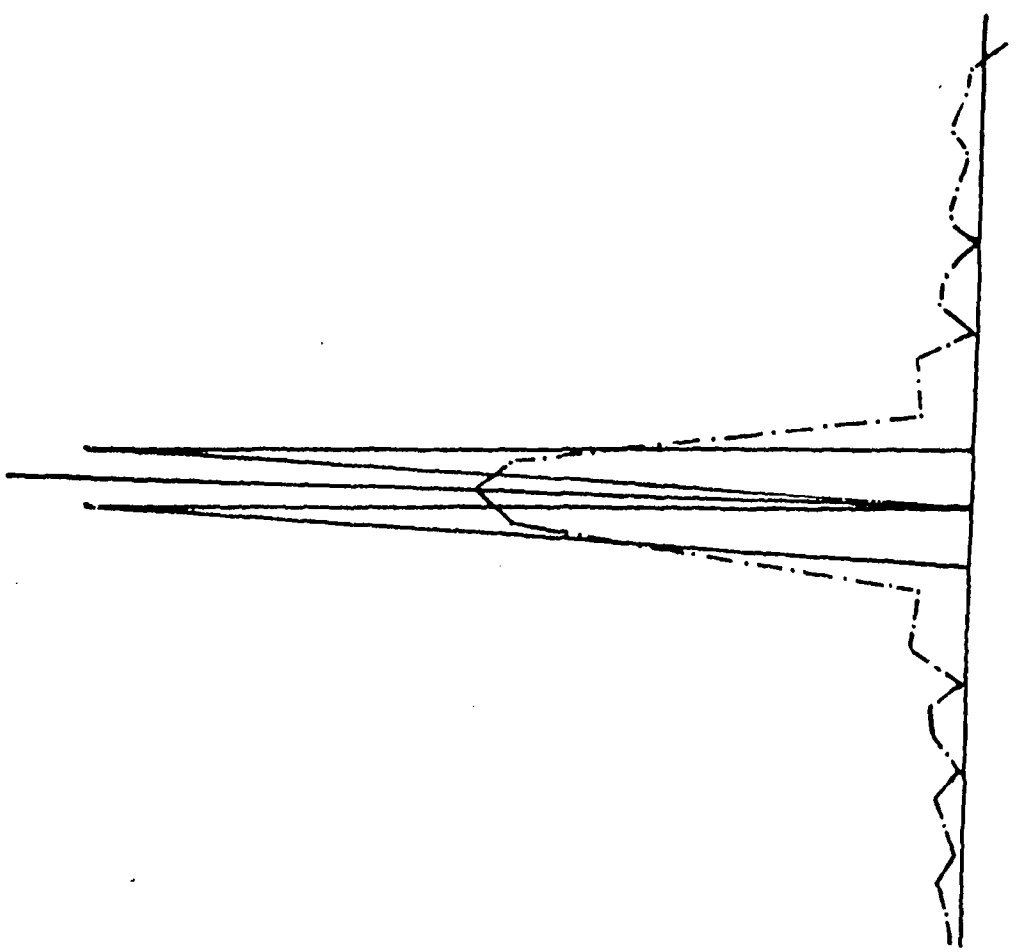

Figure 1

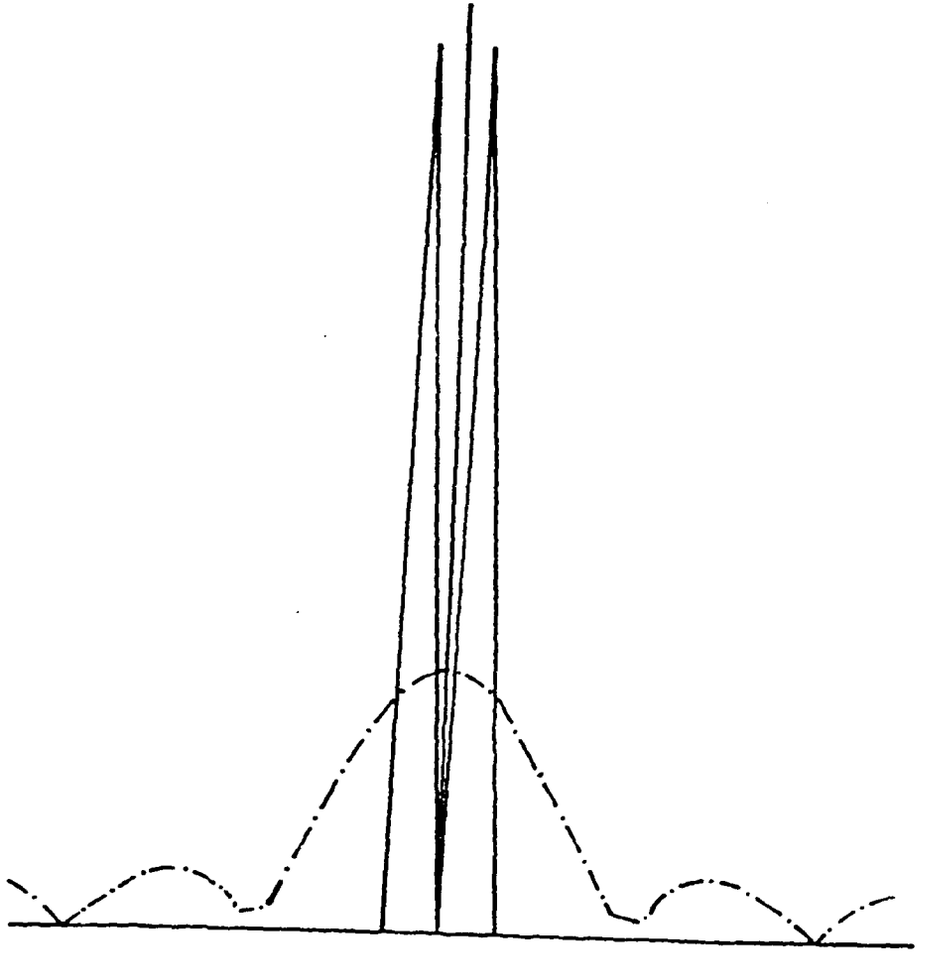

Figure 2

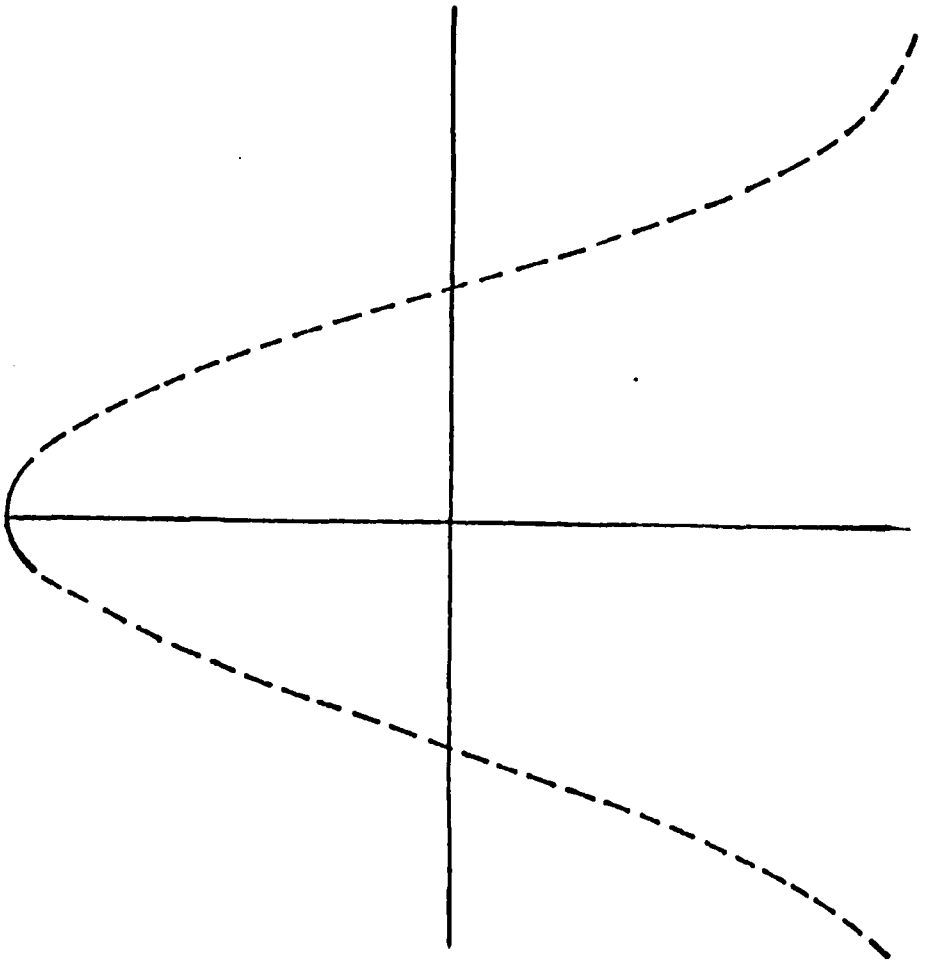

Figure 3

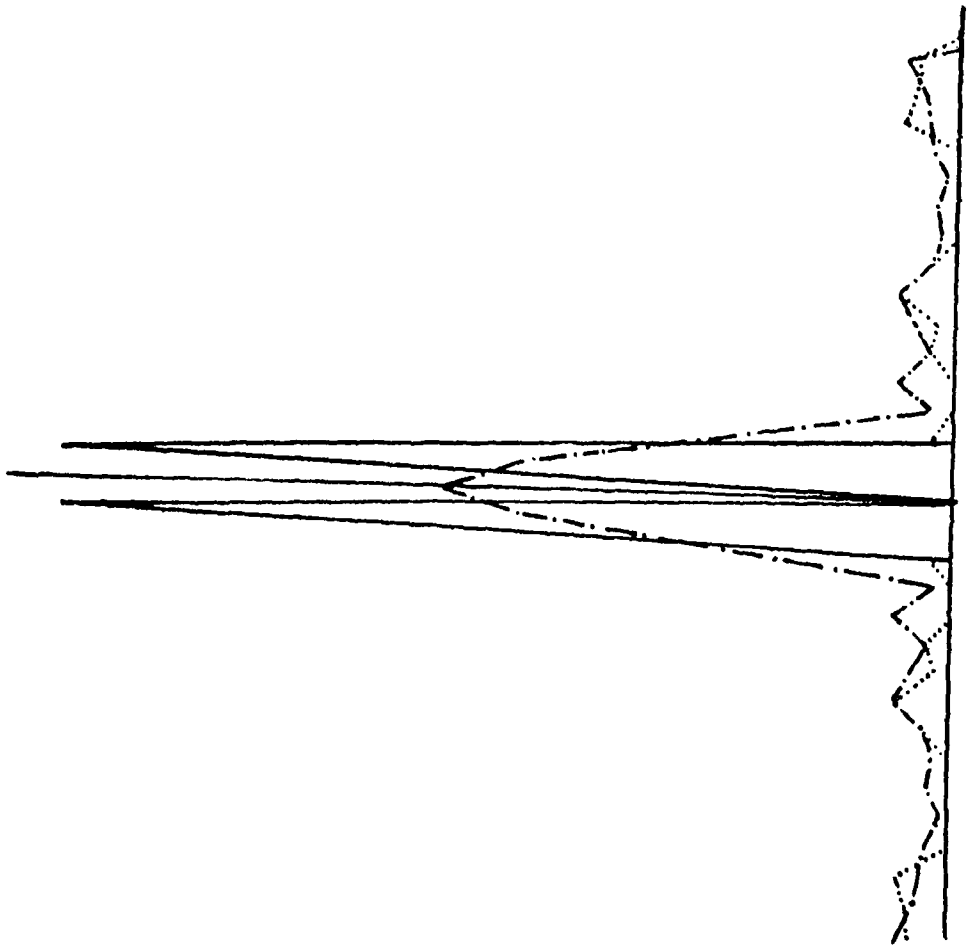

Figure 4

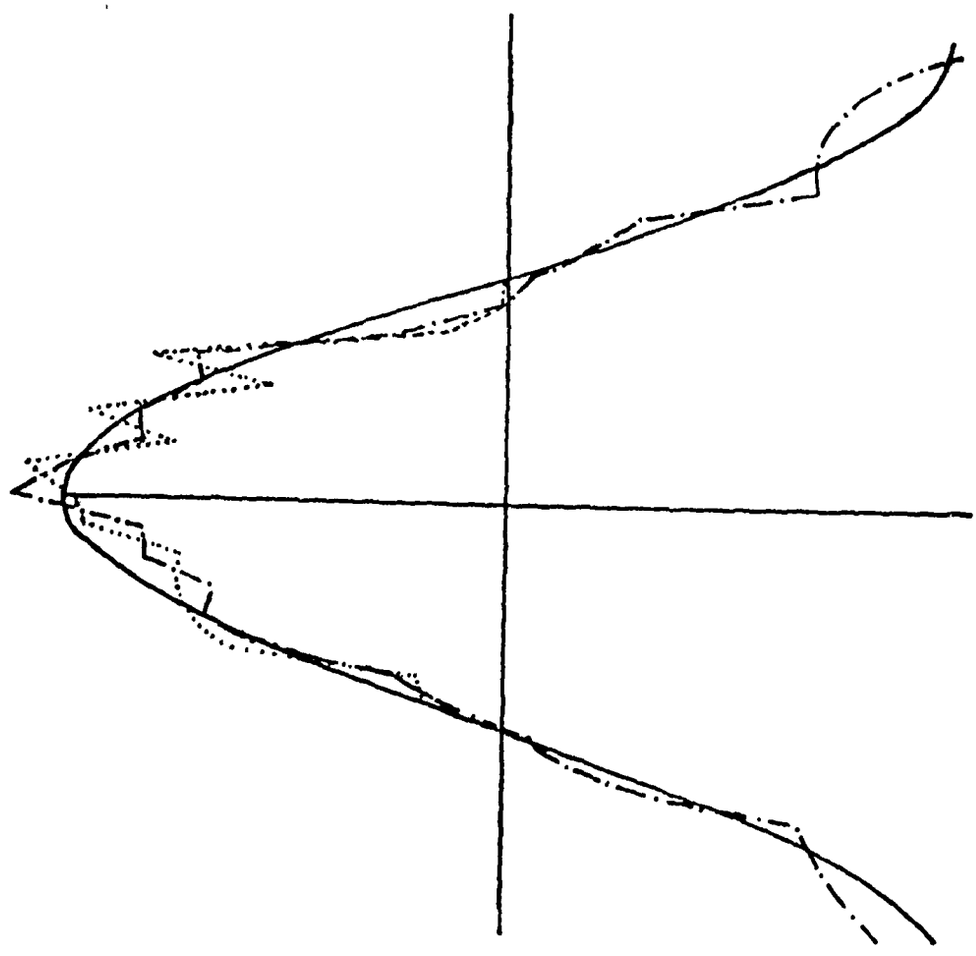

Figure 5

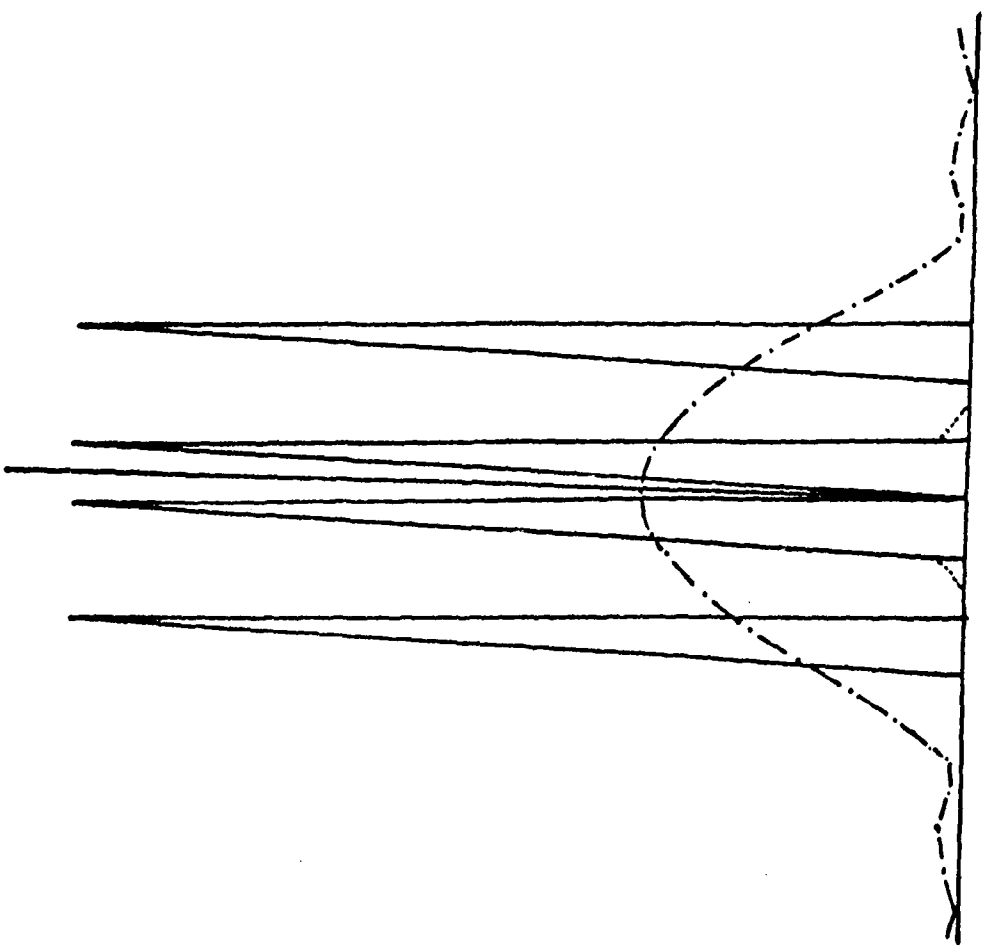

Figure 6

292-09

White-light prefiltering for real-time digital image transmission of still and moving color video images

G. Eichmann and R. Stirbl

Department of Electrical Engineering, The City College of the City University of New York
New York, N.Y. 10031

Abstract

Signal-dependent noise encountered when sampling video signals at low sampling rate, while using an adaptive video delta modulator both as a source encoder and a video digitizer, is combated by using a white-light reflective transform optical preprocessor. While the white-light preprocessor works on black and white images, its main advantage is that it can simultaneously process, using a single source, many color channels. Further, the relative lack of both spatial and temporal coherence aids in reducing speckle and interference noise effects. Experimental results on color video images, that have been preprocessed using a white-light optical transform preprocessor and digitally encoded by sampling with an adaptive delta modulator close to the Nyquist rate, are presented.

Introduction

Along with the development of sophisticated monitoring and communication equipment the need for real-time digital video transmission is apparent. Digital signal transmission offers many advantages over analog transmission when operating over a channel that is corrupted by noise. This is due to the fact that quantized levels are more easily discriminated from the effects of noise. In addition, the digital format allows for time multiplexing, error-coding and correcting as well as encrypting, procedures that are not available on an analog channel. However, when the standard four MHz video signal is sampled at the Nyquist rate and encoded using pulse code modulation (PCM) to four to six quantization levels, the data rate becomes 48 - 64 Mbs. In the case of color video signals, it is not uncommon to require 85 - 90 Mbs digital bandwidth for color PCM encoded digital video signals. This high digital bandwidth is usually unacceptable in many applications.

Various digital encoding alternatives have been explored to reduce the digital bandwidth to an acceptable level. One such solution is a hard-wired adaptive delta modulator (ADM) that works at video rates. In order to compress the digital bandwidth to its ultimate limit it is necessary to operate the ADM close to its Nyquist rate. However, when an ADM runs near its Nyquist rate, a new noise source, and effect that is signal dependent and it termed edge busyness, appears. This noise source is due to the adaptive property of the ADM leading to oscillatory sampling behaviour near the Nyquist rate. For an ADM this noise source is the fundamental limitation in reducing the digital video bandwidth. This signal dependent noise source is combated by preprocessing the color video images by a white-light reflective transform analog preprocessor. While the white-light preprocessor works on black and white images, its main advantage is that it can simultaneously process, using a single source, many color channels. Further, the relative lack of both spatial and temporal coherence aids in reducing optical speckle and interference noise effects. Experimental results on color video images, that have been preprocessed using a white-light optical transform preprocessor and digitally encoded by sampling with an ADM close to the Nyquist rate, is presented.

Background

In an ADM, the step size algorithm is signal dependent. The algorithm of the ADM used in our work was developed by Schilling and Song [1]. In this algorithm, the step size is dependent on the previous transmitted bit and is given as

$$E_{k+1} = \mathrm{Sgn}\,[S_k - X_k]$$

$$X_k = X_{k-1} + Y_k \qquad (1)$$

$$Y_k \begin{cases} Y_{k-1}\,(E_k + \tfrac{1}{2}E_{k-1}) & Y_{k-1} > Y_{min} \\ 2Y_{min}E_k & Y_{k-1} < 2Y_{min} \\ Y_{max} & Y_{k-1} > Y_{max} \end{cases}$$

where E_{k+1} is the transmitted digit, S_{k+1} is the present sample of the input to the encoder, Y_{k+1} is the step size of the ADM, X_{k+1} is the encoder's estimate of the input sample and Y_{min} and Y_{max} is the minimum and maximum allowable step size of the ADM, respectively. Fig. 1 shows the relationship among the clock pulse, the input signal, the estimate and the output bit stream. Notice that the system responds to the rising edge of each clock pulse. Observe that when the estimate X_{k+1} is less than the sample of the input signal S_{k+1}, the transmitted bit is a one and the step size is increased by the factor of one and a half. Thus, the estimate rises exponentially. When an overshoot occurs, the transmitted bit is a minus one and the step size decreases by a factor of one-half. This form of adaptive encoding takes the human observer vision into account.

292-04

Due to the different initial conditions, scanning from line to line, as well as frame to frame, a vertical edge encountered in the image will occur at different positions in the scan. As the sampling rate decreases the error between the steps, and especially near a vertical edge, increases. Fig. 2 illustrates what can occur when the encoder encounters a high contrast vertical edge for two different initial predictor values. Here we see the dotted trace reaches the correct value in five steps, as opposed to a previous or a following scan line trace, shown as a solid line, that takes seven steps. This error in the ADM is called the slope overload noise. The difference is not highly visible when the sampling rate is high, but as the rate is lowered, its visibility increases. Fig. 3 shows the combination of one-dimensional slope overload error and the two-dimensional line to line difference at the same high contrast boundaries which causes an image degradation known as "edge busyness". As a function of time, at low sampling rates, the edge seems to "wiggle" about a vertical line. This noise not only degrades image quality, but also leads to visual fatigue. The slope overload noise can be reduced by sampling at a faster rate. However, if we wish to compress the bandwidth, it is not an acceptable solution.

White-light preprocessor

The purpose of the white-light preprocessor is to manipulate the spatial frequencies of the image. Since the high spatial frequencies are due to the high contrast edges and the high contrast edges leads to edge busyness, the selective filtering of the high spatial frequencies can effect the signal dependent noise. While an all digital implementation of both transform processing and ADM encoding is possible, in general, digital image transforms are time-consuming. Analog transform processors, because they operate on the full image at the speed of light, are natural candidates for real-time image processing applications.

Highly coherent analog spatial transform processors suffer the disadvantage that they are sensitive to positional tolerance errors, dirt noise on the lenses as well as problems with speckle noise. Furthermore, for color image processing, a number of color channels must be created to simultaneously process a color image. By decreasing both spatial and temporal coherence of the source, some of these objections can be circumvented.

It is known that a white-light source can acquire spatial coherence by passing its output through a pinhole. In this case, the light appears to emanate from a single point source. The light radiating from the pinhole has a weaker intensity, as compared to a laser source, and its region of spatial coherence is rather restricted. However, using a low light level camera and constricting the size of the input images, these problems can be overcome.

The arrangement for the white-light preprocessor follows the physical description of the narrowband transform processor. The source is a broad-band 200 W Mercury-Xenon arc lamp. Its output is first spatially filtered by focusing it on a pinhole. The size of the pinhole, 370um diameter, was chosen as a compromise. A small pinhole would block most of the output light as well as it would create a chromatic diffraction pattern. A large pinhole, in turn, will restrict the region of lateral coherence. The light from the pinhole is collimated by an F/8 6" diameter lens. The angular spread of the collimated beam is inversely proportional to the lateral coherence of the white-light system. Instead of the usual lens configuration, we have chosen a reflective system. There are two possible reflective systems. In Fig. 4(a) a fully reflective transform, while in Fig. 4(b) a transmissive filtering system is shown. While the second configuration leads to the use of off-axis parabolic mirrors, we have used the first, single parabolic mirror, configuration. For this geometry the object, the transform and the image planes are all formed in the focal plane of the parabolic mirror. By mounting the object off-axis and moving it out of the focal plane, see Fig. 5, the three regions are fully separated. For stationary objects the color transparency was immersed in a liquid-gate holder. For moving images a 16mm pin-registered film projector was used. The projector was placed on its vibration-isolated stand. While we expected problems due to the vibration and the lack of index-matching gate, the time-averaging effect of the moving frame tended to compensate for these defects.

The spatial filtering is performed with a mirror whose reflectivity is adjusted by a transparency in front of it. Both continuous as well as binary filtering can be performed. Binary filtering tends to degrade image quality abruptly. Continuous-tone, in particular logarithmic, filtering tends to work better, The preprocessing is completed by converting back the conditioned image and focusing it on a color video camera. The three color channels; R, G and B are encoded as well as decoded by three hard-wired video delta modulators. The resultant images can then be viewed either on a color monitor or recorded, using an RGB to NTSC color signal converter, on a video recorder. Stationary and moving color images, using 8 Mbs per color channel, can be digitally transmitted with good fidelity.

Summary

Experimental results were presented on the real-time encoding of moving and stationary color video images. To compress the digital bandwidth, a white-light analog preprocessor has been utilized to condition the video image for digital encoding. The preprocessor allows the encoding of color video images with 8 Mbs per color channel.

Acknowledgments

This work was supported in part by a grant from AFOSR #77-3217 and a contract from RADC F-19628-80-C-0095.

References

1. Song, C.L., J. Garodnick and D.L. Schilling, "A variable step-size robust delta modulator", IEEE Trans. on Comm., vol. COM-19, p. 1033 (1971).

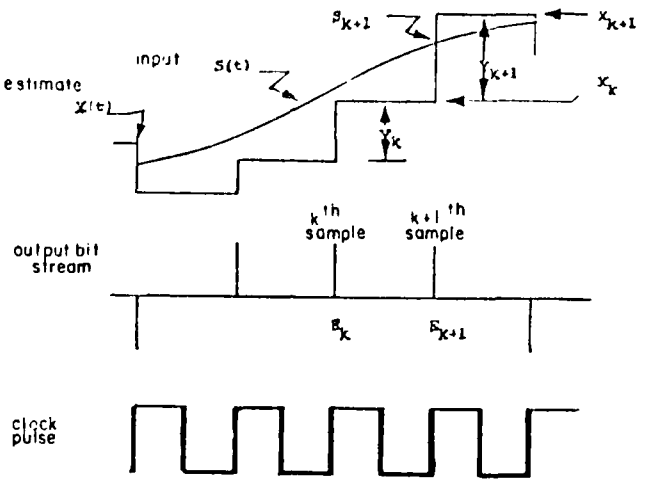

Figure 1 Delta Modulator waveforms; the input, the estimate, the output and the clock

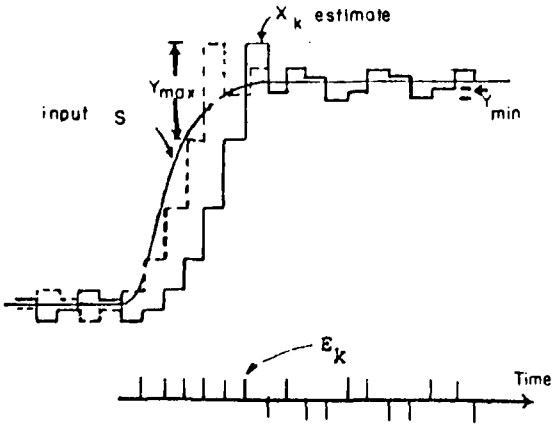

Figure 2 Adaptive Delta Modulator Waveform

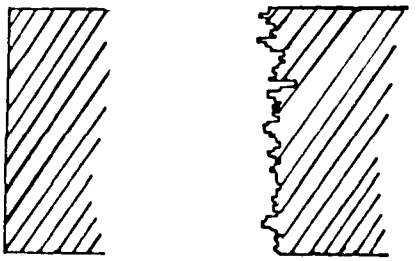

Figure 3 The effect of edge busyness on an edge

(a) Edge before ADM encoding

(b) Edge after ADM encoding

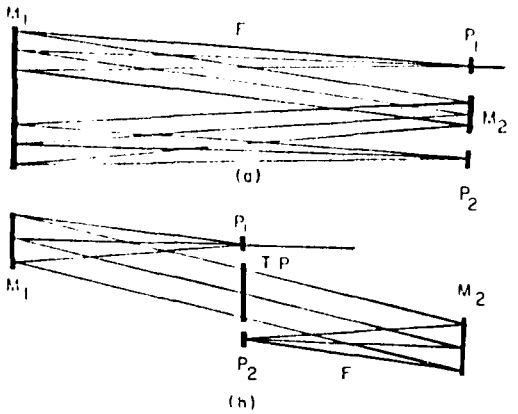

Figure 4 Reflective transform configuration

(a) on-axis parabolic mirror and reflective spatial filter

(b) off-axis parabolic mirro. and transmissive spatial filter

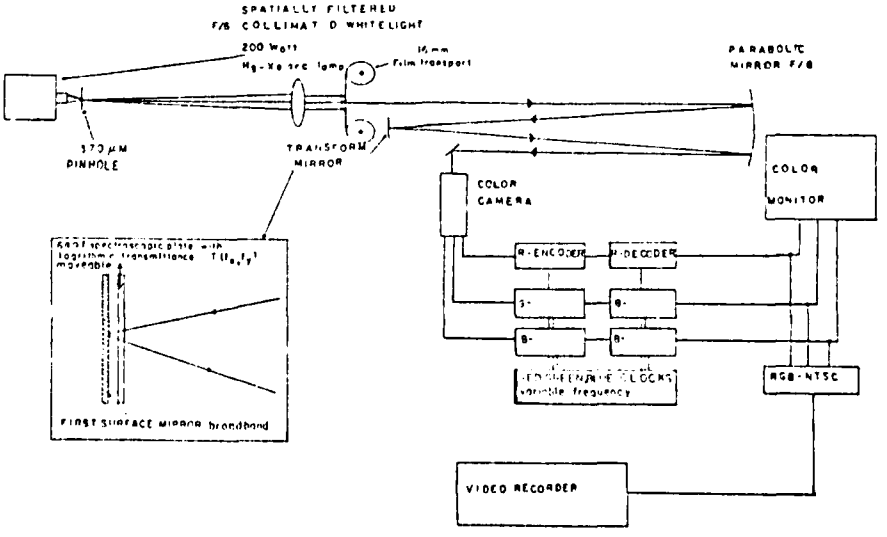

Figure 5 White -light color video preprocessor for digital encoding of video color images

III. Professional Staff

1. Co-Principal Investigators

   D. L. Schilling - Professor

   G. Eichmann - Professor

2. Research Associates

   R. Mammone - Assistant Professor

   T. Saadwai - Assistant Professor

   F. Hemmati - Research Assistant Professor

3. Visiting Scholars

   B. Z. Dong

4. Graduate Students

   B. Coetzer

   M. Jankowski

   J. Keybl

   M. Nicholson

   C. Putman

   R. Stirbl

IV. Publications

This section lists written publications resulting from AFOSR support of this project from the initial starting date.

1. R. Mammone and G. Eichmann ,"Restoration of discrete Fourier Spectra using Linear Programming ", submitted to Journal of the Optical Society of America

2. R. Mammone and G. Eichmann, "Superresolving Image Restoration using Linear Programming", Applied Optics, vol. 21, pp. 496-501 (1982)

3. R. Mammone, Robust Superresolving Restoration with Applications, Ph.D. dissertation, City University of New York, 1981

4. "White-light prefiltering for real-time digital image transmission of still and moving color video images", (with R. Stirbl) presented at 1981 Fall SPIE Seminar on Processing Images and Data from Optical Sensors, San Diego, California.

5. "Hybrid white-light filtering for real-time digital still and moving color image transmission", (with R. Stirbl and J. Keybl) J. Optical Soc. America, Vol. 70, 1589 (1980).

6. "Optimal Restoration of Linearly Degraded Images", (with R. Mammone) J. Optical Soc. America, Vol. 70, 1580 (1980).

7. "Hybrid Video Encoding for Real-Time Image Transmission",(with R. Stirbl and R. Mammone) Conference Record, SPIE Seminar on Optical Signal Processing for C3/I, 1979.

8. "Number Theoretic Transform Modular Residue Processors",(with J. Keybl and R. Mammone) Conference Record,

AD-A117 737 CITY COLL NEW YORK . F/G 17/2
ACQUISITION, IMAGE AND DATA COMPRESSION.(U)
APR 82 D L SCHILLING, G EICHMANN AFOSR-81-0169
UNCLASSIFIED AFOSR-TR-82-0567 NL

SPIE Seminar on Optical Signal Processing for C3/I, 1

9. "Superresolution Using Prolate Spheroidal Wavefunc Filtering ",(with R. Mammone) J. Opt. Soc. America, v 1442, 1979

10."Hybrid White-light Video Filtering for Real-time Color Image Transmission"(with R. Stirbl and J. Keybl Opt. Soc. America, vol. 69, 1435, 1979

11."Quasi-Monochromatic Incoherent Optical Image Proc Conference Record, 1978 International Symposium on Op Computing, London, England.

12."Hybrid Image Source Encoding for Real-time Image Transmission", (with R. Mammone, R. Stirbl and R. Silber),Conference Record, 1978 Fall SPIE Seminar on Signal Procesing, San Diego, Calif.

13. "Switched Frequency Diversity in a Rayleigh Fadi (with F. Hemmati), to be published in the IEEE Trans.

14. "The Effect of Frequency-Selective Fading on a N FH-FSK System Operating with Partial Band Tone Intefe (with L. B. Milstein), IEEE Trans. on Comm., May 1982

15. Theory of Spread Spectrum Communications - A Tut (with R. L. Pickholtz, L. B. Milstein), IEEE Trans. o

16. "The Effect of Multiple-Tone Interfering Signals Sequence Spread Spectrum Communications System", (wit S. Davidovici), IEEE Trans. on Comm., May 1982.

17. "Performance of a Spread Spectrum Communications Over a Frequency-Selective Fading Channel in the Pres Interference", (with L. B. Milstein), IEEE Trans. on

18. "Comparison of Performance of 16-ary QASK and MS Frequency Selective Rician Fading Channel", (with L. R. L. Pickholtz), IEEE Trans. on Comm., Nov. 1981.